Mercury and other trace element wet deposition in Alaska: spatial patterns, controlling factors, and source regions

A draft report to the Alaska Department of Environmental Conservation

Authors:

Daniel Obrist, Division of Atmospheric Sciences, Desert Research Institute, Reno, NV, USA

Christopher Pearson, Division of Hydrologic Sciences, Desert Research Institute, Reno, NV, USA

Christopher Moore, Division of Atmospheric Sciences, Desert Research Institute, Reno, NV, USA

September 20, 2016

Executive Summary

Our team conducted a detailed analysis of wet deposition patterns of mercury from five stations across Alaska and trace metals from three stations to determine the levels of deposition compared to other areas and the factors that influence that deposition. Additionally, we were tasked with making recommendations on how to best monitor the overall deposition of mercury to the State of Alaska. Data was included from the National Atmospheric Deposition Program (NADP) Mercury Deposition Network (MDN) sites Dutch Harbor (AK00), Nome (AK04), Glacier Bay National Park in Bartlett Cove (AK05), Gates of the Arctic National Park in Bettles (AK06), and Kodiak Island (AK98). Our analysis included *four main approaches*:

- Summary statistics of Hg wet deposition, precipitation amounts, and precipitation Hg concentration by year, season, and sites along with statistical tests to assess significant differences, such as Analyses of Variance (ANOVA), Analyses of Covariance (ANCOVA), subsequent post-hoc Bonferroni tests, and non-parametric Kendall Tau tests.
- Principle components analyses and correlation analyses and matrices to determine the association of mercury in wet deposition to that of other trace elements as well as determine relationships among other trace metals to identify possibly common sources.
- Mapping and spatial interpolation of Hg deposition to visualize the key patterns of Hg concentrations and Hg deposition across the State of Alaska.
- Intensive analysis of air mass backtrajectories for the year 2014, including every major storm event, to determine source areas contributing to deposition at the three sites Kodiak Island (AK98), Gates of the Arctic (AK06) and Nome (AK04). Analyses included weighing of trajectories according to their deposition contributions to create frequency maps of contributing areas to annual Hg deposition.

Major findings:

For *Hg concentrations in deposition* across the five deposition stations, we found the following main patterns:

- Mercury concentrations in precipitation at the two northern stations (Nome and Gates of the Arctic) were consistently and significantly higher than the two lowest-latitude sites (Kodiak Island and Glacier Bay).
- These differences in Hg concentration between stations were largely explained by different precipitation regimes, with high amounts of precipitation at the lower latitude stations leading to washout effects compared to dryer, northern deposition sites.
- Differences in Hg concentrations between sites still existed after the effects of precipitation differences were removed although the influence of precipitation was strong. After the correction, Gates of the Arctic (AK06) and Nome (AK04) still had the highest Hg concentrations in precipitation and Kodiak Island still statistically had the lowest Hg concentrations. This suggested that other factors contributed to higher Hg concentrations in wet deposition at these stations as well.

For *Hg deposition loads (area-based loads)*, we report the following main patterns:

- Highest annual Hg deposition loads were always observed at Kodiak Island (AK98), and lowest deposition loads were always observed at Gates of the Arctic (AK06), and these differences were substantial. For example, Kodiak Island (AK98) exceeded deposition at Dutch Harbor (AK00) by a factor 2.64 (in 2009), 2.40 (in 2011), 2.10 (in 2012), and 2.55 (in 2014).
- These patterns also are to a large degree explained by precipitation differences. Across all stations and collection years, precipitation overwhelmingly controlled annual Hg deposition and annual precipitation alone explained 73% of the variability in observed annual Hg deposition across all stations and monitoring years.
- In comparison to Hg deposition loads across the contiguous Unites States, our analyses revealed that annual Hg deposition loads for all of Alaska were among the lowest anywhere in the United States. In comparison to 2014 data, three stations in Alaska (Nome, Glacier Bay, and Gates of the Arctic), were below the minimum deposition load of any of the 99 contiguous United States deposition stations. The two other stations (Dutch Harbor and Kodiak Island) fell below the 5th percentile of annual deposition loads observed across the lower 48 States.
- Based on observations and spatial interpolations, we find distinct zones of highest Hg deposition in Alaska along the southern and southeastern coasts (confined to 50-100 miles inland), and similarly high Hg depositions in isolated mountain areas near the southern coast due to orographic precipitation enhancement. Lower Hg deposition amount are observed along the southwestern coastal region, including Kodiak Island and the western and eastern Aleutians. For most of the state, particularly in the interior and far northern regions, Hg deposition are estimated to be very low.

Detailed air mass backtrajectory analysis for 2014 revealed the following patterns:

- For Gates of the Arctic (AK06), trajectory frequency maps indicated almost identical source origins of precipitation and Hg wet deposition, suggesting that the origin of Hg deposition was closely related to the origin of precipitation. For both source areas of precipitation and Hg deposition, trajectories reached far into the Bering Sea as well as into the Gulf of Alaska.
- For Kodiak Island, there was a similarly close agreement of the source regions for precipitation and Hg wet deposition; here, the major origins for both were usually the Gulf of Alaska with additional contributions derived from the eastern Pacific Ocean up to about 2,500 km south of Kodiak Island.
- For Nome, the origins of precipitation and Hg wet deposition were quite different; for Hg deposition, we found increased source contributions relative to that of precipitation in the western Pacific Ocean near the East Asian continent, which could be due to long-range transport from East Asia. We find origins for both precipitation and Hg deposition in a wide source area across the Bearing Sea, the central Pacific Ocean, and the western Pacific Ocean.

Our analysis of *wet deposition of auxiliary trace elements* from Dutch Harbor, Nome, and Kodiak Island showed the following major patterns:

- Similar to Hg, higher trace metal concentrations were generally observed at the northern station Nome compared to Kodiak Island further to the south, with concentrations at Dutch Harbor in-

between. Yet, washout effects on trace metal concentrations were much smaller or absent for most other trace elements, and one element (Se) even showed increased concentration with increased precipitation.

- The order of annual deposition loads of many trace elements among stations deviates in parts from that observed for Hg. Relatively high deposition of As were observed at Nome, and As, Pb, and Zn were relatively high at Dutch Harbor; however, the current sparse data record adds uncertainties to interpretations of such annual deposition patters.
- Across all sites, we find two distinct associations of trace elements: Cr and Ni are clustered, and so are As and Pb, which may be attributable to different source origins. Sources of Ni and Cr are often considered driven by crustal (e.g., dust) sources), while As and Pb are attributable to anthropogenic inputs, including by long-range transport from Asia. Mercury, nor any of the other trace elements analyzed, does not consistently associate with any of these four elements, suggesting more diffuse and possibly different source origins for these elements.
- Calculations of enrichment factors (i.e., elemental enrichment compared to the upper continental crust) show low enrichment factors for Cr and Ni in support of predominantly crustal sources, while high enrichment factors for Pb and Se suggest additional anthropogenic and natural sources. For most other elements, including Hg, enrichment factors are in-between these elements not indicating a clear attribution to either crustal or anthropogenic source origins.
- Backtrajecotry frequency analyses are in support of influence from Asian long-range transport for deposition of As and Pb. All other elements, however, show diffusive sources from upwind ocean areas.

Recommendations:

Based on our analyses, we have the following recommendations for continued monitoring of Hg deposition and other trace elements:

- Due to generally low wet Hg concentrations across stations, Hg wet deposition for the state could be well represented with two measurement sites, one station representing an area of high precipitation regimes and one station in interior Alaska with inherently low precipitation. Because of their long data record, we suggest to maintain Kodiak Island and Gates of the Arctic for continued Hg wet deposition monitoring into the future. Deposition to other areas in Alaska could be constrained by extrapolation of observed Hg concentrations multiplied by respective precipitation patterns.
- Due to *additional atmospheric Hg deposition processes,* low measured wet Hg deposition in the State of Alaska, however, does not indicate a lack of detrimental Hg impacts from atmospheric deposition because Hg wet deposition is generally a minor component of total atmospheric deposition (<10-20%). We recommend to move towards a comprehensive monitoring strategy that includes other forms of deposition (in particular dry deposition) and other input pathways (e.g., runoff for aquatic ecosystems). Terrestrial Hg deposition is dominated by dry deposition of the gaseous elemental Hg^0, which is supported in recent studies from the north slope of Alaska in the arctic tundra which showed that wet deposition is almost negligible (in the range of a few percent). For most rivers, wetlands, lakes, and even for ocean

basins, major source contributions can be traced to upland watershed sources, rather than direct atmospheric wet Hg deposition.

- Given the dominance of Hg^0 deposition, we strongly recommend adding dry deposition monitoring of Hg^0, which best is achieved by direct measurement of surface-atmosphere exchange of Hg^0 at the ecosystem level using micrometeorological techniques. An alternative method includes monitoring of litterfall deposition (analog to the NADP litterfall Hg network), although this does not directly represent net Hg^0 deposition, and this should include non-forested sites (e.g., tundra) as well. Of secondary importance is quantification of dry deposition of oxidized Hg^{II}: however, while Hg^{II} dry deposition is important along the arctic coast in springtime, it may not be a major source of deposition in much of interior Alaska.
- Multi-tracer monitoring strategies have the advantage to determine associations among elements and identify common source regions or origins, but results can be inconclusive. Depending on specific questions to be addressed, a comprehensive monitoring strategy should be developed that includes other typical source tracers (e.g., Fe, Al, or Ti for dust; Cl, Na, Mg for ocean sources; gaseous tracers such as CO, CO_2, and O_3 as combustion tracers; ^{222}Rn as a boundary layer tracer) to facilitate better source apportionment both for wet deposition as well as for gaseous species (e.g., Hg^0). Continued monitoring of trace elements should further be based on which elements are most important in regard to environmental impacts.

Contents

1 Introduction

1.1. Mercury and other persistent contaminants in Alaska

Most of Alaska falls into the northern arctic-boreal zone dominated by arctic and subarctic tundra and boreal forests. The state has a wide range of ecoregions (Gallant et al., 1995), including: the Arctic Foothills and the Brooks Range mountains dominated by tundra graminoid and herbaceous plants to the north; the Interior Highlands and Bottomlands dominated by spruce and hardwood forests in central Alaska; the Alaskan Peninsula mountains, Aleutian Islands, and Alaska Range to the southwest and south with scrub communities; and the Arctic coastal and Coastal Western Hemlock Sitka Spruce Forests in the southeast. Significant assessments of contaminant impacts have been focused particularly on the Arctic study domain, including large international efforts by the Arctic Monitoring and Assessment Programme (AMAP), a working group of the Arctic Council (AMAP, 2009a; AMAP, 2009b; AMAP, 2011).

The focus on northern latitudes is driven by reports that show significant neurotoxicity as well as immunological, cardiovascular, and reproductive effects in Arctic populations from exposure to contaminants, particularly mercury (Hg), persistent organic pollutant (POPs), and lead (Pb) (AMAP, 2011). Although the proportion of childbearing-age women who exceed blood level guidelines for Hg, polychlorinated biphenyls (PCBs, a POP), and Pb has been decreasing – possibly driven by nutritional changes – the most recent AMAP report expresses great concern about effects of Arctic climate warming on access to non-local foods. In addition, delivery of contaminants to the Arctic is expected to increase in the future due to changes in synoptic atmospheric transport patterns and an expected increase in contaminant source fluxes from within northern regions with increased development, resource extraction, and transportation activities.

The additional pollutant input is of particular concern since, the organic form of Hg, methylmercury (MeHg), can be a major health issue for northern populations that consume large quantities of seafood and marine mammals as part of their traditional diet (Stow et al., 2011). Risks associated with high levels of MeHg exposure include long-term neuro-developmental delays in children exposed in utero, impaired cardiovascular health in adults, and disruption of immunological and endocrine functions (Karagas et al., 2012; Tan et al., 2009). Blood MeHg in more than 50% of some northern populations exceeds concentrations equivalent to the U.S. EPA's reference dose (Bjerregaard and Hansen, 2000; Van Oostdam et al., 1999; Walker et al., 2006). The impact of Hg is not limited to humans, wildlife is also affected. Hg bioaccumulates in aquatic and terrestrial food webs and is present at elevated concentrations in biota such as fish, seals, polar bears, and land mammals that are a major part of the traditional diet of northern peoples (Baeyens et al., 2003; Dietz et al., 2009; Douglas et al., 2012; Evans et al., 2005; Lawson and Mason, 1998; Loseto et al., 2008; Macdonald and Bewers, 1996; Outridge et al., 2008; Walker et al., 2006; Watras and Bloom, 1992). As a result, northern Hg contamination has shown large-scale detrimental effects on wildlife and human health – including beluga whales, ringed seals, Arctic foxes, avian and indigenous populations such as the Inuit (Ackerman et al., 2016; Bocharova et al., 2013; Braune et al., 2014; Eagles-Smith et al., 2016; Laird et al., 2013; Leitch et al., 2007).

In addition, northern boreal and arctic areas also are significantly affected by other persistent contaminants, including polycyclic aromatic hydrocarbons (PAHs), POPs, and other heavy metals such as cadmium and lead (AMAP, 2005; AMAP, 2009a; AMAP, 2011). These contaminants are problematic since they are toxic, highly persistent in the environment, and primarily supplied to the region by atmospheric transport and deposition.

Long-range transport via the atmosphere provides enhanced Hg and other pollutant input (Dommergue et al., 2010; Steffen et al., 2008) and springtime photochemical events lead to additional Hg deposition to snow and ice along the high Arctic coast (Douglas and Sturm, 2004; Lindberg et al., 2002). In remote lakes and rivers far from the industrial development of population centers, studies have found Hg values exceeding the U.S. EPA aquatic life total Hg standard for adverse chronic effects to biota (Schuster et al., 2011). High levels of historically accumulated Hg have also been found in surface soils and permafrost cores (Hedge et al., 2015; Schuster et al., 2008). Wildland fires in boreal zones can release substantial amounts of Hg into the atmosphere or to streams and lakes (Amirbahman et al., 2004a; Amirbahman et al., 2004b; Biswas et al., 2008; Kelly et al., 2006; Porvari et al., 2003; Sigler et al., 2003; Taylor, 2007; Turetsky et al., 2006a); and avian Hg exposure can be elevated in remote areas of Alaska, including locations in the Aleutian Islands, the North Slope of Alaska, and east-central Alaska (Ackerman et al., 2016; Eagles-Smith et al., 2016).

1.2. Atmospheric Hg sources

Table 1. U.S EPA Toxics Release Inventory 2014 (in pounds).

Facility	Fugitive Air Emissions	Point Source Air Emissions
TESORO ALASKA - KENAI REFINERY.MILE 22.5 KENAI SPUR HWY, KENAI ALASKA 99611 (KENAI PENINSULA)	0	15
TESORO LOGISTICS GP LLC-NIKISKI TERMINAL.MILE 19 KENAI SPUR HWY, KENAI ALASKA 99611 (KENAI PENINSULA)	0	0
KENAI PIPE LINE COMPANY-KPL FACILITYY.MILE 22.5 KENAI SPUR HWY, KENAI ALASKA 99611 (KENAI PENINSULA)	0	0
US DOD USAF EIELSON AFB AK.2310 CENTRAL AVE STE 100, EIELSON AFB ALASKA 99702 (FAIRBANKS NORTH STAR)	0	8
RED DOG OPERATIONS.90 MILES N OF KOTZEBUE, KOTZEBUE ALASKA 99752 (NORTHWEST ARCTIC)	5	2
POGO MINE.38 MILES NE OF DELTA JUNCTION, DELTA JUNCTION ALASKA 99737 (FAIRBANKS NORTH STAR)	0	3
HECLA GREENS CREEK MINING CO.13401 GLACIER HWY, JUNEAU ALASKA 99801 (JUNEAU)	0	6
FORT KNOX MINE.1 FORT KNOX RD, FAIRBANKS ALASKA 99712 (FAIRBANKS NORTH STAR)	1	0
DOYON UTILITIES FT WAINWRIGHT AK.3564 NEELY RD, FORT WAINWRIGHT ALASKA 99703 (FAIRBANKS NORTH	0	2
COEUR ALASKA INC KENSINGTON GOLD PROJECT.3031 CLINTON DR SUITE 202, JUNEAU ALASKA 99801 (JUNEAU)	0	1
AURORA ENERGY LLC.1206 FIRST AVE, FAIRBANKS ALASKA 99701 (FAIRBANKS NORTH STAR)	0	7
GOLDEN VALLEY ELECTRIC ASSOC HEALY POWER PLANT.25 HEALY SPUR RD, HEALY ALASKA 99743 (DENALI)	0	3
Total	**6**	**47**

Both natural and anthropogenic sources of atmospheric Hg exist in Alaska. The EPA Toxics Release Inventory (TRI) lists the following fugitive and point-source air sources in the State of Alaska for 2014 for Hg and Hg compounds (Table 1; EPA, 2014); the total reported air emissions of Hg for Alaska amounts to 53 pounds. Further, there is indication of potentially important contributions of local or regional sources, including natural emission sources such as wildfires (Brunke et al., 2001; Friedli et al., 2001; Mitchell et al., 2012; Obrist et al., 2008b; Turetsky et al., 2006b; Webster et al., 2016; Wiedinmyer et al., 2006), volcanic emissions (Ferrara et al., 2000; Mather and Pyle, 2004; Nriagu and Becker, 2003; Pyle and Mather, 2003), and degassing from Hg-enriched soils and possibly background soils (Agnan et al., 2015a; Gustin et al., 2008). For example, studies show substantial biomass burning Hg emissions from boreal forests (Friedli et al., 2001; Turetsky et al., 2006a), and in a recent biomass emission inventory for the western U.S. (although without including Alaska), Webster, Kane et al. (2016) indicated particularly high Hg emission potential from forest fires in northern forests, which is attributed to high fire

intensities and substantial soil heating. Although the importance of the natural sources is known, many natural emission processes are poorly quantified across Alaska.

Alaska also is likely extensively impacted by increasing global Hg emissions because of long-range atmospheric transport (Brooks et al., 2008; Mason et al., 1994; Schuster et al., 2002; Streets et al., 2011a). Hg inputs in many northern areas may originate in large part from lower latitudes, with Hg transported via the atmosphere (Dommergue et al., 2010; Steffen et al., 2008). Hg input to northern areas has increased since pre-industrial times as evident by higher Hg levels in the upper layers of lake sediments and by measurements from ice cores and peat records (Boutron et al., 1998; Hermanson, 1998; Mann et al., 2005; Shotyk et al., 2003). Sediment Hg levels in Arctic lakes and areas of the Arctic Ocean such as Hudson Bay show 20th century increases which are consistent and similar to the increases observed in the lower latitudes (Fitzgerald et al., 2005; Hare et al., 2010; Muir et al., 2009; Semkin et al., 2005).

1.3. Atmospheric Hg cycling and deposition

Three main forms of atmospheric Hg – gaseous elemental mercury (GEM): gaseous oxidized mercury (GOM); and particulate-bound Hg (HgP) – are currently defined operationally, although little is known about their exact chemical composition (Schroeder and Munthe, 1998). What is well known, however, is that GEM, GOM, and HgP have profoundly different behaviors in the atmosphere. GOM is highly water-soluble, quickly deposits to surfaces, and is scavenged by rain or cloud drops. HgP is generally limited to the atmospheric lifetime of particles, typically less than 10 days (Corbitt et al., 2011; Schroeder and Munthe, 1998; Slemr et al., 1985). In contrast, elemental GEM has low solubility in water and a long atmospheric lifetime of 0.5 to 2 years (Bergan and Rodhe, 2001; Selin et al., 2007). As a result, speciation of airborne mercury, and specifically the presence of oxidized forms with high deposition velocities, has been considered to define local, regional, and global deposition loads, including in wet deposition (Selin and Jacob, 2008).

Homogenous and heterogeneous-phase redox processes in the atmosphere transform Hg between different forms; hence, speciation of atmospheric Hg may not represent original emissions to the atmosphere. Well-known chemical transformations, for example, occur during "Mercury Depletion Events" (MDE; Schroeder et al., 1998) in the polar atmosphere during which dominant GEM can completely oxidize to GOM and PHg, which in turn lead to increases in surface deposition (Lindberg et al., 2001b; Lu et al., 2001). It has been estimated that MDEs can increase Hg deposition to the Arctic by 120 to 300 Mg each year (Ariya et al., 2004; Skov et al., 2004), but there is little knowledge of the spatial extent of MDEs (Van Dam et al., 2013). MDEs are considered to be driven by active halogen chemistry (particularly by reactive bromine), and a similar oxidation pathways also are observed over salt-rich water such as the Dead Sea (Obrist et al., 2010) and across the marine boundary layer (Engle et al., 2008; Laurier et al., 2003; Mason et al., 2000; Sigler et al., 2009; Sprovieri et al., 2003). Oxidation of GEM also occurs in the higher troposphere, whereby high-altitudes observations show that air masses are often enhanced with GOM or PHg (Faïn et al., 2009b; Murphy et al., 2006; Selin et al., 2007; Sheu et al., 2010; Swartzendruber et al., 2006).

1.4. Long-range transport

Long-range transport of Hg from mid-latitude source regions is a main source of Hg deposition to northern ecosystems (Durnford et al., 2010). Although global anthropogenic emissions have been fairly stable in recent years, regional decreases in emissions from Europe, Russia, and North

America have been offset by increases from the Asian continent with varying impacts on Arctic and boreal regions (Streets et al., 2011b; Wilson et al., 2010). Across some arctic areas, large-scale changes in Hg pollution patterns have been observed during recent decades, with source origins changing in the 1970s from previous European-dominated locations increasingly to Asian locations (Castello et al., 2014; Douglas et al., 2012; Faïn et al., 2009a).

Research flights in the early 2000s showed high levels of atmospheric Hg in East Asia and over the western Pacific ocean, well above global background values due to Asian pollution (Friedli et al., 2004b), and many studies since have confirmed consistently enhanced atmospheric Hg levels in this region (e.g., Agnan et al., 2014). Measurements at a remote station in Okinawa, Japan and at high-elevation observatories at the US west coast, including Mt. Bachelor Observatory in Oregon, Cheeka Peak Observatory in Washington, and Storm Peak Laboratory in the Rocky Mountains, showed evidence that enhanced Asian Hg levels are subject to trans-pacific transport eastwards to reach the west coast of the United States within several days (Friedli et al., 2004a; Jaffe et al., 2003a; Jaffe et al., 2005; Weiss-Penzias et al., 2006; Weiss-Penzias et al., 2007). These measurements are consistent with previously observed long-range transport of other air pollutants from Asia to the United States, including sulfate, nitrogen oxides, hydrocarbons, carbon monoxide (CO), ozone (O3), and aerosols (Andreae et al., 1988; Husar et al., 2001; Jaffe et al., 1999; Jaffe et al., 2003a; Jaffe et al., 2003b; Jaffe et al., 2003c; Obrist et al., 2008a; Parrish et al., 1992; Price et al., 2004). These events, also termed Asian Long-Range Transport (ALRT) events, are considered significant sources of atmospheric mercury to the United States. Net eastward outflow of Hg from Asia was estimated at 1460 metric tons per year and 600 tons from China alone (Jaffe et al., 2005; Weiss-Penzias et al., 2007). Modeling studies support the notion of significant foreign Hg imports with 5 to 36% of North American Hg deposition attributed to Asian Hg emissions (Seigneur et al., 2004) (2004), with highest contributions in the western US. Similarly, other studies indicate that only around 20% of deposition in the US directly originates from North American anthropogenic sources with the rest from natural emissions, re-emissions, and intercontinental transport (Selin and Jacob, 2008; Strode et al., 2008).

1.5. Summary and conclusions from a previous atmospheric Hg modelling study (Jaeglé 2010)

In a 2010 report entitled "Atmospheric Long-Range Transport and Deposition of Mercury to Alaska" submitted to the Alaska Department of Environmental Conservation, Jaeglé (2010) conducted a detailed study of atmospheric sources of Hg contamination over Alaska. The study included literature review of sources and processes focusing on Alaska, and the use of the GEOS-Chem global atmosphere-ocean-land Hg Model to address the main sources of Hg deposition to Alaska. In this section, we shortly summarize the main findings of the report by Jaeglé (2010). We here shortly summarize the main conclusions of this report.

In a literature review, Jaeglé (2010) summarizes major sources of atmospheric Hg in Alaska: these include 0.1 Mg yr^{-1} reported by the U.S. EPA National Emission Inventory program, mainly concentrated around Fairbanks and Juneau City. They discuss a study on wildfire Hg emissions that estimated fire-related Hg emissions in Alaska of 12 Mg yr^{-1} (Wiedinmyer and Friedli, 2007), although others suggest emissions several-fold lower. They further list natural Hg emissions from mineral deposits that cover large areas and are related to past Hg mining operations in the region.

In a first overview of MDN Hg wet deposition data in Alaska, they discuss three years of deposition data at Kodiak Island (AK98), showing highest deposition fluxes in early summer (May-July) and much lower deposition fluxes winter and fall deposition. They report a mean annual deposition at

Kodiak Island of 4.8±2.6 µg m^{-2}. At much shorter time records at Gates of the Arctic (AK06; 29 weeks), they report low deposition values, possibly attributable to local variability in precipitation. A third station, Ambler (AK99; 14 weeks) had insufficient time coverage for significant analysis. They conclude that Alaskan sites have low Hg wet deposition compared to other MDN sites in the 48 conterminous United States.

They further provide an overview of several Hg studies from the region, including: atmospheric Hg^0 observations, particularly from the Arctic site Barrow that is heavily influenced by coastal mercury depletion events (MDE); observation in snow and sea ice; and historic records of deposition in lake sediment, which are not further discussed here. They further present results from the Western Airborne Contaminant Assessment Project (WACAP; NPS, 2008), with the following main conclusions: lichen Hg concentrations in Alaska were about an order of magnitude lower than those of the other states; snow deposition fluxes in Alaska, in the range of 300-500 ng m^{-2} yr^{-1}, were significantly lower than in the 48 conterminous states (1000-3000 ng m^{-2} yr^{-1}); and sediment records in four Alaska lakes also show lower Hg fluxes compared to other lakes. Yet, fish concentrations in Alaska lakes show elevated concentrations exceeding human contaminant health threshold, which was surprising and not fully explained. Possible reasons for this include high dissolved organic carbon levels in Alaska rivers and lakes leading or different biological and biogeochemical characteristics and higher rates of Hg bioaccumulation in Alaska.

Table 2. Estimated emissions from and deposition to Alaska (from Jaeglé 2010)

	Alaska
Emissions, Tg/yr	**39**
Anthropogenic	0.1
Biomass Burning	0.3
Land	37.6
- Land geogenic	*26.2*
- Land soil+vegetation	*5.5*
- Land/snow/ice re-emission	*5.9*
Ocean	1
Deposition, Tg/yr	**25**
Wet Deposition	7
Dry Deposition	18
-Dry dep. of Hg^0	*15*
- Dry dep. of Hg^{II}+Hg^P	*3*
- Hg^{II} loss to sea-salt	*0*

Using GEOS-Chem model simulation, which was constrained by observations of atmospheric Hg concentrations as well as wet deposition in Alaska and Canada, the report provided an emission and deposition budget for Alaska. In summary, their model predicts that sources are dominated by land emissions, in particular by natural geogenic emissions and re-emissions from land and snow/ice. Deposition is dominated by plant uptake of Hg^0, and dry deposition of Hg^{II} dominates over wet deposition. They attribute wet and dry deposition maxima in spring due to enhanced oxidation of Hg^0 to Hg^{II}.

Comparing pre-industrial simulations with modern day simulations, the results predict that emission in Alaska increased by 13% over pre-industrial emissions, mainly due to increased soil re-emission and small contributions from regional anthropogenic emissions. However, the model predicts that deposition has increased by a factor of 2.1, which is attributed to increased global anthrophonic emissions. Using sensitivity analyses, source-receptor analysis were performed to quantify the role of anthropogenic contributions to Hg deposition over Alaska (**Table 3**). Anthropogenic emissions contribute 34-37% of deposition, with Asian anthropogenic emissions the largest single source (22-24% of total deposition) as compared to only 3% from N. American emissions. Legacy anthropogenic emission (i.e., re-emissions) account for 13-14%, and biomass burning for 10% of Alaska deposition. The report did not provide data on the respective contributions from wet versus dry deposition. In predicting future changes in emission and depositions, the model predicts increased deposition by 35.8%, with the largest component driven by increased anthropogenic emissions from Asia.

Table 3. Modelled contributions to Hg deposition from various sources (from Jaeglé 2010)

	Globe	Alaska
Natural	**39%**	**43%**
Biomass Burning	**10%**	**10%**
Anthropogenic	**35%**	**34%**
Asia	*21%*	*22%*
N. America	*3%*	*3%*
Europe	*4%*	*5%*
Rest of the world	*7%*	*4%*
Legacy anthropogenic	**16%**	**13%**
Total	**100%**	**100%**

Key recommendations made to the Alaska Department of Environmental Conservation by Jaeglé (2010) include: continuation of wet deposition measurement at Kodiak Island to reflect deposition to the North Gulf of Alaska; continuation of wet deposition at Gates of the Arctic to track wet deposition over interior Alaska; measurement of atmospheric Hg^0 at Barrow to assess MDE; new measurement of Hg^0 in the interior Alaska such as Bettles to constrain atmospheric levels in central Alaska; and long-wet deposition measurement at a deposition site in south eastern Alaska to represent deposition to this region of Alaska.

2 Goals

The main goal of this report are to analyze wet deposition patterns of mercury from five measurement stations in Alaska. The stations with available Hg wet deposition data provided for analyses in this study are shown in ***Table 4***, and include Hg wet deposition stations in Dutch Harbor (AK00), Nome (AK04), Glacier Bay National Park in Bartlett Cove (AK05), Gates of the Arctic National Park in Bettles (AK06), and Kodiak Island (AK98). Temporal coverage of available wet deposition data differ among stations, with the earliest record starting in September 2007 and records of most stations terminating in September or October 2015. Data were provided to the authors of this study through the National Atmospheric Deposition Program (NADP) Mercury Deposition Network data portal. We accepted most quality control and assurance protocols of the NADP and accepted data with quality rating A (considered fully qualified with no problems) and B (considered valid data with minor problems, used for summary statistics). Yet, an exception to this is that we rejected outlier values based on the 1.5x interquartile range (IQR) rule as several statistical tests are highly sensitive to such outliers.

3 Materials and Methods

3.1. Mercury deposition network operation and protocols

Weekly Hg deposition data was taken from the National Atmospheric Deposition Program (NADP) Mercury Deposition Network (MDN). Samples are collected each week by a specially modified wet-deposition collector. Prior to deployment, sample bottles are pre-charged with 20.0 mL of 0.12 M hydrologic acid preservative. Bottles are collected weekly and sent off for analysis by a central laboratory. Precipitation is measured separately at each site by a weighing-bucket rain gage with a sensitivity of 0.01 inches. Sampling periods greater than one week occur randomly throughout the record and are weighted accordingly.

Each sample is assigned a quality rating (A, B, or C) based on sample quality and collector performance. Samples with a rating of C are not included in any analyses. The net sample volume collected in the bottle is used for precipitation during weeks with missing rain gage data. Trace samples are assigned a precipitation value of 0.127 inches.

After collection, Hg collection bottles are sent off for sample preparation and analysis. Samples are unpacked in a clean-air station and preserved with additional 0.2 N BrCl in HCl reagent. Once fully preserved, samples are placed on a shaker for at least 4 hours. After shaking, 50-100 mL aliquots are poured into 125 mL Teflon bottles for analysis. 200 µL of 20% hydroxylamine hydrochloride is added prior to injection in the analyzer. Sample analysis follows EPA Methods 1669 and 1631 where Hg is quantified by atomic fluorescence after sequential dual-gold trap adsorption.

3.2 Trace Metal Analysis

We are still awaiting methods details from the State of Alaska for analysis of trace metals.

3.3. Statistical analyses

This analysis was separated into two major sections with two distinct datasets:

- Dataset #1: Alaska NADP Hg Deposition Dataset
- Dataset #2: State of Alaska Trace Metal Dataset

All statistical analyses were performed using the statistical software program “R” (R-Core-Team, 2014). Outliers for both the Trace Metal Dataset and NADP Hg Deposition Dataset were determined using the 1.5 x IQR rule. Datasets were Log10-transformed and back-transformed during outlier testing in order to account for the skewed right/log-normal distribution of the data. Summary statistics are shown throughout this report using both all data and with outliers removed. The trace metal dataset contained multiple elements with numerous values below detection limit (BDL). Maximum-likely hood estimation (MLE) summary statistics were calculated along-side of 1/2 MDL substitution. When applicable, non-parametric ranked-based tests were performed on the trace metal dataset. Boxplots and scatterplots were made using the ggplot2 package (Wickham, 2009).

Analysis of Variance (ANOVA) and Analysis of Covariance (ANCOVA) were performed using the aov function in the R stats package (R-Core-Team, 2014). Testing was performed on Log10-

transformed data using a type-III ANVOA to account for unbalanced factor levels in the dataset. Trace metal ANOVAs were performed on the ½ MDL substituted datasets.

Trace metal correlations were assessed by the non-parametric Kendall Tau test to account for BDL substitution and tied rankings. Kendall's test does not require any assumptions about the underlying distribution of the dataset and is less sensitive to tied values in the ranking process. Correlation testing was performed using the psych package (Revelle, 2014) and visualized with the corrplot package.

A principal component analysis (PCA) using the R package ade4 (Dray and Dufour, 2007) was performed on the ranked trace metal dataset. The trace metal PCA was performed on ranked data to account for BDL values and non-normal distributions. Season was defined as follows for both datasets: spring (March, April, May), summer (June, July, August), fall (September, October, November), winter (December, January, February).

3.4. Mapping and Spatial Interpolation

Mapping and spatial interpolation/extrapolation and was performed in ArcGIS®. Inverse distance weighting (n=5; p=0.5) was used to interpolate/extrapolate precipitation weighted mean concentrations (pwm) across Alaska. The processing extent was allowed to extend beyond the sampling region to all of Alaska. Pwm values were taken from NADP MDN annual estimates and averaged for all available years. This dataset was then combined with annual normal precipitation (2007-2015) from the NCEP Climate Forecast System Version 2 (CFSv2) 6-hourly Products (Saha, 2011) to estimate deposition totals across the entire region. Precipitation data was accessed and compiled using Google Earth Engine (Google Earth Engine Team, 2015). Deposition maps produced during this study are limited by the spatial distribution, temporal coverage, and number of sampling points (n=5) available. Maps are intended to visualize large scale patterns and should not be used to predict deposition at individual sites due to the uncertainty with spatial interpolation/extrapolation.

3.5. Back-trajectory modeling and determination of deposition source areas

Backtrajectories were generated using the National Oceanic and Atmospheric Administration Air Resources Laboratory's Hybrid Single Particle Lagrangian Integrated Trajectory (HYSPLIT) Version 4 Model. The model and associated files are freely available for download and use on PCs under: http://ready.arl.noaa.gov/hyreg/HYSPLIT_pchysplit.php. The model was implemented with meteorological data that has already been prepared for by NOAA for use in the HYSPLIT model available under: http://ready.arl.noaa.gov/archives.php. Data used for this project was the Global Data Assimilation System (GDAS) 0.5 degree meteorological data. We performed an intensive analysis of the backtrajectories analyses for each individual precipitation event for the entire year of 2014 at each station with available Hg wet deposition for that year (Nome, Gates of the Arctic and Kodiak Island). Individual precipitation events were selected based on measurable precipitation data, averaged to an hourly time resolution. A single event was registered if there was not more than a 2 hour interruption in precipitation. If a storm lasted several hours without an interruption of storm activity, the event was classified as a single precipitation event; if there was an interruption in measureable activity >2hr in duration, the

storm was separated into two events. Using this method, the number of individual precipitation events identified for 2014 were 247 (Kodiak Island), 182 (Nome) and 148 (Gates of the Arctic).

A single air parcel trajectory was then calculated for each precipitation event, with the end time initialized to coincide with the center of each precipitation period and the end latitude/longitude set to that of the particular site. For the other trace metals dataset (121 samples), the end time of each trajectory was set to the sample date. 2013 GDAS meteorological data were unavailable at the time, which resulted in the loss of only 27 potential trajectories. Further, the altitude at which all backtrajectories was initiated was set consistently to 2,000 m a.s.l. The output of each HYSPLIT run (trajectory) represents the calculated latitude, longitude and altitude of an air parcel with these final coordinates over the previous 10 days, with temporal resolution of 1 hour, i.e. 240 3D coordinates per trajectory.

In order to delineate major source origins of wet deposition at these stations, each backtrajectory was then weighted according to its contribution to annual Hg deposition as a fraction of the total annual Hg deposition sum. In other words, each of the 240 3D coordinates in each trajectory output was allocated a scalar value representing the measured Hg or trace metal deposition value for that precipitation event. We then calculated the residence time of each weighed backtrajectory in 2˚ x 2˚grid cells, with the fractional residence time of the time spent in a particular grid cell based on the time of the entire trajectory. For example, if a 10-day backtrajectory spent 12 hours of its time in a specific grid cell, it would receive a weighting of 5% for that particular grid cell. The weighting of a backtrajectory residence time in a grid cell was then combined with the weighting of that trajectory as a fraction of total annual deposition, so that both the contribution to annual deposition as well as the residence time in grid cells were fully weighted. Finally, the sum of all backtrajectory weights for each grid cell were summed up and represented as a normalized frequency for each grid cell. We performed this both for 2014 Hg wet deposition, whereby the weighting occurred as the contribution of each trajectory to annual Hg wet deposition, and 2014-15 trace metal deposition. Each weighted and normalized, 2˚ x 2˚ grid of values was finally converted to a raster file using the Python computing language package GDAL (GDAL, 2016; PythonSoftwareFoundation) and mapped and visualized in ArcGIS®.

4 Mercury concentrations in weekly-measured deposition samples: differences between stations, seasons, and effects of different precipitation regimes

In this section, we provide a summary overview and statistics of all available weekly data of measured Hg concentrations from the five wet deposition stations. It is important to note that the data coverage (see section 4.1) differed among stations, e.g., some stations had data from 2007 to 2015 while others had a much more limited data coverage (e.g., starting in 2013). Comparisons among stations, therefore, potentially show inter-annual as well as seasonal biases due to different temporal coverage. Still, due to the multi-year data coverage for Hg deposition measurements at most stations, we considered such effects minor. In section 4.1., we provide an overview of the locations of wet deposition stations and an overview of the temporal coverage for each station. In section 4.2., we provide summary statistics of all precipitation samples as well as individually

among sites. In section 4.3., we evaluate outlier concentrations and discuss reasons for a limited number of unusually high deposition concentrations. In section 4.4., we analyze in detail differences among sites, and show that some of the differences were related to different precipitation regimes. In section 4.5., we address seasonal patterns of observed concentrations.

4.1. Locations of Hg wet deposition stations and temporal coverage of available data

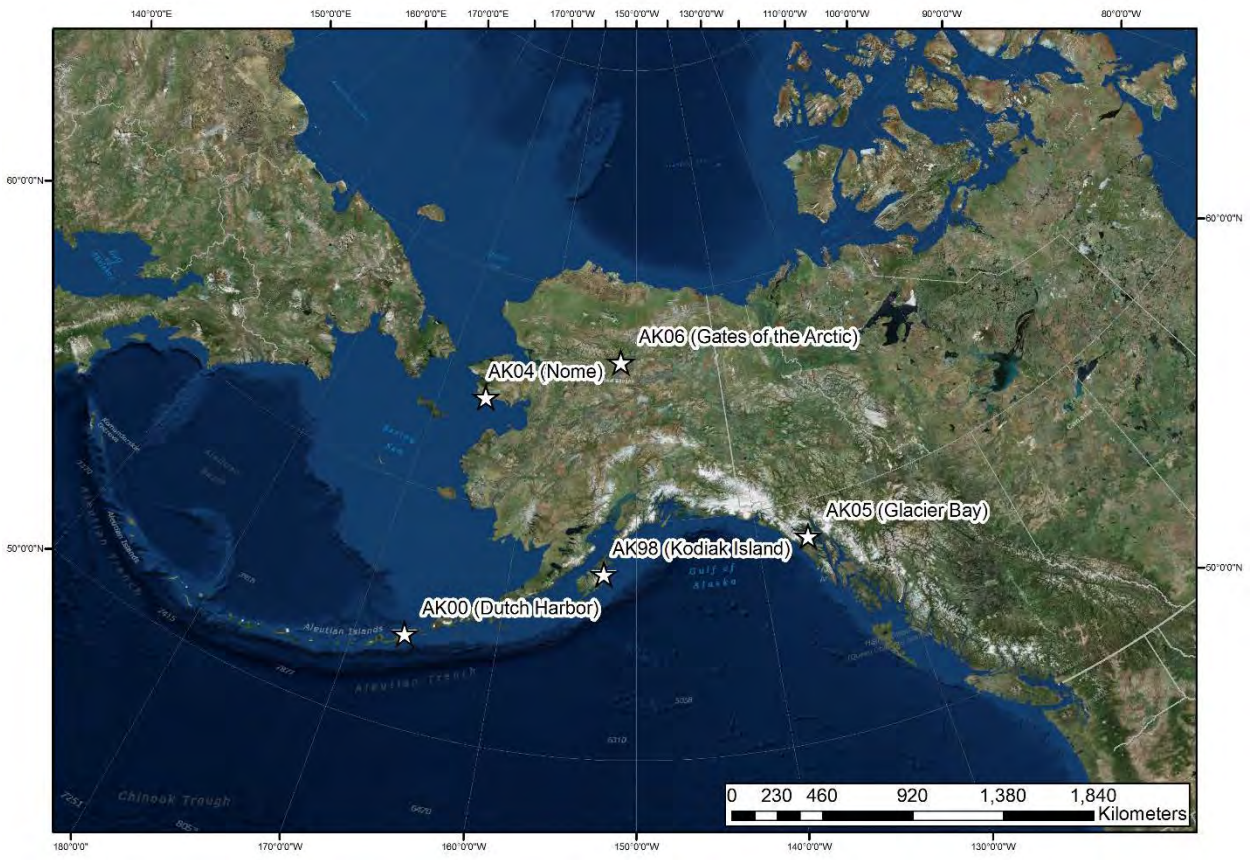

Figure 1. Locations and site ID of the five Hg wet deposition stations in Alaska used for this analysis.

The five stations with available data on Hg wet deposition are shown in **Figure 1**, and details of the stations are listed in ***Table 4***. All stations had different temporal coverages in measurements (***Table 4***): the longest available data record was for Kodiak Island (AK98) which started with deposition measurements in September 2007 and continued to measure through September 2015. Using valid data only with quality assignments A and B (via NADP protocols), the station had a total of 321 available Hg concentration data and 351 data points for Hg deposition loads. Note that differences in the number of concentration and deposition observations occur because of zero precipitation weeks (i.e. no sample); zero precipitation values result in a deposition value of zero, but no concentration measurement. A time series graph of available data (**Figure 2**) shows that periods of missing data were experienced particularly from June through September 2009 and May

through November 2010. These were attributed to difficulties with finding trained operators, funding gaps or periods when there was some contamination associated with samples.

The second longest data set was available for Gates of the Arctic (AK06) in Bettles, with data starting in November 2008 through October 2015. This station showed a total of 216 data points of measured Hg concentrations and 267 loads, which accounted for 74% of the observation period. Another multiyear Hg deposition record was available for Dutch Harbor (AK00) Harbor with measurements from September 2009 through September 2015. Of the total duration, 145 concentration observations and 152 deposition data points were available, covering only 49% of the measurement period. Two shorter time records were also available for Glacier Bay (AK05) from March 2010 to May 2013 and for Nome (AK04) which was operated from September 2013 to September 2015. For Glacier Bay, a total of 137 concentration and 144 load data points resulted in a time coverage of 87% for the deposition record, while for Nome (AK04) 83% of the weeks the sampler was deployed had successful measurements.

Table 4. Overview of available data coverage for each station

Station ID	AK06	AK04	AK05	AK98	AK00
Station Name	Gates of the Arctic National Park	Nome	Glacier Bay National Park	Kodiak	Dutch Harbor
Latitude	66.906	64.506	58.457	57.719	53.845
Longitude	-151.683	-165.396	-135.867	-152.562	-166.505
Elevation (m)	630	15	2	7	58
Start Measurements	11/11/2008	9/25/2013	3/16/2010	9/18/2007	9/26/2009
Stop Measurements	10/27/2015	9/29/2015	5/21/2013	9/29/2015	9/30/2015
# of Weeks	362	103	165	418	312
# of Hg Concentrations (QR A and B)	216	67	137	321	145
# of Hg Depositions (QR A and B)	267	85	144	351	152
Data Coverage (Deposition)	74%	83%	87%	84%	49%

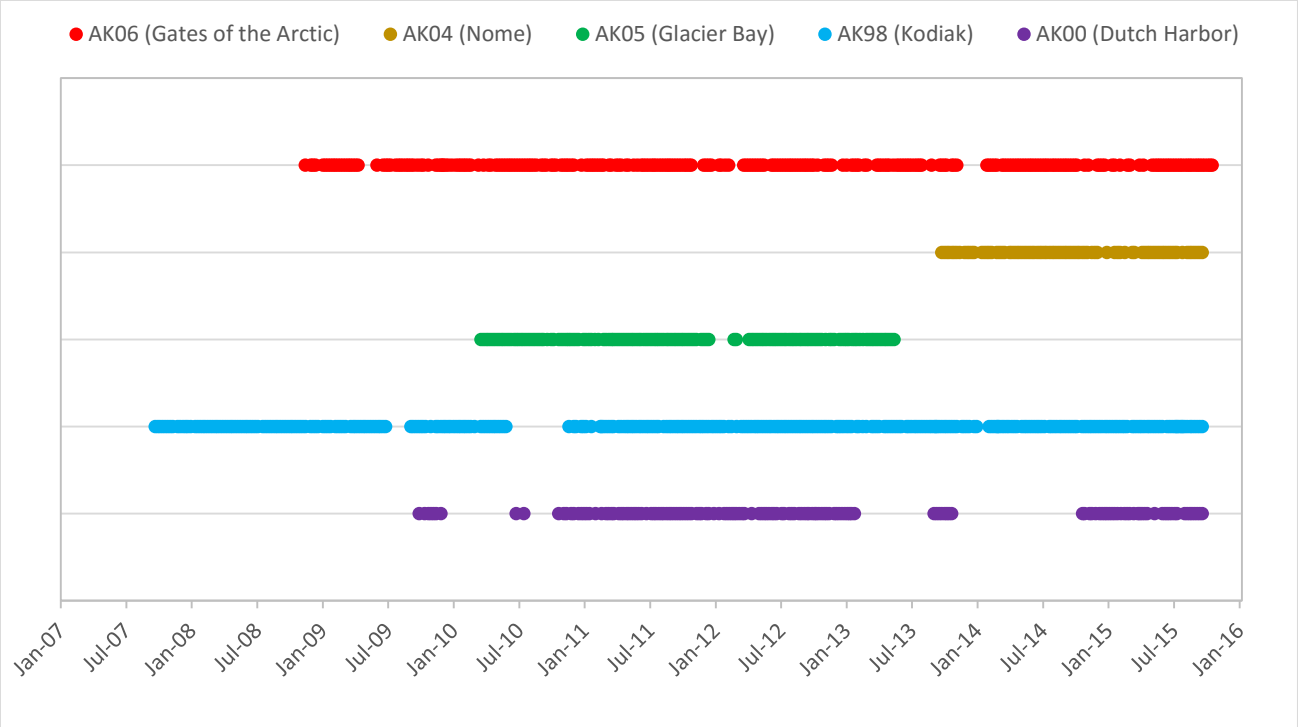

Figure 2. Time series of available MDN measurements based on deposition data. Gaps in the record correspond to interruptions (>1 week) in sample collection.

4.2. Summary statistics of weekly concentrations and differences in concentrations among sites

Using all available data, we generated box-and-whisker plots of measured weekly Hg wet deposition concentrations of all five stations which are shown in **Figure 3**.

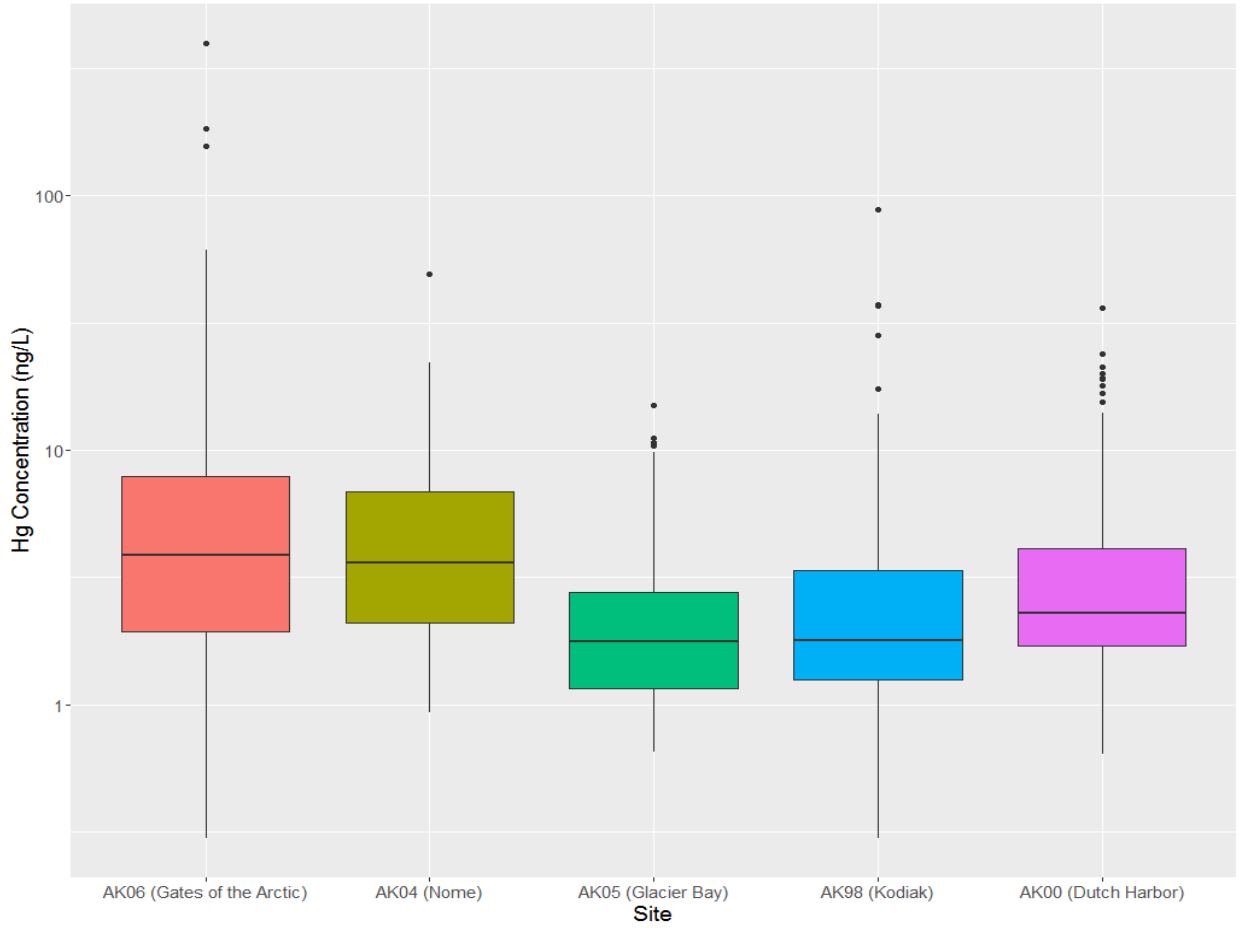

Figure 3. Box-and-whisker plots of Hg concentrations in wet deposition of five Alaskan deposition stations of all data, including outliers (marked as dots above and below whiskers). Lines of box plots show first, second, and third quartiles, and whiskers indicate 1.5 interquartile ranges.

Median Hg concentrations (**Table 5**) were in the following order, from highest to lowest: Gates of the Artic (3.6 ng L^{-1}) > Nome (3.6 ng L^{-1}) > Dutch Harbor (2.3 ng L^{-1}) > Kodiak Island and Glacier Bay (both 1.8 ng L^{-1}). The distribution of mean values followed the same order, although mean values were higher compared to median values due to skewed distributions in concentrations. To address the skewness and non-normal distribution of data, we log_{10}-transformed all data for statistical analyses. Minimum Hg concentrations among stations were 0.3 ng L^{-1}. Maximum concentrations strongly varied among stations, with by far the highest concentrations reported for Gates of the Arctic with concentrations of up to 396 ng L^{-1}. Such high values were unreasonably high compared to the majority of data from this and other datasets. These high Hg concentrations can be statistically characterized as outlier values based on the interquartile range (IQR) rule to determine outliers (i.e., 1.5 x IQR above the third quartile or below the first quartile). In the section below, we discuss reasons for unusually high Hg concentrations that likely led to these outlier values and provide justification for removal of these values from further statistical and graphical analyses.

Table 5. Summary statistics of Hg concentrations observed at the five deposition stations, and ANOVA analysis and post-hoc comparisons to test for statistical differences in Hg concentrations among different stations. ANOVA analyses were performed after removal of outliers (concentrations > 26.14 ng L^{-1}).

Station ID			AK06	AK04	AK05	AK98	AK00
Station Name			Gates of the Arctic National Park	Nome	Glacier Bay National Park	Kodiak	Dutch Harbor
Hg concentrations (ng L^{-1})							
# Outliers Removed (>26.14 ng L^{-1})			11	1	0	4	1
Mean			5.3	5.5	2.6	2.7	4.0
Median			3.6	3.5	1.8	1.8	2.3
Standard Deviation			4.9	5.0	2.5	2.4	4.4
Minimum			0.3	0.9	0.7	0.3	0.6
Maximum			26.1	22.0	15.0	17.4	24.0
ANOVA	Df	SS	RSS	AIC	F-value	P-value	
Season	3	90.91	502.35	-440.70	62.46	<0.001	
Site	4	57.06	468.51	-503.25	29.40	<0.001	
Season:Site Interaction	12	8.60	420.04	-614.03	1.48	0.1268	
Post-Hoc Comparisons							
Season	Diff	Lower	Upper	P-value			
Spring-Fall	0.4722	0.3016	0.6429	<0.001			
Summer-Fall	0.9155	0.7492	1.0818	<0.001			
Winter-Fall	0.1919	0.0174	0.3664	0.0245			
Summer-Spring	0.4433	0.2725	0.6141	<0.001			
Winter-Spring	-0.2803	-0.4591	-0.1015	<0.001			
Winter-Summer	-0.7236	-0.8983	-0.5489	<0.001			
Site	Diff	Lower	Upper	P-value			
AK04-AK00	0.2498	-0.0333	0.5328	0.1129			
AK98-AK00	-0.3614	-0.5528	-0.1701	<0.001			
AK05-AK00	-0.4630	-0.6903	-0.2358	<0.001			
AK06-AK00	0.1261	-0.0812	0.3333	0.4577			
AK98-AK04	-0.6112	-0.8689	-0.3536	<0.001			
AK05-AK04	-0.7128	-0.9981	-0.4275	<0.001			
AK06-AK04	-0.1237	-0.3934	0.1459	0.7193			
AK05-AK98	-0.1016	-0.2963	0.0931	0.6106			
AK06-AK98	0.4875	0.3166	0.6584	<0.001			
AK06-AK05	0.5891	0.3788	0.7994	<0.001			

4.3. Sampling artifacts observed under low precipitation events

We consider very high Hg concentrations suspect since wet deposition concentrations in remote, northern areas are generally in the range of 5 to 10 ng L^{-1} (Sanei et al., 2010). We consider that at low amounts of precipitation, collection of wet deposition can lead to significant quality control issues. We only used quality-tested MDN data with quality ratings A ("fully qualified with no problems") and B ("valid data with minor problems, used for summary statistics"). Quality rating data C, which are considered "invalid data not used for summary statistics", are not considered in any of our analyses. Still, we found problems with data quality of wet deposition at low precipitation amounts even when using only quality rating data A and B. In **Figure 4**, we show correlations between wet deposition concentrations and respective precipitation amounts for precipitation amounts below 50 mm. While we expect to find relationships between Hg concentrations and weekly precipitation, we found very high Hg concentrations only at very low precipitation. Further, these cases occurred primarily at the two northernmost stations Nome (66.9° N) and Gates of the Arctic (64.5°N). For example, all 990 deposition samples of the complete dataset showed a mean precipitation of 33 mm during collection: yet, the six observations with Hg concentrations above 50 ng L^{-1} (0.7% of all data) showed extremely low amounts of precipitation (mean: 2.1 mm, maximum: 4.3 mm) and five of these observations stem from Gates of the Arctic. Similarly, the 23 values with Hg concentrations exceeding 20 ng L^{-1} show an average precipitation of 3.6 mm, a maximum precipitation of 14.5 mm, and 14 of the 23 observations originate from Gates of the Arctic. We propose that reported MDN data, particularly data from Gates of the Arctic, can be unreliable at low precipitation amounts, likely due to blank issues with sampling trains and bottles, or due to handling issues during sample collection. Both of these factors would result in unreasonably high Hg concentrations as observed during very low precipitation amounts.

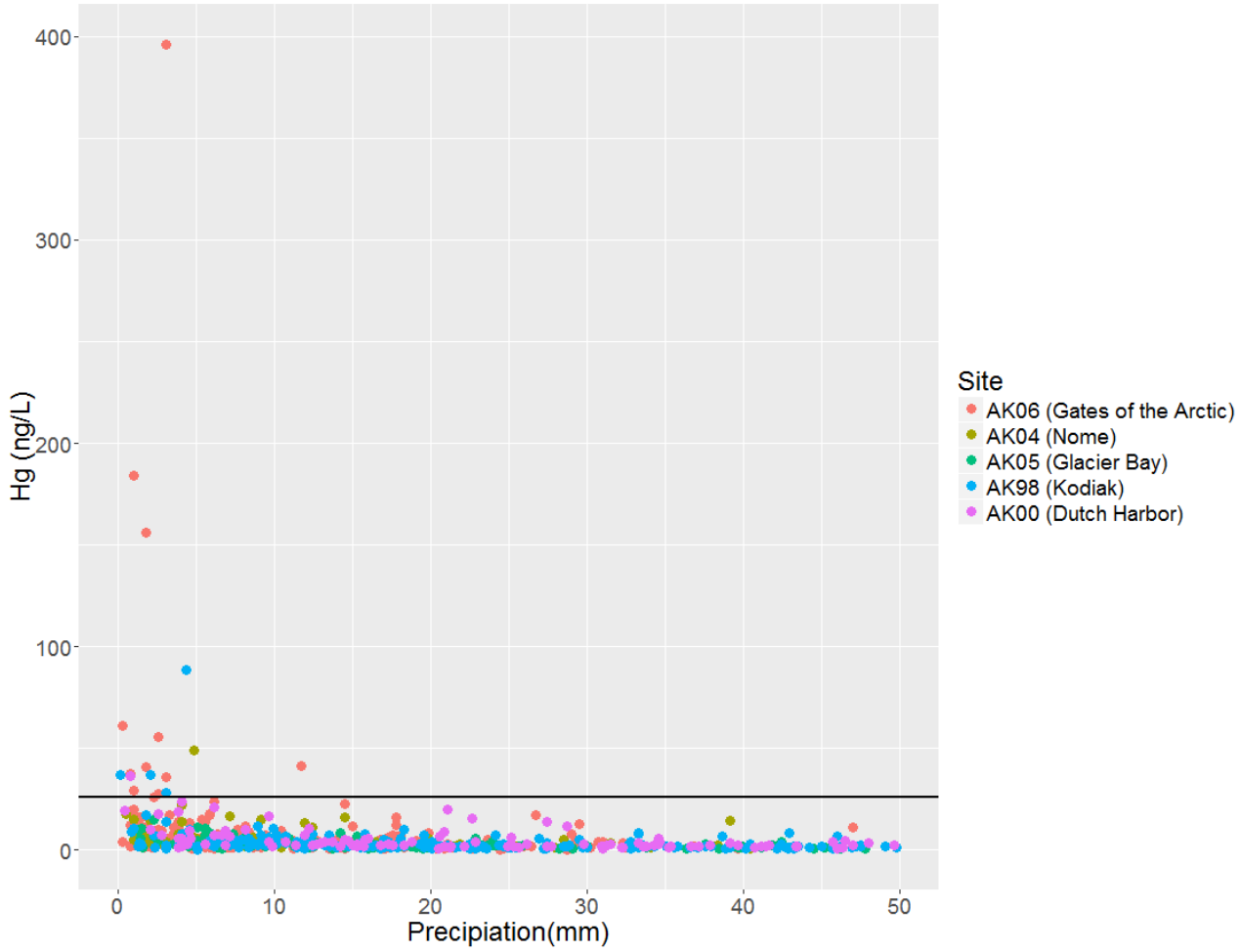

Figure 4. Scatterplot of Hg wet deposition concentrations (y-axis) and deposition amounts for weekly precipitation values <50 mm. The graph shows that very high values (e.g., above outlier concentrations of 26.14 ng L^{-1}; black line) occur predominantly at low precipitation amounts, suggesting sampling artifacts.

For summary statistics, seasonal analyses, and statistical comparison of data, we eliminated outlier concentrations (>26.14 ng L^{-1}), a value we determined by IQR outlier analysis. This resulted in removal of 1.9% of all data (17 values in total). For consistency, we selected a common outlier concentration across all stations, rather than delineate an outlier concentration for each station separately. For calculation of deposition maps (i.e., sum of deposition, seasonal and annual deposition loads, we did not remove values associated with outlier Hg concentrations because we decided to use the officially released and controlled annual MDN deposition data following official MDN protocols. However, because outliers were always associated with very low precipitation amounts, removal of outlier Hg concentrations would have very small impacts on annual deposition loads.

4.4. Site differences in Hg concentrations and wash-out effect by precipitation amounts

The highest Hg concentrations of weekly deposition samples were observed at the two northernmost sites Gates of the Arctic and Nome, with median values at these stations almost

double compared to concentrations of the lower latitude stations. Of the three stations at lower latitudes, concentrations were highest at the westernmost station in Dutch Harbor, with a median concentration 28% higher than the two coastal stations located further east on Kodiak Island and in Glacier Bay. In fact, observed concentrations at Dutch Harbor were not statistically different compared to the two northern stations, but were significantly higher compared to Kodiak Island and Glacier Bay. Therefore, based on statistical analyses (**Table 5**), two groups of stations were separated based on differences: the three stations with highest concentrations (Gates of the Arctic, Nome, and Dutch Harbor) and the two stations with the lowest concentrations (Kodiak Island and Glacier Bay). The Hg concentrations of the three stations in the high group were not significantly different from each other, but they were statistically higher than the two stations in the lower concentration group. The Hg concentrations of the two stations in the lower group were not statistically different from each other.

One possible reason for higher Hg concentrations observed at the two northern sites may be due to a wash-out effect of Hg concentrations by different storm sizes (Poissant and Pilote, 1998). It is well known that increased precipitation, e.g., due bigger storms and increasing duration of storms, lead to lower concentrations of airborne contaminants compared to smaller storms, due to initially higher scavenging of airborne (particulate-phase and gaseous) contaminants that are washed out (wash-out effect: Ferrara et al., 1986; Poissant and Pilote, 1998). To examine this possibility, we performed a detailed analysis of the precipitation amounts at each site.

Figure 5 and **Table 6** show box-and-whisker plots and summary statistics of weekly precipitation amounts of the five stations, along with statistical differences between stations. Weekly precipitation amounts were much lower at Gates of the Arctic and Nome, and these stations showed median weekly precipitation amounts three to five times lower compared to the three lower latitude sites. The differences were statistically significant between the northern and lower-latitude sites, but no statistical differences were observed among the two northern or among the three lower-latitude sites (based on post-hoc comparison tests, not shown).

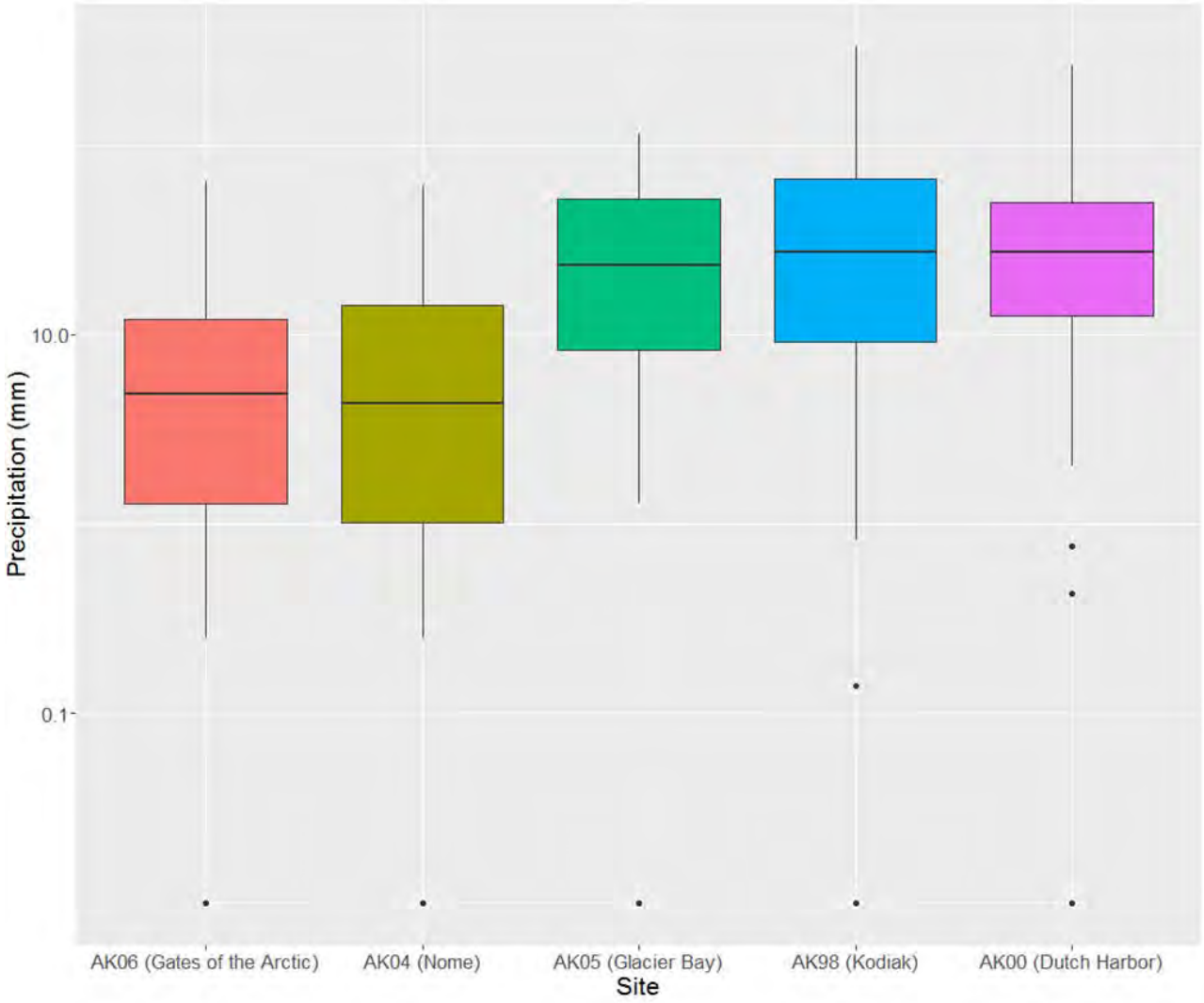

Figure 5. Boxplot of weekly precipitation totals for all sample collection weeks at each of the five MDN monitoring stations in Alaska.

Table 6. Precipitation summary statistics for all observation weeks for each of the five MDN monitoring stations in Alaska.

Station ID	AK06	AK04	AK05	AK98	AK00
Station Name	Gates of the Arctic National Park	Nome	Glacier Bay National Park	Kodiak	Dutch Harbor
Precipitation (mm)					
n	2349	733	956	2207	1076
Mean	1.03	1.24	4.99	6.26	5.19
Median	0	0	1.27	0.25	1.52
Standard /Deviation	2.94	3.22	8.28	14.04	9.33
Minimum	0	0	0	0	0
Maximum	78.99	38.35	63.25	263.91	94.23
# of zeros	1530	468	365	1029	335
Percentage Zeros	65.1	63.8	38.2	46.6	31.1

*A,B, and C QR Data Included

To delve deeper into the possibility of a "washout" effect, we analyzed the impact of storm size on Hg concentrations across the five stations by regression analyses. **Figure 6** shows the linear regressions between the Hg concentration and total weekly precipitation amount for each station, as well as for the entire dataset combined (black line) and **Figure 7** provides the statistics of all linear regressions. At each station, we observed strong and statistically significant negative correlations between Hg concentrations and precipitation amounts. The slopes of the linear regressions, using $\log_{10}$-transformed Hg concentrations (in ng L^{-1}) and $\log_{10}$-transformed precipitation (in mm), varied between -0.28 and -0.46. Yet, in spite of the range of slopes, ANCOVA analyses used to test for differences between slopes among stations showed that that slopes were not statistically different between the five sites. Hence, a common relationship between wet deposition concentrations and precipitation was best described by the following common inverse linear regression:

(1) $$log_{10}Hg_{conc.}[ng\ L^{-1}] = 0.844 - 0.347 \times log_{10}Precip[mm]$$

These observations were well aligned with observations that Hg wet deposition concentrations were often related to precipitation amounts. These "washout" effects occurred during storm events when Hg concentrations were highest at the beginning of an event and then decreased over time (Ferrara et al., 1986; Glass and Sorensen, 1999). The effect was attributed to scavenging of HgP and GOM (Poissant and Pilote, 1998; Schroeder and Munthe, 1998). In a study in the western United States, we previously saw similar linear correlations of $\log_{10}$-transformed Hg concentrations and precipitation (Faïn et al., 2011), an effect which has been observed by others as well in many areas of the U.S. (Lamborg et al., 1995; Landis et al., 2002; Lyman and Gustin, 2008; Mason et al., 1997).

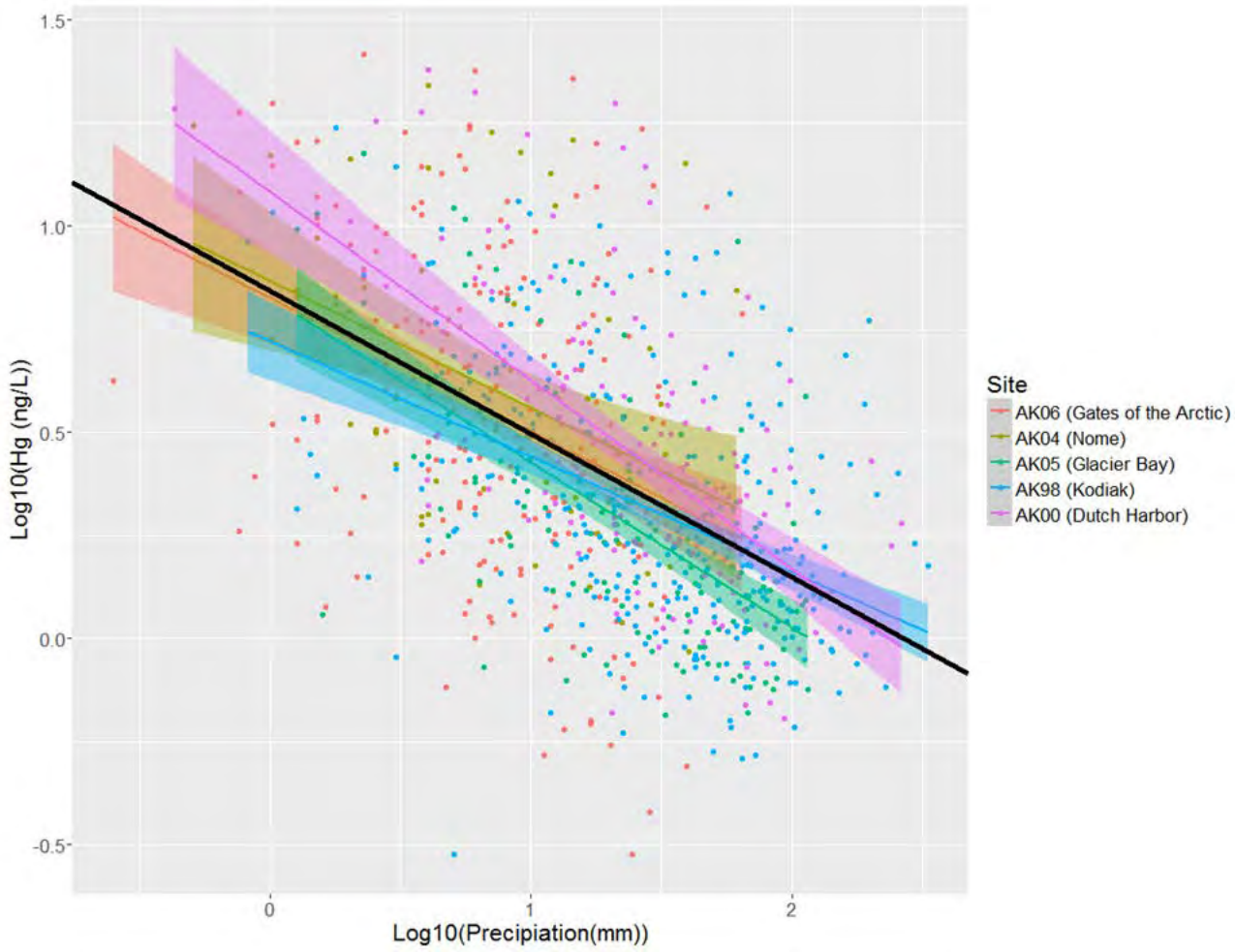

Figure 6. Scatterplots of observed Hg concentrations and precipitation amounts, separated by station. The black line shows the overall regression using all sites/all data.

Table 7. Linear regression analysis between Hg concentrations (log-transformed) and respective Hg concentrations. All linear regressions are statistically significant. ANCOVA results show that slopes are not statistically different between the five sites (P = 0.058), but that intercepts of the regression lines differ significantly between the five sites (P<0.01).

Station ID	AK06	AK04	AK05	AK98	AK00	
Station Name	Gates of the Arctic National Park	Nome	Glacier Bay National Park	Kodiak	Dutch Harbor	All Sites
Log10(Prcp(mm)) vs Log10(Hg(ng L^{-1}))						
Intercept	0.8266	0.8674	0.8268	0.7213	1.0832	0.8439
Slope	-0.3145	-0.3078	-0.3999	-0.2801	-0.4567	-0.3474
R^2	0.1134	0.1589	0.3802	0.2040	0.3508	0.2750
P-value	<0.001	<0.001	<0.001	<0.001	<0.001	<0.01
*Outliers (>26.14 ng L^{-1}) Removed for Regression Analysis						

Log10(Hg(ng L^{-1}))~Log10(Precipitation(mm))*Site					
	Df	Sum Sq	Mean Sq	F value	Pr(>F)
Log10(Prcp)	1	31.03	31.03	345.55	<0.01
Site	4	2.54	0.63	7.06	<0.01
Log10(Prcp):Site	4	0.81	0.20	2.25	0.0622
Residuals	859	77.14	0.09		

Log10(Hg(ng L^{-1}))~Log10(Precipitation(mm))+Site					
	Df	Sum Sq	Mean Sq	F value	Pr(>F)
Log10(Prcp)	1	31.03	31.03	343.56	<0.01
Site	4	2.54	0.63	7.02	<0.01
Residuals	863	77.95	0.09		

The fact that weekly precipitation amounts differed among stations and the observed relationships of Hg concentrations to weekly precipitation, however, does not yet provide full evidence that storm sizes really differed between sites. Different weekly precipitation amounts could have been shaped both by different storm sizes or different storm frequencies. In **Figure 7** below, we re-analyzed the daily precipitation statistics of all five stations over the entire measurement period. The cumulative distribution functions, shown in **Figure 7**, in fact support the presence of much smaller precipitation sizes at Gate of the Arctic and Nome. For example, the mean size of daily precipitation events at the northern stations was a factor of 4 to 6 lower than daily precipitation sizes at the three lower-latitude stations. The lower magnitude of daily precipitation at the two northern sites also drove the cumulative distribution of daily precipitation at those two sites to be quite different than the other sites as shown in **Figure 7**. The higher fraction of low precipitation events is shown by separation of the AK06 and AK04 lines from the other sites occurring below 1 mm. This separation indicated that a much larger fraction of precipitation occurred as small (< 1 mm) storms at the northern two stations. The three coastal, lower latitude sites, on the other hand experienced much higher fractions of daily storms above 2 mm with relatively similar cumulative frequencies.

The cumulative effect of larger precipitation events at the lower latitude sites, when coupled with the observed relationships between Hg concentration and weekly precipitation amounts, clearly indicates that washout is impacting Hg concentrations measured at the lower latitude sites, with lower concentrations as the typical precipitation event size increases. We therefore propose that washout and subsequent dilution effects driven by different precipitation patterns explain a large degree of the differences in Hg concentrations between sites, in particular between the dry northern sites and lower-latitude sites.

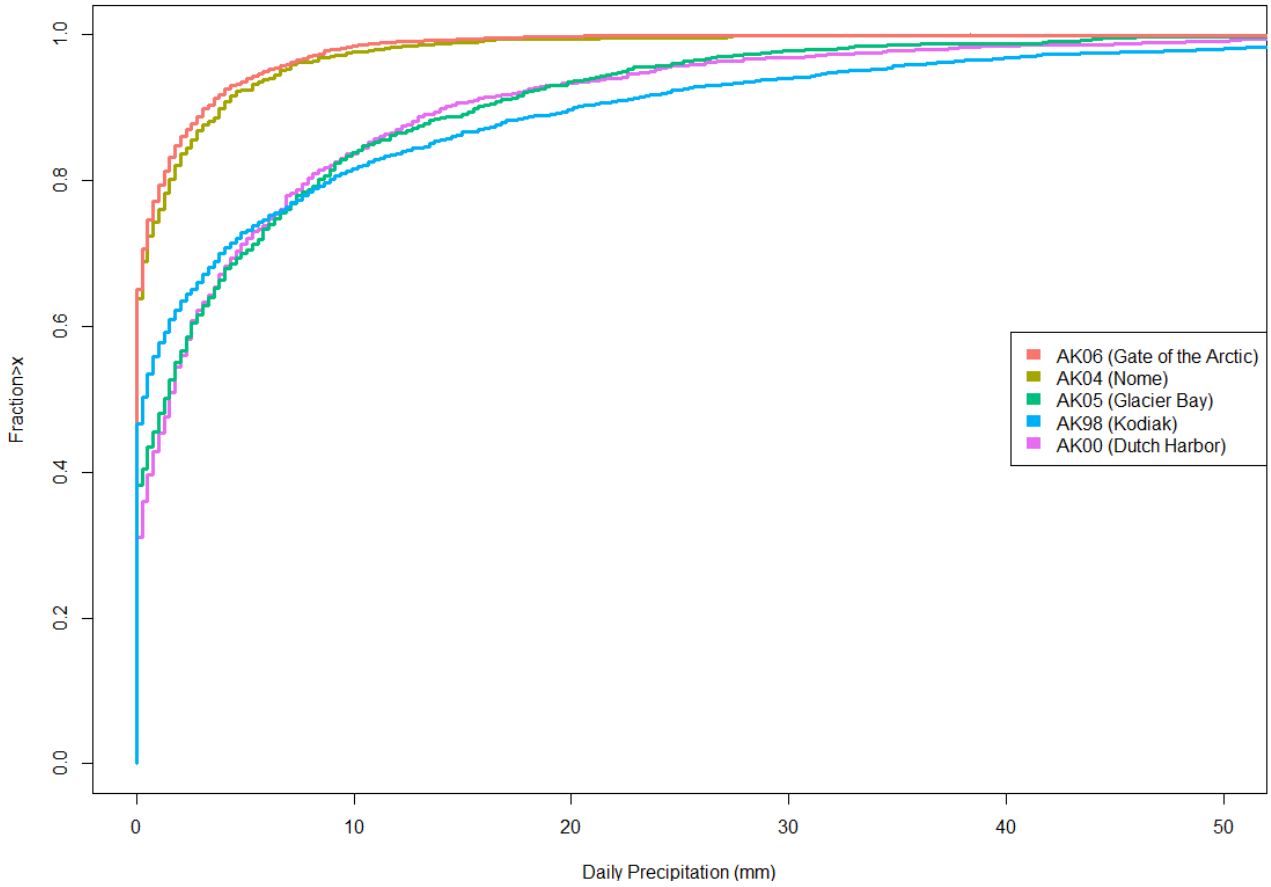

Figure 7. Empirical cumulative distribution plot of daily precipitation at five monitoring stations in Alaska (plot has been cropped at 50 mm). Distinct differences in storm size are observed between the northern (red and gold lines) and southern stations (green, blue, and purple lines).

Our dilution observation further led us to attempt to quantify the contribution of washout on Hg concentrations using calculated linear correlations between the two variables, effectively standardizing Hg concentrations by subtracting the linear regression trend. A "precipitation-corrected" Hg concentration (Hg_{corr}) was calculated using the following equation, with the intercept and slope of the linear regression as given below:

$$\log_{10}(Hg_{corr}[ng\ L^{-1}]) = \log_{10}(Hg[ng\ L^{-1}]) - \frac{1}{2}intercept + slope \times log_{10}(precipitation[mm]) \quad (2)$$

The differences in concentrations were significantly reduced and in parts even completely disappeared from the original Hg concentration differences as shown **Figure 8** showing the precipitation-corrected Hg concentrations, (Hg_{corr}; i.e., Hg concentrations minus linear trend). For example, when the precipitation size correction was applied to the median Hg concentrations, the difference between the highest concentration station (Gates of the Arctic: 3.9 ng L^{-1}) and lowest concentration station (Glacier Bay: 1.8 ng L^{-1}) dropped from 110% difference to only 20% difference (median values of Hg_{corr} at Gates of the Arctic: 2.7 ng L^{-1} versus Glacier Point: 2.2. ng L^{-1}). Some differences in Hg concentrations between stations even completely disappeared when the correction was applied. For example, a difference in median Hg concentration at Nome (3.6 ng L^{-1}) that exceeded that at Kodiak Island (1.8 ng L^{-1}) by 101% disappeared almost completely after correcting for different precipitation amounts (median values for Hg_{corr} of 2.6 and 2.7 ng L^{-1}, respectively).

ANOVA analyses and summary statistics (**Table 8**) show that even for Hg_{corr}, however, there remained significant statistical differences among sites ($P<0.01$), indicating that precipitation patterns alone did not explain all observed differences among stations. Using a post-hoc Bonferroni comparison after the ANOVA, we determined that differences remained statistically significant between stations: Gates of the Arctic, followed by Nome, showed the highest Hg_{corr} concentrations, which for Gates of the Arctic was significantly enhanced compared to all other stations, but Nome. The lowest Hg_{corr} was observed for Kodiak Island, which showed statistically lower concentrations compared to all other stations. The concentration ranking of the lower latitude stations changed, however, so that Dutch Harbor no longer showed statistically higher concentrations compared to Glacier Bay.

The statistical differences in Hg_{corr} indicated that differences in Hg concentrations between stations persisted even after Hg concentrations were corrected for precipitation amounts. *Based on these results, our first conclusion is that the two northern stations, Nome and Gates of the Arctic, had statistically enhanced Hg concentrations in weekly deposition samples, compared to those at Kodiak Island and Glacier Bay, largely due to higher precipitation amounts and increased washout effects (due to large storm sizes) at the lower latitude sites. However, differences among sites still existed after precipitation differences were removed, indicating that in addition to precipitation other factors are influencing Hg wet deposition across Alaska.*

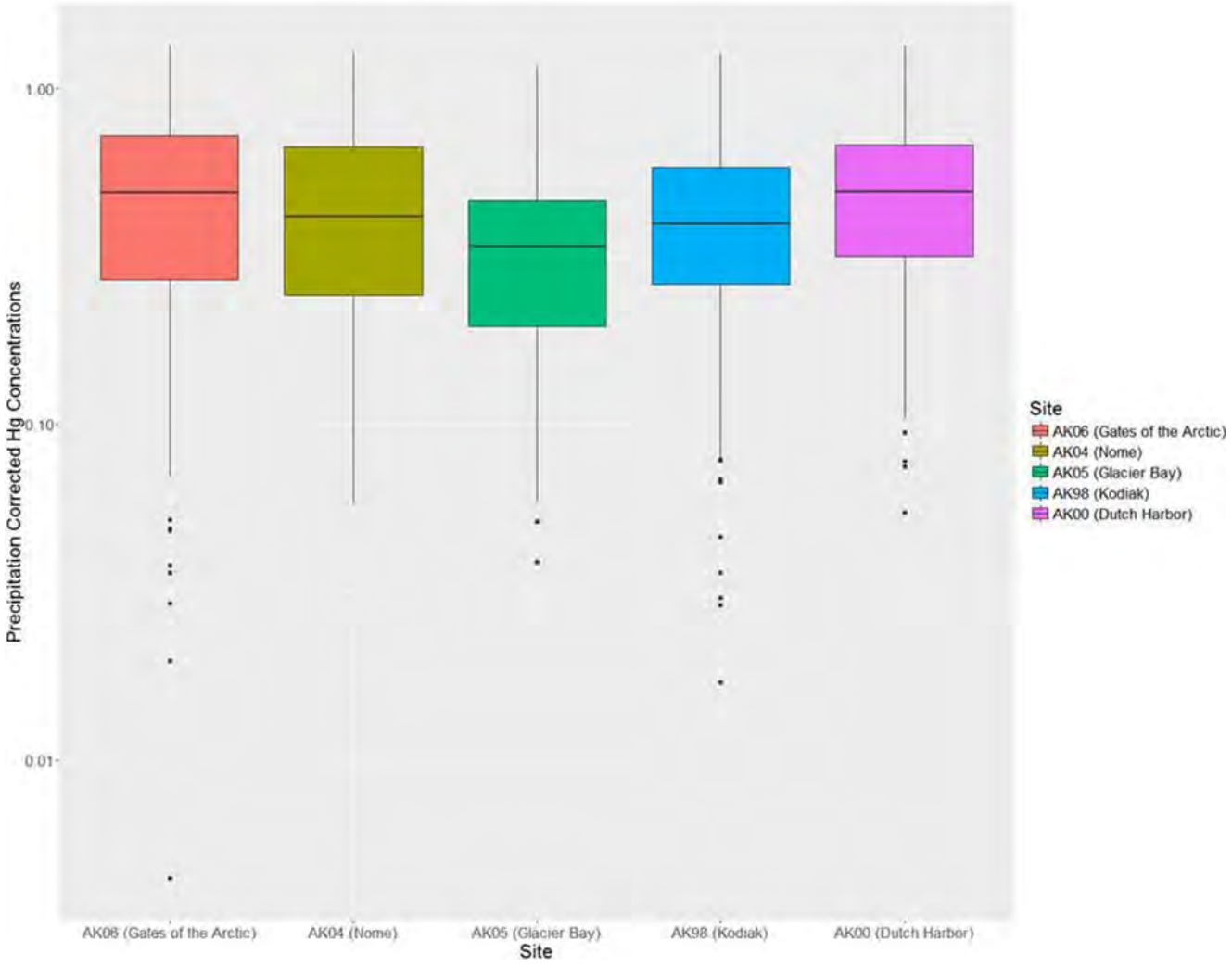

Figure 8. Summary boxplot of precipitation corrected Hg concentrations for each monitoring station. Hg_{corr} was calculated by subtracting the linear regression trend between Hg concentrations and weekly precipitation amounts. Note that the absolute Hg_{corr} values are not meaningful (concentrations are adjusted to an average precipitation amount) and only the comparisons among sites are relevant.

Table 8. ANOVA and post-hoc comparison results for precipitation corrected Hg concentrations.

Log10(Hg_Corrected))~Season*Site						
	Df	SS	RSS	AIC	F-value	P-value
Season	3	11.0284	72.651	-2122.6	50.6476	<0.001
Site	4	3.4207	65.043	-2220.7	11.7821	<0.001
Season:Site Interaction	12	2.4138	64.036	-2250.3	2.7713	0.001
Post-Hoc Comparisons						
Season	Diff	Lower	Upper	P-value		
Spring-Fall	0.1504	0.0845	0.2163	<0.001		
Summer-Fall	0.3249	0.2606	0.3893	<0.001		
Winter-Fall	0.0875	0.0200	0.1550	0.005		
Summer-Spring	0.1746	0.1086	0.2405	<0.001		
Winter-Spring	-0.0628	-0.1319	0.0063	0.090		
Winter-Summer	-0.2374	-0.3050	-0.1698	<0.001		
Site	Diff	Lower	Upper	P-value		
AK04-AK00	0.0648	-0.0395	0.1690	0.435		
AK98-AK00	-0.0818	-0.1630	-0.0005	0.048		
AK05-AK00	0.0016	-0.0644	0.0676	1.000		
AK06-AK00	0.1274	0.0473	0.2075	<0.001		
AK98-AK04	-0.1465	-0.2569	-0.0362	0.003		
AK05-AK04	-0.0632	-0.1629	0.0364	0.414		
AK06-AK04	0.0626	-0.0468	0.1721	0.521		
AK05-AK98	0.0833	0.0080	0.1586	0.022		
AK06-AK98	0.2092	0.1213	0.2971	<0.001		
AK06-AK05	0.1258	0.0518	0.1999	<0.001		

4.5 Seasonal patterns of Hg concentrations

We also explored how Hg concentrations in wet deposition changed among seasons. An ANOVA analysis (**Table 8**) of all Hg deposition concentrations at the five sites showed that significant seasonal differences existed (variable "season": $P<0.01$), and post-hoc seasonal comparisons showed that Hg concentrations differed among all individual seasons. The ANOVA analysis also showed that seasonal patterns were very consistent among the five stations (i.e. no significant interactions of "Season" x "Station"). The patterns are well reflected in **Figure 9** below that shows all stations with very pronounced and similar seasonal patterns. Across all stations, the highest Hg concentrations occurred in the summer, followed by spring, winter, and lowest in fall. These patterns were surprisingly consistent among the five stations, with median concentrations at each

station following the same order. The only exception to this was Dutch Harbor where fall concentrations were slightly above those in winter (2.0 versus 1.9 ng L^{-1}).

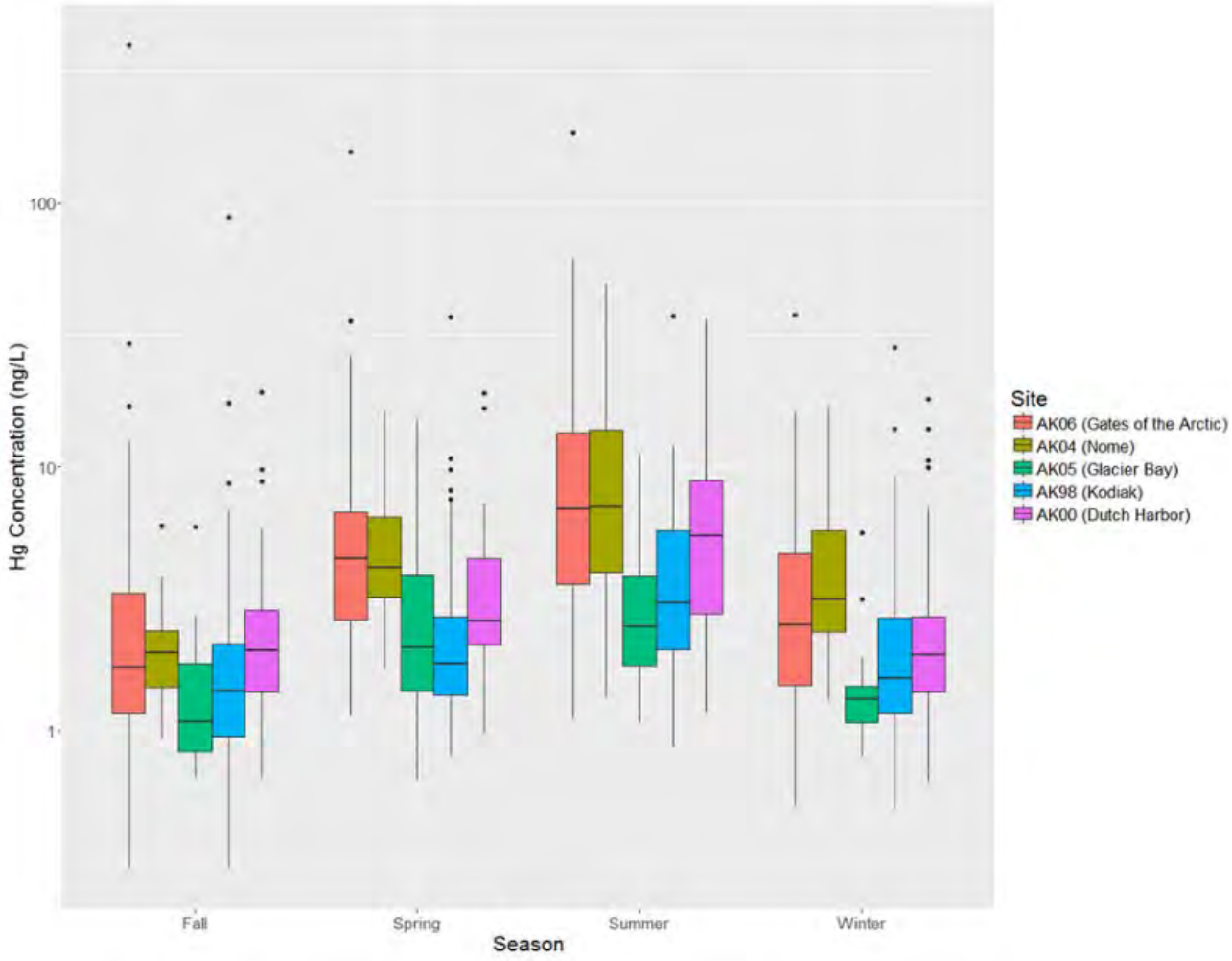

Figure 9. Summary boxplot of Hg concentrations separated by monitoring station and collection season. Similar seasonal trends are observed at each site with the highest concentrations occurring in summer and lowest concentrations in fall.

The patterns suggest enhanced summertime Hg concentrations, an effect that could be related to increased photochemical formation of oxidized mercury in summer that may have led to increased atmospheric scavenging and higher Hg concentrations in precipitation. Yet, similar to the differences in Hg concentrations among stations discussed above, seasonal patterns also could have been compounded by different weekly precipitation amounts. Indeed, seasonal precipitation was generally lowest in summer, highest in fall and winter, suggesting different wash-out effects as discussed above (**Figure 10**).

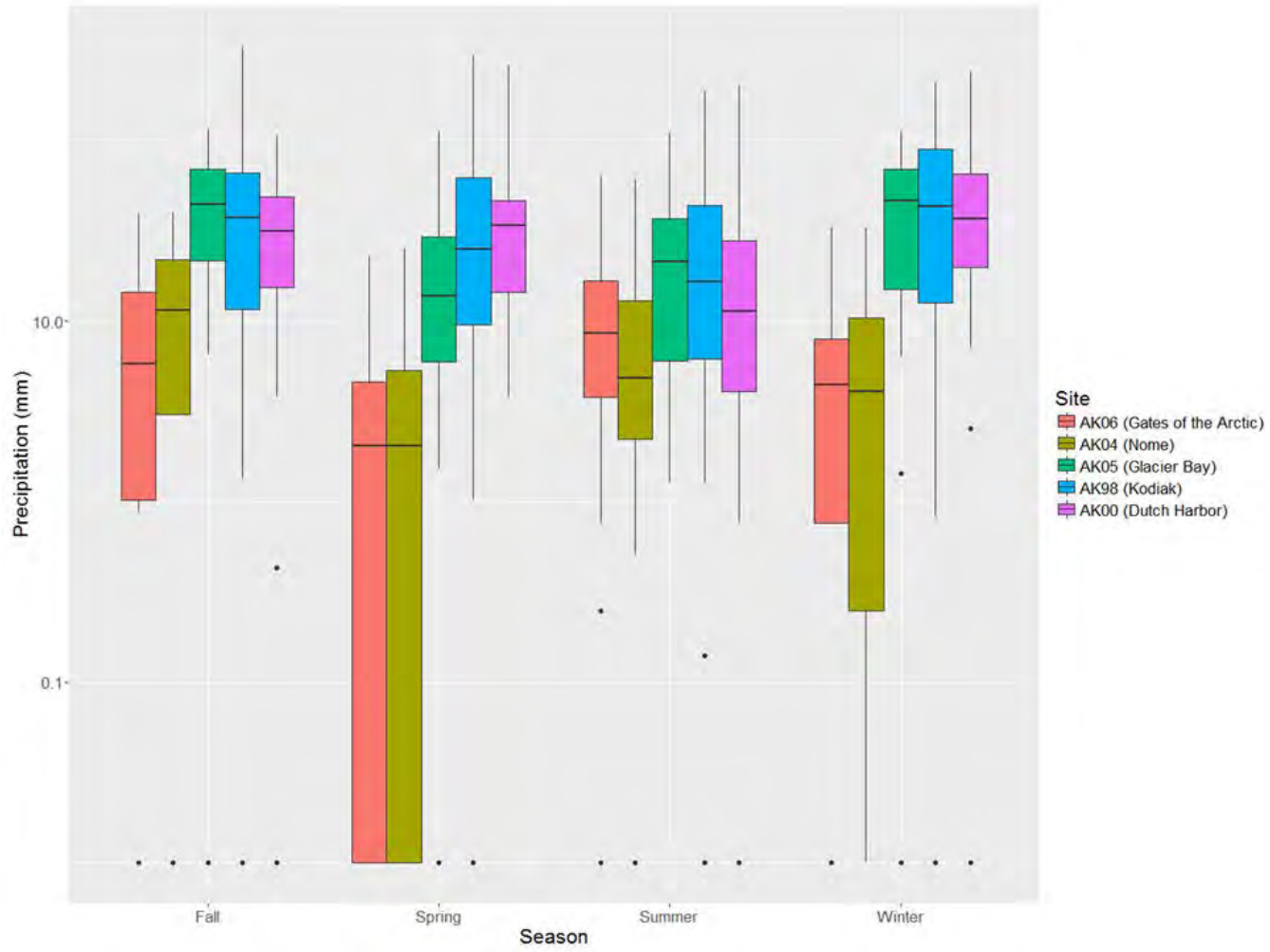

Figure 10. Box and whisker plot of weekly precipitation totals grouped by site and season.

To explore the impacts of precipitation on the seasonal differences, we conducted a detailed analysis of the correlations of Hg concentrations and precipitation amounts for each season. These correlations show statistically significant effects of precipitation on Hg concentrations in all seasons, and an ANCOVA analysis shows that the dilution effects also was similar among all seasons (**Table 9**; no significant interaction term of "Season" x "Precipitation"). Yet, it also was evident that the regression lines were shifted between different seasons (**Figure 11**), in particular with higher Hg concentrations across the entire precipitation spectrum in summer and with lower concentrations in fall compared to winter and winter. These patterns suggested that even when adjusted for the different precipitation regimes, summer concentrations of Hg in wet deposition were higher compared to those in winter.

We further tested if seasonal differences persisted when correcting for different precipitation amounts by calculating precipitation-adjusted Hg_{corr} concentrations (analogue to section 4.4). ANOVA analysis and post-hoc Bonferroni comparisons showed that some differences among seasons persisted and that the order of Hg_{corr} concentrations followed the same order as the

uncorrected Hg concentrations (summer > fall> spring/winter). Using the corrected data, only the statistical difference between spring and winter concentration persisted.

Our second conclusion therefore is that Hg concentrations were different among seasons, with consistently highest concentrations in summer and lowest concentrations in fall. Part of these differences could be explained by having the lowest precipitation amount in summer, but much of the difference remained after removing the precipitation effect.

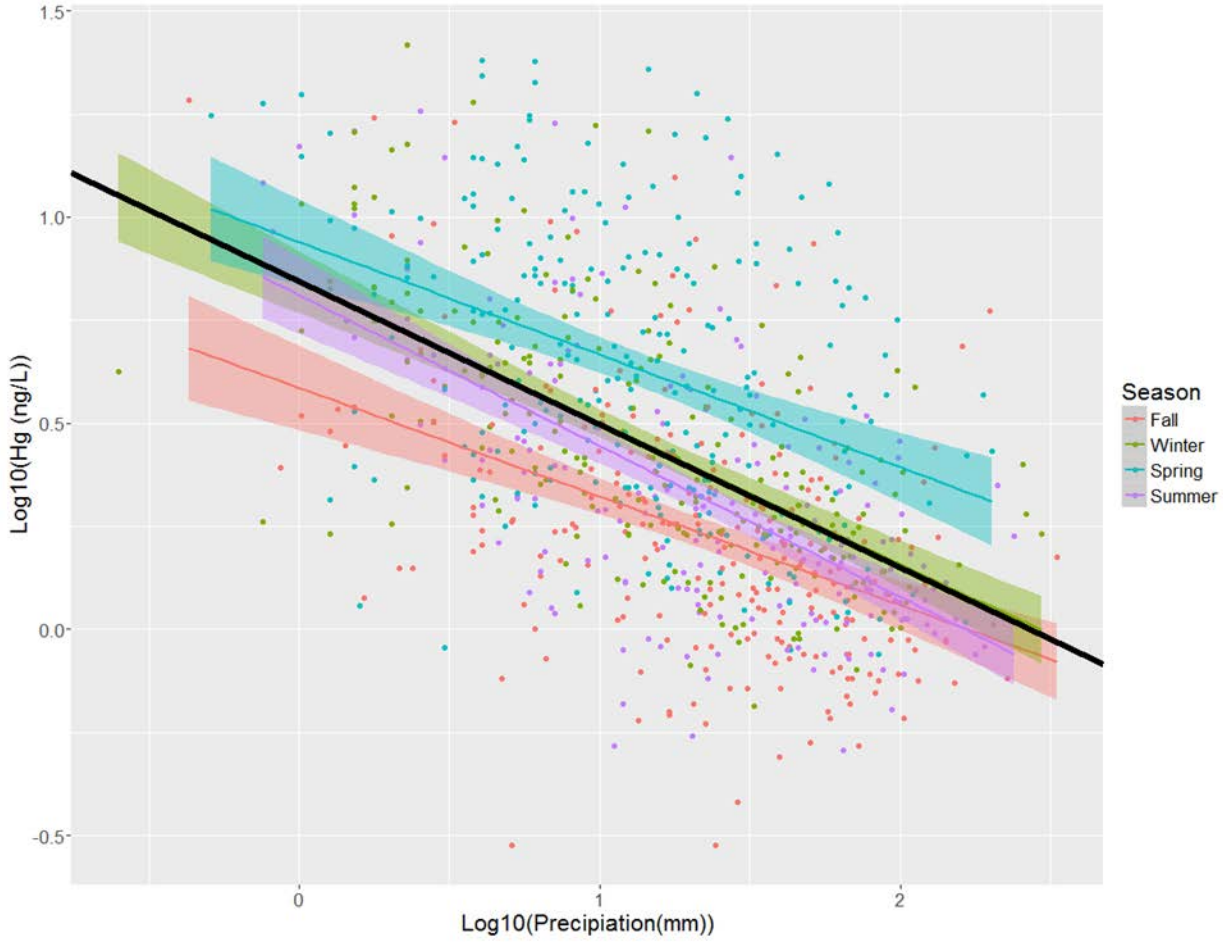

Figure 11. Linear regression analysis between Precipitation and respective Hg concentrations separated by season (both log10-transformed). The black line shows the regression for all seasons. All linear regressions are statistically significant.

Table 9. ANCOVA results showing that slopes are not statistically different between the four season (P = 0.131), but that intercepts of the regression lines differ significantly between the four season (P<0.01).

Log10(Hg(ng L^{-1}))~Log10(Precipitation(mm))*Season					
	Df	Sum Sq	Mean Sq	F value	Pr(>F)
Log10(Prcp)	1	31.03	31.03	400.99	<0.01
Season	3	13.39	4.46	57.69	<0.01
Log10(Prcp):Season	3	0.46	0.16	2.00	0.112
Residuals	861	66.63	0.08		
Log10(Hg(ng L^{-1}))~Log10(Precipitation(mm))+Season					
	Df	Sum Sq	Mean Sq	F value	Pr(>F)
Log10(Prcp)	1	31.03	31.03	399.61	<0.01
Season	3	13.39	4.46	57.49	<0.01
Residuals	864	67.10	0.08		

4.6. Inter-annual patterns of Hg concentrations

Overall no statistical differences were observed by year for the five sites (**Figure 12** and **Table 10**). This was likely due to the high variability of the concentrations throughout the measurement period and the varying levels of data collection per year by site (See Section 5.1).

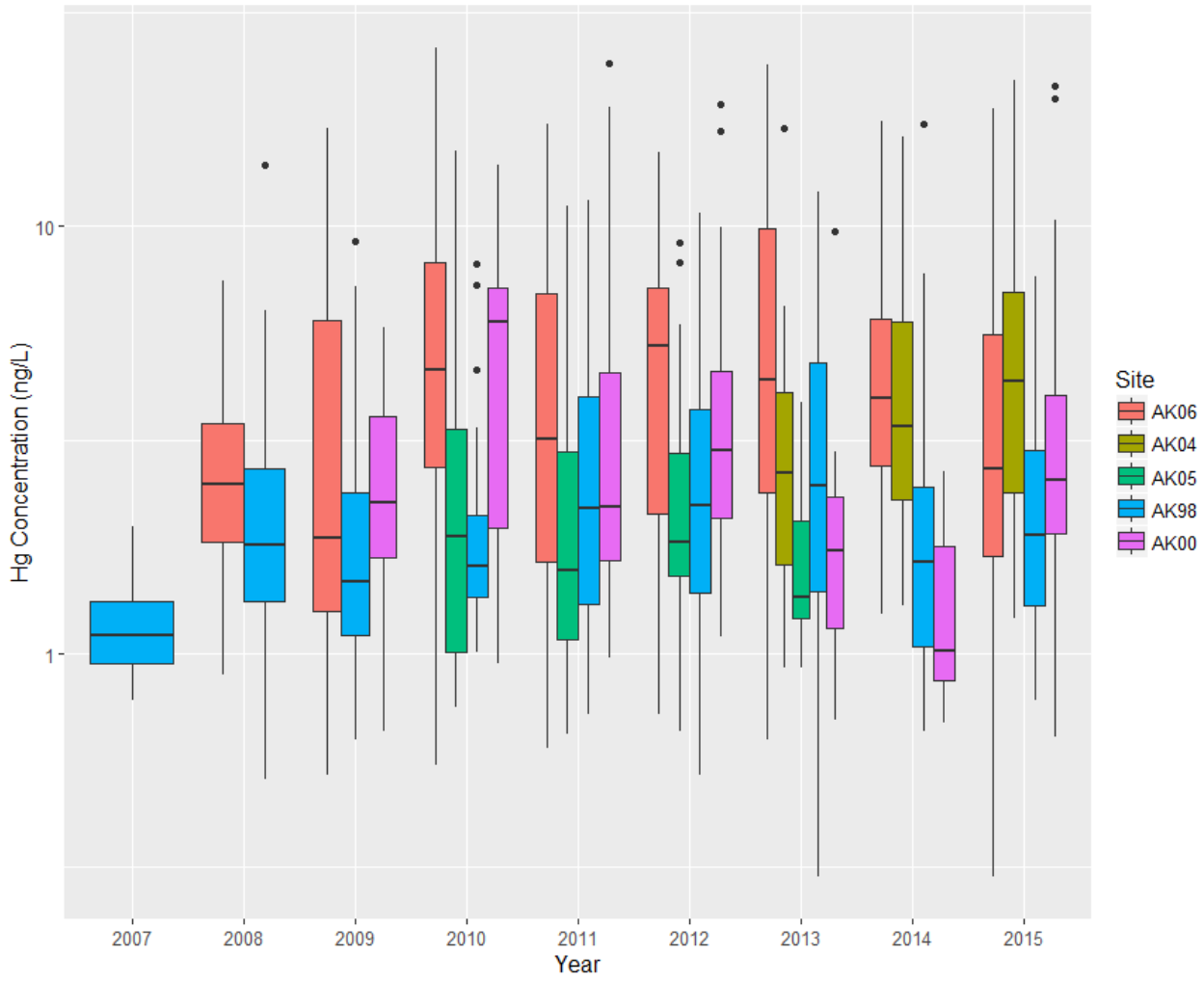

Figure 12. Summary boxplot separated by year and station (Outliers >26.14 ng L^{-1} removed).

Table 10. ANOVA results testing for significant effects of site and year on Hg concentrations (outliers >26.14 removed prior to analyses). Results show no significant effect for either year or site.

Log10(Hg(ng L^{-1}))~Site*Year						
	Df	SS	RSS	AIC	F-value	P-value
Site	4	4.1573	526.78	-422.99	1.7083	0.146
Year	1	0.5182	523.14	-423.01	0.8517	0.3563
Site:Year Interaction	4	4.1553	526.78	-422.99	1.7074	0.1462

5 Mercury deposition loads: site differences, inter-annual variability, and relationships to precipitation patterns

5.1. Annual Hg deposition load differences

Figure 13 shows annual Hg deposition loads measured for the five stations across multiple years. As discussed above, the temporal coverage of available data differs strongly between stations. In addition, according to MDN protocols, annual deposition values require a substantial data coverage based on stringent completeness criteria, including percentage of summary period for which valid samples exist (≥ 75%); percentage of summary period for which precipitation amounts are available, either from the rain gage or from the sample volume (≥ 90%); and percentage of total measured precipitation associated with valid samples (≥ 75%). For calculation of annual wet deposition loads, the protocol requires calculation of precipitation-weighted annual Hg concentration multiplied by annual precipitation records of the stations.

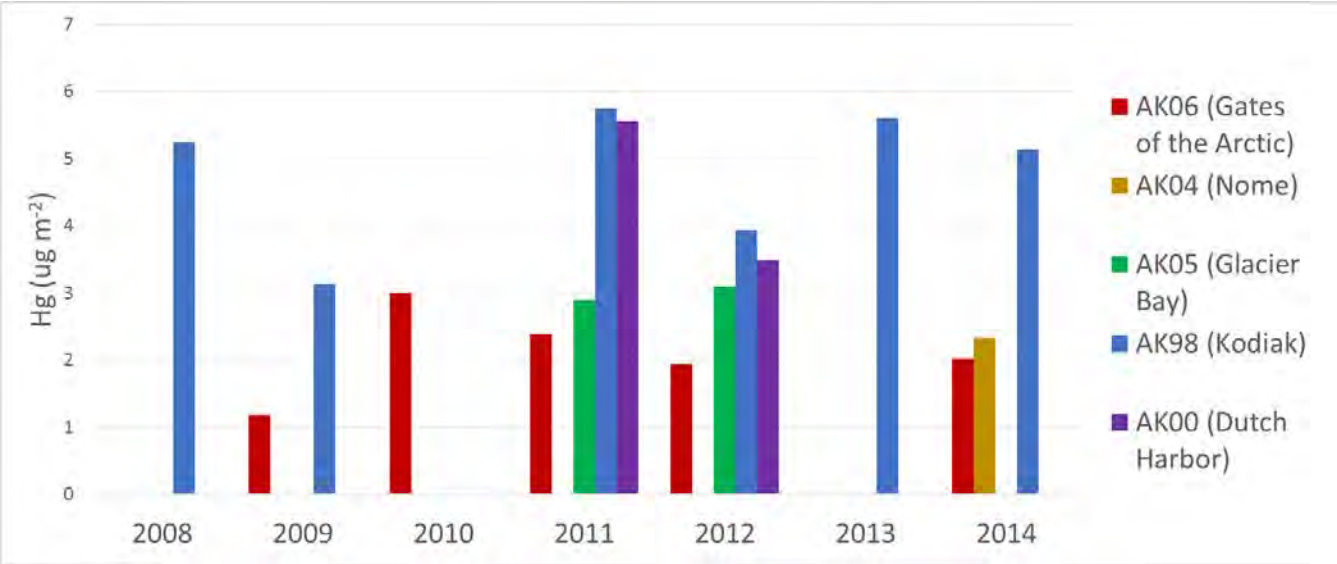

Figure 13. Summary plot of NADP MDN annual Hg deposition estimates for five monitoring sites in Alaska.

The strong differences in temporal coverage of annual Hg deposition complicated direct comparisons of annual deposition loads among station and assessment of inter-annual variability, but some useful pertinent conclusions still can be drawn. The 16 annual Hg deposition values from the five stations averaged 3.55±1.48 µg m^{-2}, with a minimum of 1.94 µg m^{-2} (Gates of the Arctic) in 2012 and a maximum of 5.74 µg m^{-2} at Kodiak Island in 2011. In fact, the highest Hg deposition loads were always observed at Kodiak Island when data were available, and lowest deposition loads were always observed at Gates of the Arctic when data were available. The differences were large: for example in the four years of corresponding deposition coverage at these two stations, Kodiak Island deposition exceeded that of Dutch Harbor by a factor of 2.6 (in 2009), 2.4 (in 2011), 2.0 (in 2012), and 2.6 (in 2014). Second highest deposition loads were consistently observed at Dutch Harbor, with loads that were only slightly below those in Kodiak Island in the two years of corresponding measurements.

Statistical tests showed that annual deposition was statistically different among stations, and a post-hoc Bonferroni comparison showed that this difference was driven largely by a statistical difference between the highest (Kodiak Island) and lowest (Gates of the Arctic) station (**Table 11**; $P<0.05$), although statistically significant differences also were evident between Dutch Harbor and Gates of the Arctic. In addition, if we used a statistical significance of 10% rather than 5%, we also found significant differences between Kodiak Island and Glacier Bay and Kodiak Island and Nome. Therefore, we can summarize annual deposition loads across these five stations as follows: the highest deposition at Kodiak Island (4.80±1.04 μg m^{-2}) was not statistically different from the second highest station Dutch Harbor (4.52±1.47 μg m^{-2}), but statistically different from all other stations. Substantially lower deposition was observed at Gates of the Arctic (2.11±0.67μg m^{-2}), and intermediate values were observed for Glacier Bay (3.00±0.14 μg m^{-2}) and Nome (2.34 μg m^{-2}).

Table 11. ANOVA results showing significant effects of site (i.e. location) on annual Hg deposition. No significant inter-annual differences were observed.

Annual Hg(ng m^{-2})~Site+Year

	Df	SS	RSS	AIC	F-value	P-value
Site	4	17.0294	19.1524	16.8775	10.0268	0.0132
Year	6	7.1782	9.3012	1.3208	2.8176	0.1378
Post-Hoc Comparisons						
Site	Diff	Lower	Upper	P-value		
AK04-AK00	-2.1795	-5.3809	1.0219	0.1790		
AK05-AK00	-1.5160	-4.1299	1.0979	0.2727		
AK06-AK00	-2.4091	-4.5961	-0.2221	0.0345		
AK98-AK00	0.2833	-1.8509	2.4176	0.9797		
AK05-AK04	0.6635	-2.5379	3.8649	0.9099		
AK06-AK04	-0.2296	-3.0930	2.6338	0.9969		
AK98-AK04	2.4628	-0.3606	5.2862	0.0818		
AK06-AK05	-0.8931	-3.0801	1.2939	0.5351		
AK98-AK05	1.7993	-0.3349	3.9336	0.0919		
AK98-AK06	2.6924	1.1096	4.2753	0.0055		

Using all data and stations, we did not observe significant effects of year of collection among stations ($P = 0.14$). Still, there seemed to be substantial inter-annual variability in observed deposition values at individual stations. For example, using the five years of measurements at Kodiak Island, values ranged from 3.14 (in 2009) to 5.61 (in 2013), or a factor of 1.8 difference, with a coefficient of variability (CV: Stdev/mean) of 22%. The inter-annual comparison of Gates of the Arctic showed values from 1.19 (2009) to 3.00 (2010), or a factor of 2.5 difference, with a CV of 32%. Although the temporal coverage was too low to delineate clear patterns of high- versus low-deposition years, the available data suggested generally low deposition in 2009 (e.g., lowest deposition year both at Gates of the Arctic and Kodiak Island) while the year 2011 showed high

deposition loads higher (e.g., highest deposition year for both Dutch Harbor and Kodiak Island). However, the order of years was not fully consistent among stations.

Table 12. Summary statistics of NADP MDN annual estimates of precipitation-weighted mean concentration, deposition, and precipitation for five monitoring sites in Alaska.

Station ID	AK06	AK04	AK05	AK98	AK00
Station Name	Gates of the Arctic National Park	Nome	Glacier Bay National Park	Kodiak	Dutch Harbor
# of Years	5	1	2	6	2
Hg PWM concentrations (ng L^{-1})					
Mean	5.980	6.153	1.887	2.167	2.875
Standard Deviation	2.474		0.515	0.431	0.581
Median	5.509	6.153	1.887	2.177	2.875
Minimum	3.224	6.153	1.523	1.628	2.464
Maximum	9.997	6.153	2.251	2.709	3.286
Hg deposition (ng m^{-2})					
Mean	2.108	2.338	3.002	4.801	4.518
Standard Deviation	0.665	NA	0.145	1.035	1.466
Median	2.018	2.338	3.002	5.191	4.518
Minimum	1.188	2.338	2.899	3.137	3.481
Maximum	3.004	2.338	3.104	5.743	5.554
Precipitation (mm)					
Mean	363.1	380.0	1641.7	2249.4	1657.4
Standard Deviation	52.1	0.0	370.6	515.3	845.2
Median	368.6	380.0	1641.7	2153.2	1657.4
Minimum	300.5	380.0	1379.6	1773.3	1059.7
Maximum	435.1	380.0	1903.8	3157.9	2255.1

5.2. Annual deposition loads relationships

In order to characterize the factors that may control annual deposition loads first at individual sites and then across different stations, we independently analyzed precipitation-weighted annual Hg concentrations (Hg_{pw}) and annual precipitation among stations (note that the product between the two constitutes annual deposition). **Figure 14** shows a scatter plot and linear regression between Hg_{pw} and annual precipitation. Using data of all years and all stations (16 values), the figure shows a strong linear relationship between Hg_{pw} and annual precipitation, with a regression slope that explains 59% of the variability in Hg_{pw} across all stations and collection years. The slope of -0.0189 suggests that with each 100 mm increased annual precipitation, Hg_{pw} concentration decreases by 1.9 ng L^{-1}. The patterns support a strong dependence of Hg concentrations to precipitation patterns as has been analyzed in detail using weekly Hg concentration data (section

4.4). Yet, it is important to note that in contrast to relationships analyzed in that section above, the effect of precipitation on Hg_{pw} concentrations is linear, compared to strong non-linear functions (i.e., log_{10}-log_{10} relationships).

However, Figure 14 exemplary shows that the range of different precipitation among stations and years is much larger than the range of Hg_{pw}. For example, annual precipitation differed by almost a factor of 12 between the lowest annual precipitation at Gates of the Arctic (27 mm in 2013) vs. 316 mm at Kodiak Island in 2014. Hg_{pw} on the other hand, ranged from lowest concentration of 1.5 ng L^{-1} (in Glacier Bay in 2011) to highest concentrations at Gates of the Arctic in 2010 (10.0 ng L^{-1}), a factor of 7 difference. When eliminating an unusually high Hg_{pw} concentrations at Gates of the Arctic in 2010, the spread in Hg_{pw} of the remaining 15 station years would be further lowered to a factor reduced to a factor of 4. This suggests that different annual precipitation amounts have a stronger contribution of modulating annual deposition loads compared to differences in Hg_{pw} concentrations. This effect becomes also evident when comparing the strengths of linear regression of annual deposition to both annual precipitation and Hg_{pw} concentrations: the coefficient of determination values, r^2, of linear regressions to annual precipitation of 0.71 is much higher than the r^2 value to Hg_{pw} concentrations (0.16; or 0.28 when removing the high concentration at station Gates of the Arctic in 2010). *We conclude that differences in Hg_{pw} concentrations and differences in annual precipitation amounts both contribute to substantial variability in annual Hg deposition loads between stations and years, but we find an overwhelming impact of annual precipitation that greatly dominates over different Hg concentrations. Different annual precipitation amounts alone explain 71% of the variability in observed annual deposition loads when using linear regressions between the two. The dominant role of different precipitation in determining annual deposition loads is further increased when taking into account that precipitation effects further correlates to Hg_{pw} concentrations.*

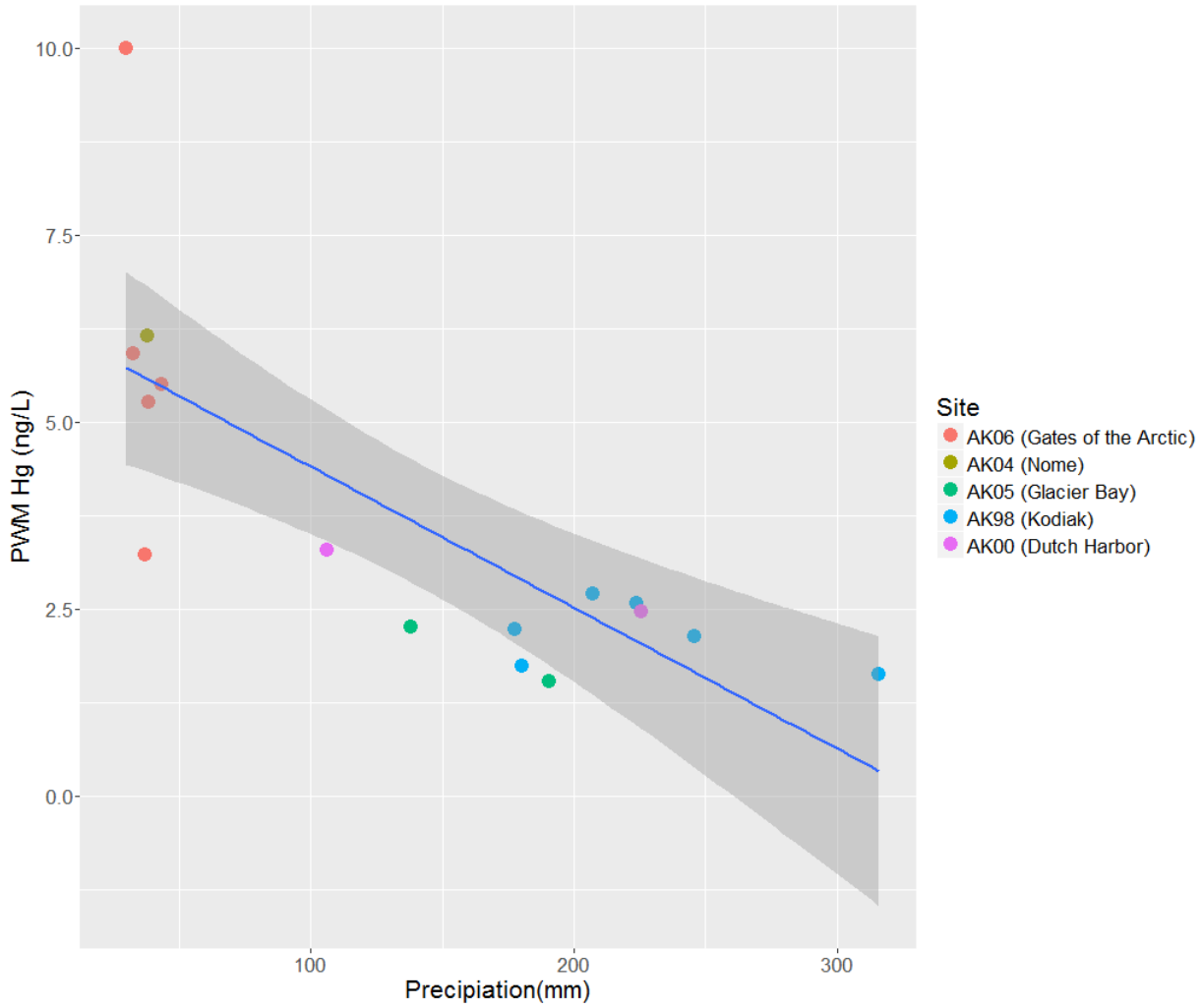

Figure 14. Plot of annual precipitation-weighted mean (pwm) Hg concentration verses annual precipitation (mm). Linear regression analysis show a significant relationship with a correlation coefficient R^2=0.557, p-value= <0.001.

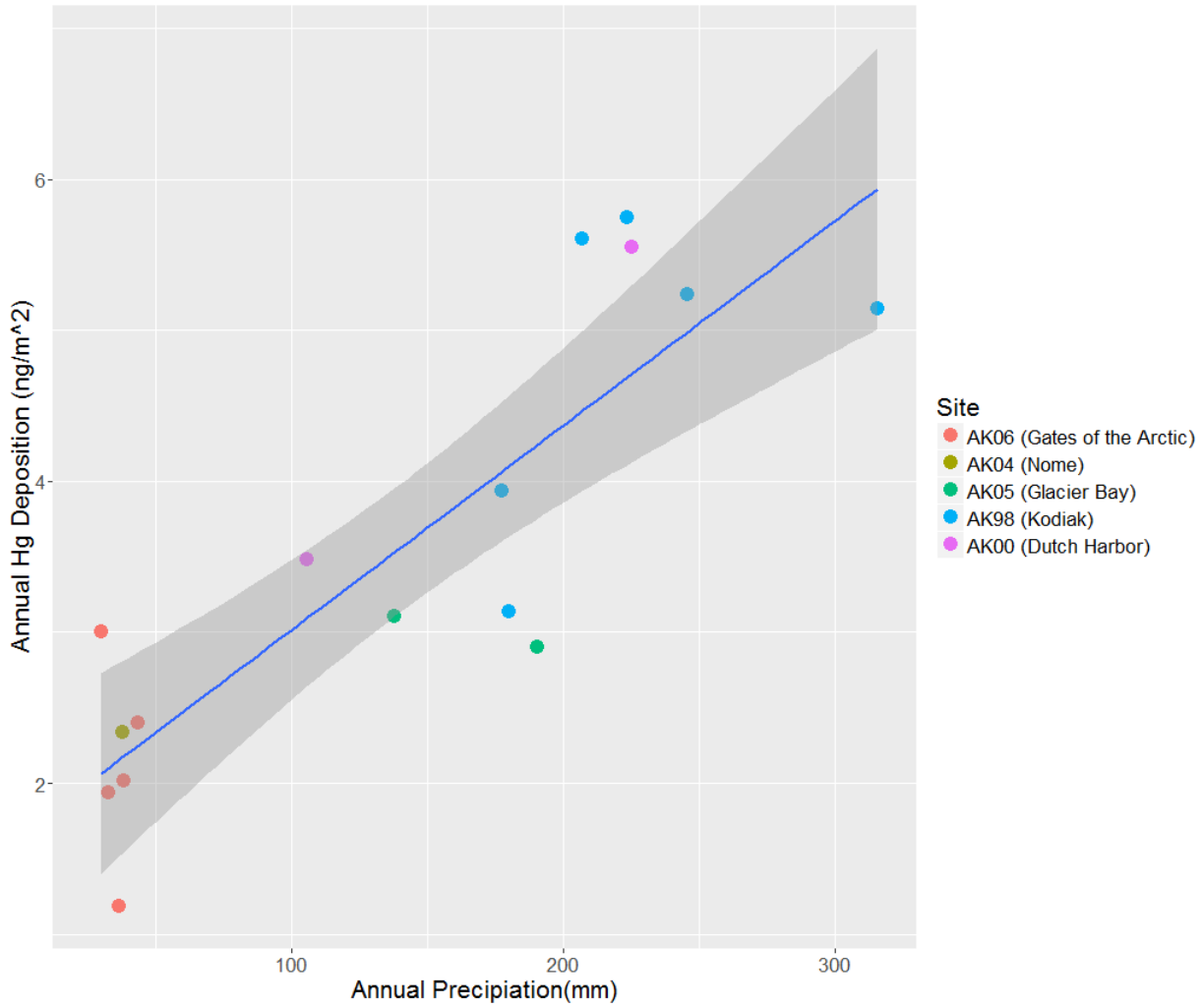

Figure 15. Plot of annual Hg deposition verses annual precipitation (mm). Linear regression analysis show a significant relationship with a correlation coefficient of R^2=0.7141, p-value= <0.001.

5.3. Composition of annual deposition loads

Not surprisingly, the statistics of weekly Hg deposition loads follow a similar order among sites as annual deposition sums. Highest to lowest medians of weekly loads are in the order of: Dutch Harbor (66.5 ng m^{-2}) > Kodiak Island (54.0 ng m^{-2}) > Glacier Bay (44.8 ng m^{-2}) > Gates of the Arctic (18.1 ng m^{-2}) > Nome (17.0 ng m^{-2}). Statistical tests show the following statistical differences: the two highest deposition sites, Dutch Harbor and Kodiak Island, are statistically significantly higher compared to all other sites, but not different from each other. The two lowest deposition sites, Nome and Gates of the Arctic, are statistically lower compared to the other sites with the exception of Nome to Glacier Bay, but do not differ from each other. Therefore, there is a group with statistically lower weekly deposition amounts in the north and a group with highest weekly deposition loads at lower-latitudes, western sites, with Glacier Bay falling in-between. These weekly deposition amounts therefore follow a very similar order as observed for calculated annual deposition amounts.

An important notion, however, is that the statistics of weekly deposition loads are substantially different from the analyses of weekly concentrations. This provides further strong evidence that deposition is in large parts driven by different precipitation patterns among sites, rather than driven by concentration differences. For example, Kodiak Island and Dutch Harbor show the highest weekly deposition loads compared to the lower-latitude sites, but concentrations show the reverse patterns with statistically highest Hg concentrations in the two northern sites. As discussed, this is due to large differences in precipitation patterns as shown by the precipitation statistics above. Therefore, in spite of much higher concentrations observed at the two northern sites (in the range of a factor 2), their inherently lower weekly precipitation amounts cause deposition loads to be the lowest among all sites.

Table 13. ANOVA analysis and post-hoc comparisons to test for statistical differences in Hg deposition among different stations.

Log10(Hg(ng m^{-2}))~Season*Site						
	Df	SS	RSS	AIC	F-value	P-value
Season	3	26.08	790.03	-63.13	9.81	<0.01
Site	4	154.14	918.08	67.36	43.48	<0.01
Season:Site Interaction	12	63.04	826.98	-40.81	5.93	<0.01
Post-Hoc Comparisons						
Season	Diff	Lower	Upper	P-value		
Spring-Fall	0.1432	-0.0865	0.3729	0.3764		
Summer-Fall	0.4640	0.2414	0.6866	<0.01		
Winter-Fall	0.2389	0.0037	0.4741	0.0448		
Summer-Spring	0.3208	0.0929	0.5487	0.0017		
Winter-Spring	0.0957	-0.1445	0.3359	0.7343		
Winter-Summer	-0.2251	-0.4585	0.0083	0.0634		
Site	Diff	Lower	Upper	P-value		
AK04-AK00	-0.8474	-1.2276	-0.4673	<0.01		
AK98-AK00	-0.1692	-0.4269	0.0886	0.3775		
AK05-AK00	-0.5120	-0.8186	-0.2054	<0.01		
AK06-AK00	-1.0128	-1.2896	-0.7360	<0.01		
AK98-AK04	0.6783	0.3324	1.0241	<0.01		
AK05-AK04	0.3355	-0.0482	0.7191	0.1189		
AK06-AK04	-0.1654	-0.5256	0.1949	0.7191		
AK05-AK98	-0.3428	-0.6056	-0.0799	0.0035		
AK06-AK98	-0.8436	-1.0710	-0.6162	<0.01		
AK06-AK05	-0.5008	-0.7824	-0.2193	<0.01		

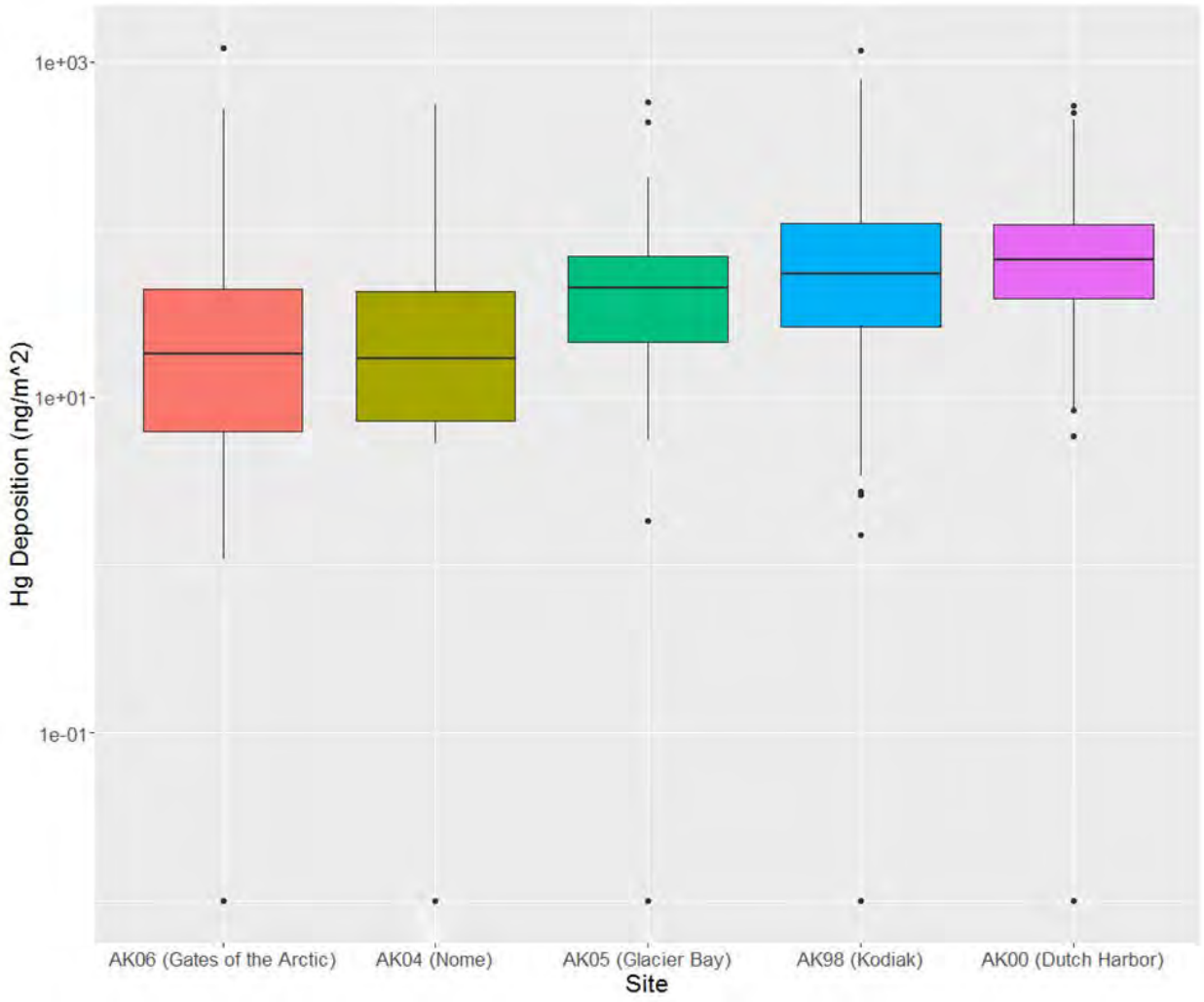

Figure 16. Box and whisker plot of weekly Hg deposition grouped by site. Deposition values of zero have been replaced with 0.01 for Log10-scale plotting purposes.

6 Scaling annual deposition and Hg deposition maps to the entire State of Alaska

6.1. Scaling protocols and resulting deposition maps

In this section, we use spatial interpolation and extrapolation techniques to create maps of deposition concentrations and deposition loads across the state of Alaska. We use similar interpolation methods as described by the National Atmospheric Deposition Program (NADP, 2016). Further, we would like to highlight the limitations and caution interpretations of deposition maps as specifically stated by the NADP network, including that: the stations and maps represent regional trends (rather than local sources); that uncertainty with maps varies geographically, have not been quantified, and high levels of uncertainty can occur due to topographic variability, near urban and industrial areas, and in regions isolated from deposition sites. The network further suggests caution when making decisions based on maps where no direct measurements were taken.

Concentration maps shown below are based on inverse distance weighting interpolation method of average precipitation-weighted Hg concentrations (Hg_{pw}) for each station. Note that this map

therefore represents different collection years and number of years for each station based on available data. For example, the maps are based on 2 years (2011 and 2012) of data for Dutch Harbor, 1 year (2014) of data for Nome, two years (2011 and 2012) for Glacier Bay, five years (2009-2014 without 2013) for Gates of the Arctic, and six years (2008-2014 without 2010) for Kodiak Island. The resulting mercury concentration distribution maps result in very coarse spatial representation of the concentrations patterns: in summary, concentrations are linked to precipitation gradients with highest concentrations observed in northern two stations with lowest annual precipitation and small storm sizes. Glacier Bay and Kodiak Island are the two stations with the lowest concentrations, but Dutch Harbor shows higher concentrations than the two other comparable lower-latitude stations. It is important to note that the use of inverse weighting procedures results in interpolation of Hg concentrations that are not fully in accordance with the observed relationships to precipitation patterns. For example, annual precipitation maps show strong gradients in annual precipitation from the southern coast of Alaska to inland and northern locations, and relatively consistent low precipitation values across much of the central, northern, and eastern Alaska. On the other hand, our interpolated Hg concentration map shows that interior and eastern Alaskan concentration maps follow only a north-to-south gradients between the lower-latitude and higher-latitude stations, but does not account for east-west gradients. While we could have attempted to use precipitation-based estimates of Hg concentrations across the state (based on strong relationships of Hg_{pw} and annual precipitation), we decided not to deviate from common NADP mapping procedures.

Figure 17a shows precipitation maps across Alaska based on precipitation data averaged for the years 2007 to 2015. The long-term NOAA precipitation maps show very strong gradients from the southern coastal locations to interior and northern Alaska, with dramatic precipitation changes within short distance (50-100 miles). Highest annual precipitation is observed along the southeastern and southcentral coasts, with maximum precipitation of approximately 610 cm yr^{-1}. High precipitation amounts in the range of 200 to 300 cm yr^{-1} are also observed in Kodiak Island and Bristol Bay and the Aleutian/Probilof Islands. Moderate precipitation is observed in the southcentral and southwestern region of Alaska, generally in the range of 100 to 200 cm yr^{-1}, whereby occasionally higher levels precipitation are observed in the mountain regions due to orographic precipitation effects. In the interior and far north regions of Alaska, however, annual precipitation sums are low and generally below 100 cm yr^{-1}.

The resulting annual deposition maps, i.e., the product of annual Hg_{pw} concentrations and precipitation, are shown in **Figure 17c**). *Based on this map, we conclude that there are distinct zones of highest Hg deposition in Alaska along the southern and southeastern coasts, with annual Hg deposition exceeding 20 µg m^{-2} yr^{-1}. The zones of highest annual Hg deposition, based on the estimated map, are confined to a zone of approximately 50-100 miles inland. Similarly high Hg depositions also occur in isolated mountain areas near the southern coast, particularly in the Alaskan Range. For example, in the Denali National Park Region, estimated Hg wet deposition of up to 15 µg m^{-2} yr^{-1} is in similar magnitude as the highest deposition amounts along the southern and southeastern coast. Lower Hg deposition amount are observed along the southwestern coastal region, including Kodiak Island and the western and eastern Aleutians. Here, estimated annual Hg deposition are in the range 5 to 10 µg m^{-2} yr^{-1}. Our estimated deposition maps indicate that in*

much of the State of Alaska, in particular in the interior and far northern regions, Hg deposition are very low. Here, annual Hg deposition generally range below 4 µg m^{-2} yr^{-1}, with many areas (e.g., north of the Brooks Range) showing deposition only in the range of 1-2 µg m^{-2} yr^{-1}.

As stated above, the estimated maps of annual deposition need to be considered with caution, as they are based on interpolation methods and include a variety of possible error terms. However, the spatial distribution represents the patterns we described with the actual measured data at the five stations: for example, we fully replicate the order and range of annual deposition among stations. Yet, we observe some differences in deposition values between the predicted deposition maps and actual observations. **Table 14** shows the respective deposition values of the prediction maps and the five stations: at some stations, estimated deposition is well within 10% of observations (e.g., Gates of the Arctic and Kodiak Island), however, in other stations we find large discrepancies over 100% (e.g., in Glacier Bay and Nome). The bias of observed versus modelled Hg deposition can be attributed in large parts to discrepancies in annual precipitation: for example, at Glacier Bay and Nome we strongly overestimate precipitation (by 90% and 117%, respectively), which accounts for the large majority of the respective biases. Reasons for the precipitation errors are mainly due to the large grid size of the modelled precipitation values as well as the strong coastal gradients. For example, the deposition station at Glacier Bay, which is situated close to Point Gustavus in the inner Bay about 50 km inland from the main coast, is located along a very large precipitation gradient, and the grid size of the precipitation maps cannot resolve these gradients leading to large local errors.

Yet another possible reason for differences between observed and predicted deposition may include issues of precipitation fetch during measurements. Precipitation gages generally show a strong bias towards under-catch of precipitation caused by wind, even with precipitation gauges that are designed with wind protection (Savina et al., 2012; Yang et al., 2000). Especially for snow collection, which at these stations accounts for a very important fraction of annual precipitation, under-catch of precipitation can range from 20 to 50% during windy conditions (Rasmussen et al., 2012). It is therefore possible that reported deposition values are at the low end of actual deposition, yet this would need to be assessed in detail in the field with additional alternative precipitation measurements.

Annual Wet Deposition Concentrations

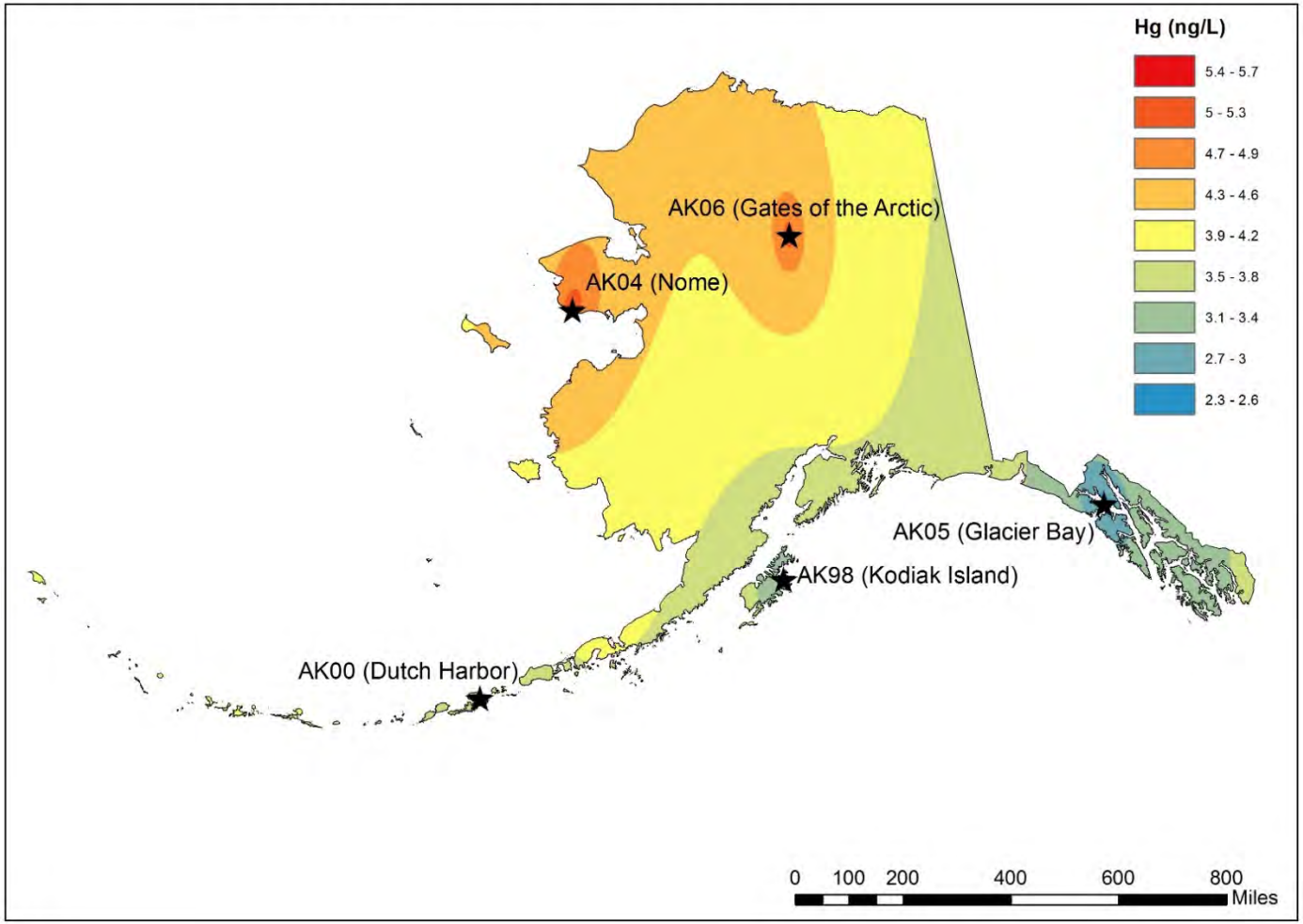

a)

b)

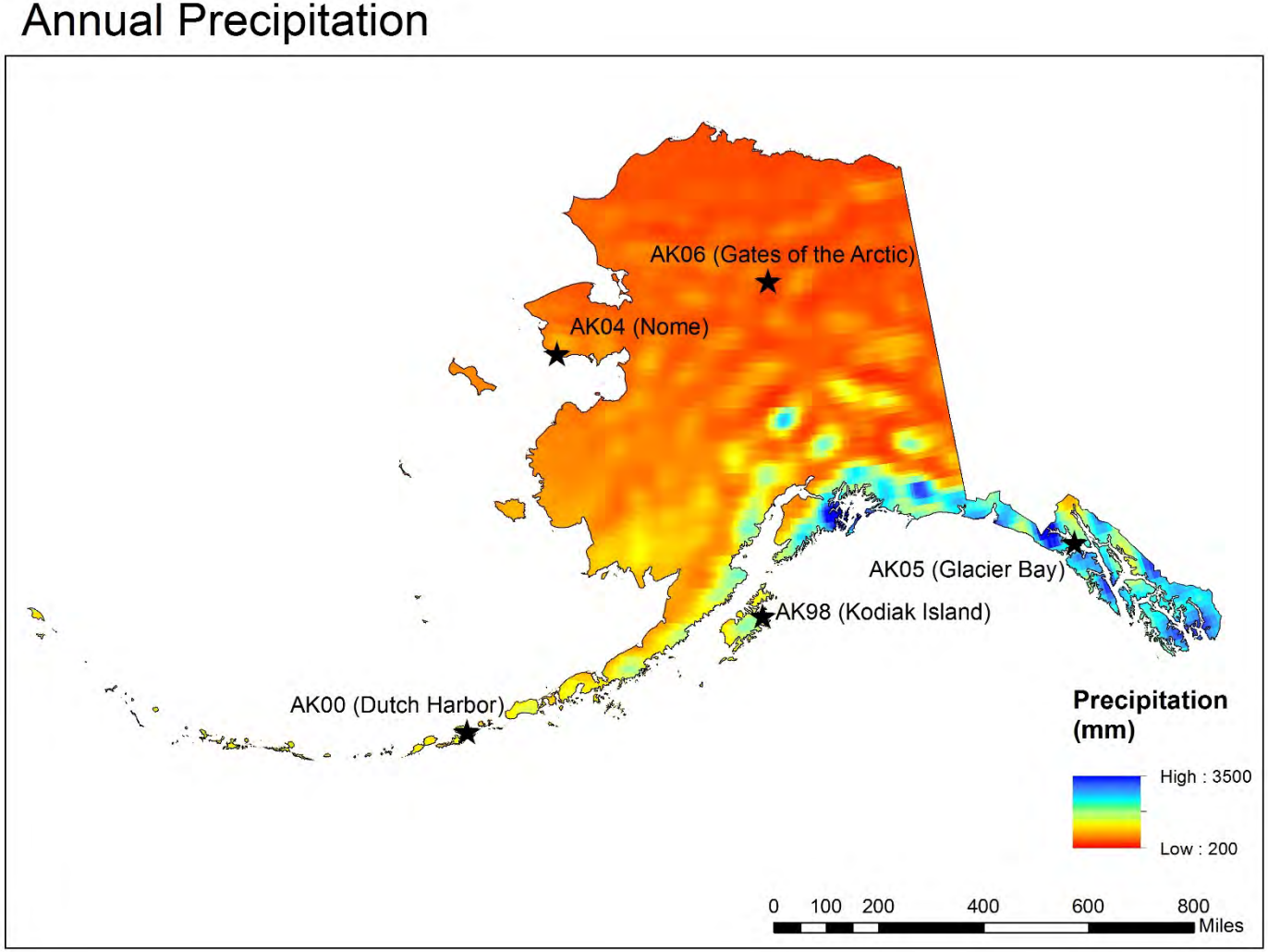
Annual Precipitation
AK06 (Gates of the Arctic)
AK04 (Nome)
AK05 (Glacier Bay)
AK98 (Kodiak Island)
AK00 (Dutch Harbor)
Precipitation (mm)
High : 3500
Low : 200
0 100 200 400 600 800
Miles

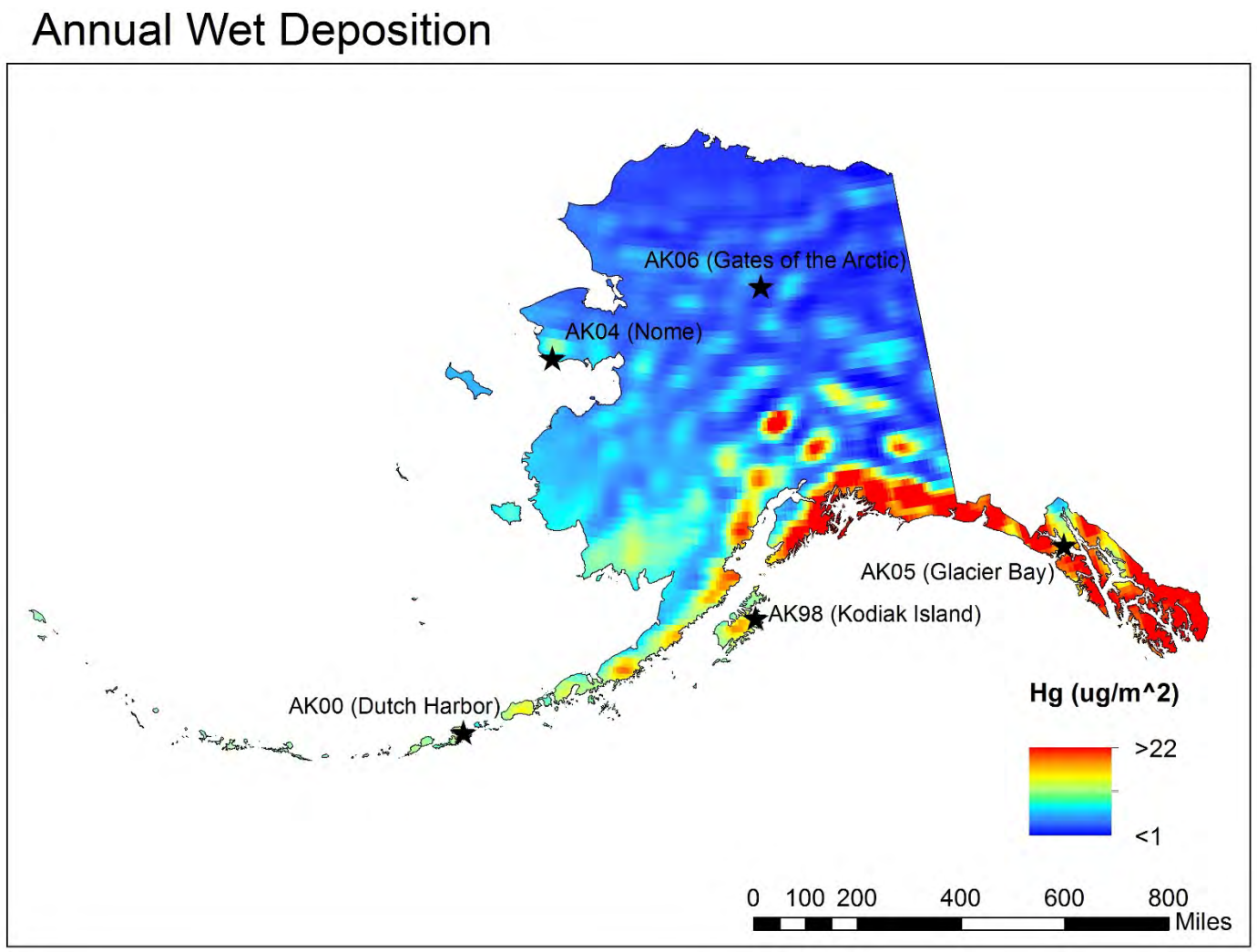

c)

Figure 17. Average Annual Hg deposition maps for the state of Alaska: A) Inverse distance weighted concentration layer; b) NCEP Climate Forecast System Precipitation 2007-2015 annual average; c) Hg deposition estimates. Maps show large-scale concentration gradients (north/south) largely due to precipitation differences with total loading being highly dependent on precipitation.

Table 14. Comparison of MDN measured precipitation and Hg deposition with NCEP Reanalysis Precipitation and modeled Hg deposition values. % bias results are similar for both precipitation and Hg deposition.

Station ID	AK06	AK04	AK05	AK98	AK00
Station Name	Gates of the Arctic National Park	Nome	Glacier Bay National Park	Kodiak	Dutch Harbor
Precipitation (mm)					
MDN Precipitation	363.1	380.0	1641.7	2249.4	1657.4
NCEP Precipitation	349.4	824.8	3112.4	1996.7	1861.1
% Bias	-3.8	117.1	89.6	-11.2	12.3
Hg Deposition (µg m^{-2})					
MDN Deposition	2.1	2.3	3.0	4.8	4.5
Modeled Deposition	2.0	4.6	7.0	5.1	5.7
% Bias	-7.5	95.0	133.5	5.2	26.6

6.2. Comparison to annual Hg wet deposition of other MDN stations

Figure 18 shows annual deposition loads observed across the contiguous United States. In general, the annual deposition loads across the lower 48 U.S. states are much higher compared to the deposition loads observed in Alaska. The 99 lower deposition values reported for the lower 48 States averaged 9.7±3.9 µg m^{-2}, with a median value of 9.0 µg m^{-2}. Only three of the Alaskan stations allowed for calculation of annual Hg deposition loads in 2014: Gates of the Arctic: (2.0 µg m^{-2}); Kodiak Island (5.1 µg m^{-2}); and Nome (2.4 µg m^{-2}), and all were very low compared to the 99 other U.S. stations. For better comparison, we compared mean annual Hg deposition of the Alaskan station to the values observed in 2014 across the lower contiguous U.S. Three of the Alaska stations, Nome (2.3 µg m^{-2}), Glacier Bay (3.0 µg m^{-2}), and Gates of the Arctic (2.1 µg m^{-2}) showed annual deposition loads below the minimum of all lower 48 contiguous U.S. States in 2014 (3.1 µg m^{-2}). Only Dutch Harbor (4.5 µg m^{-2}) and Kodiak Island (4.8 µg m^{-2}) exceeded these minimum concentrations across the lower 48 States. Even these two stations, however, also fell below the 5^{th} percentile of annual deposition observed of the lower 48 States in 2014. (5.3 µg m^{-2}). *We conclude that observed wet deposition across the five Alaskan deposition stations are the lowest in the entire United States, with three stations below the lowest deposition values observed across the 48 contiguous U.S. States.*

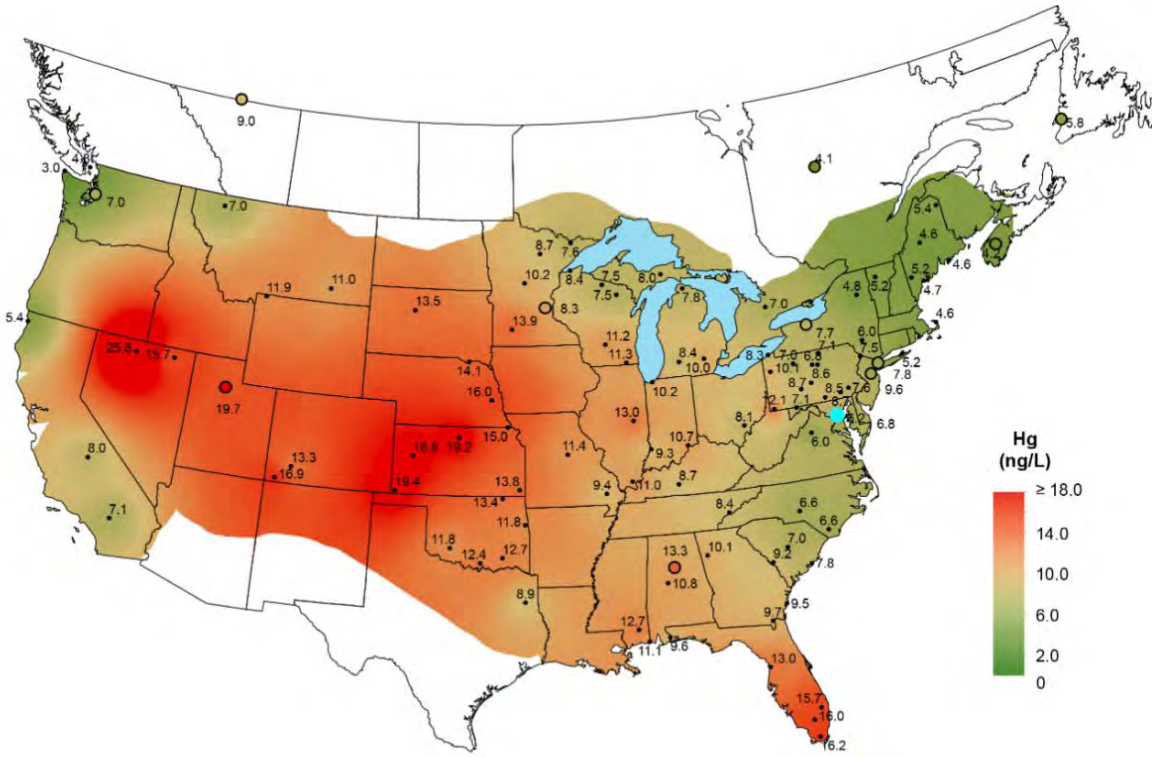

a)

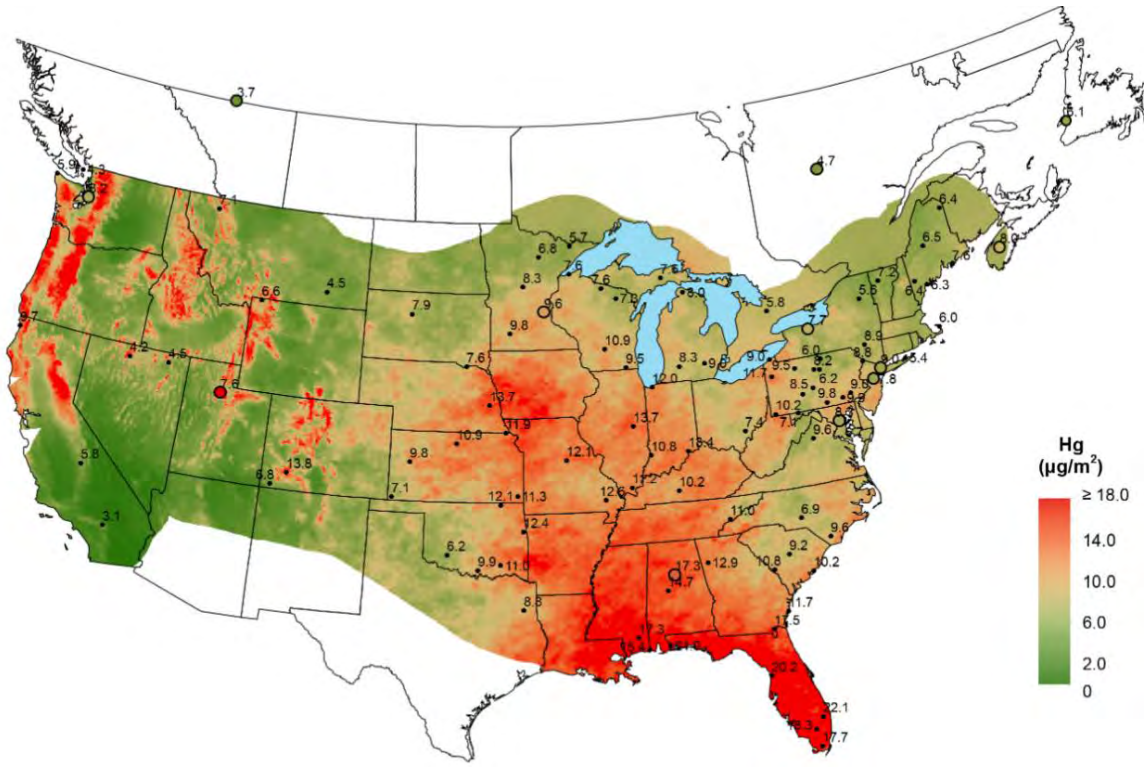

b)

Figure 18. NADP maps of annual Hg deposition a) concentration and b) load for 2014 across the lower contiguous United States.

Similarly, precipitation-weighted Hg concentrations are low in Alaska in comparison to the rest of the United States, which for the year 2014 averaged 10.6±9.1 ng L^{-1} with a median value of 8.9

ng L^{-1}. Three Alaskan stations show precipitation-weighed annual Hg concentrations below the minimum concentrations (3.0 ng L^{-1}) across the contiguous United States, including Dutch Harbor (2.9 ng L^{-1}), Glacier Bay (1.9 ng L^{-1}), and Kodiak Island (2.2. ng L^{-1}). Nome with a precipitation-weighted annual concentration of 6.2 ng L^{-1} and Gates of the Arctic (6.0 ng L^{-1}) are below the 15th percentile of concentrations of the lower 48th States. Therefore, the low deposition values across coastal regions in Alaska are driven in large parts by their very low wet deposition concentrations that are below concentrations in any other U.S. deposition stations. Although the two more northern stations also have relatively low deposition concentrations, their low annual deposition are in large parts due to low precipitation amounts.

7 Back-trajectory analyses

7.1. Intensive backtrajectory analyses for 2014

In this chapter, we present detailed and comprehensive back-trajectory analyses at three deposition stations for the year 2014. We chose 2014 because it represents a relatively average year of Hg deposition and does not show neither maximum nor minimum deposition amounts of stations that have multiple years of deposition data. In addition, 2014 is a year where we have corresponding annual deposition data at three station, including the highest deposition station (Kodiak Island), the lowest deposition station (Gates of the Arctic), as well as the intermediate station Nome. This is expected to allow comparison of source footprints between high and low deposition stations. Figures 19 a-c show all individual backtrajectories calculated for each of the stations for each Hg deposition event of the year 2014. The number of individual precipitation events identified and shown in the figures for 2014 were 247 (Kodiak Island), 182 (Nome) and 148 (Gates of the Arctic). These figures are not meant to visualize source regions as they are too busy to read; however, these individual trajectory runs form the basis of frequency maps of origin of precipitation and Hg deposition as shown in the next section.

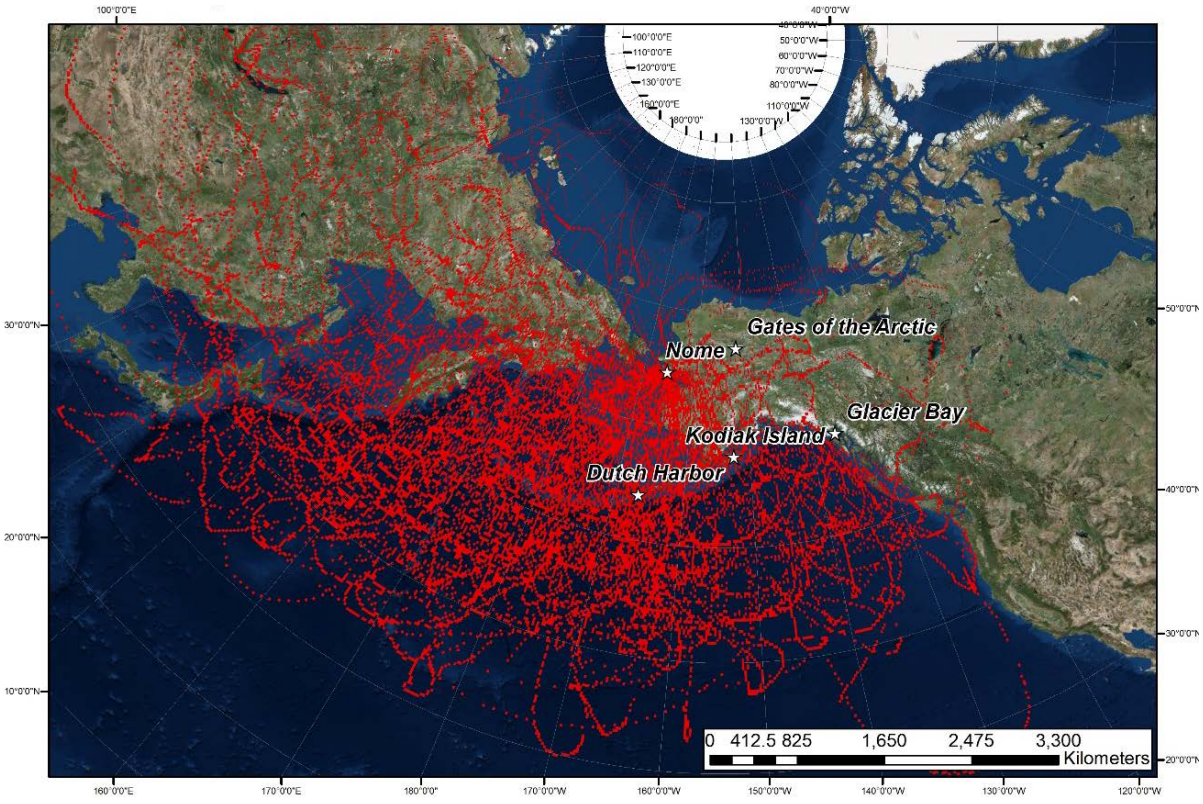
Gates of the Arctic
Nome
Glacier Bay
Kodiak Island
Dutch Harbor
0 412.5 825 1,650 2,475 3,300
Kilometers

a)

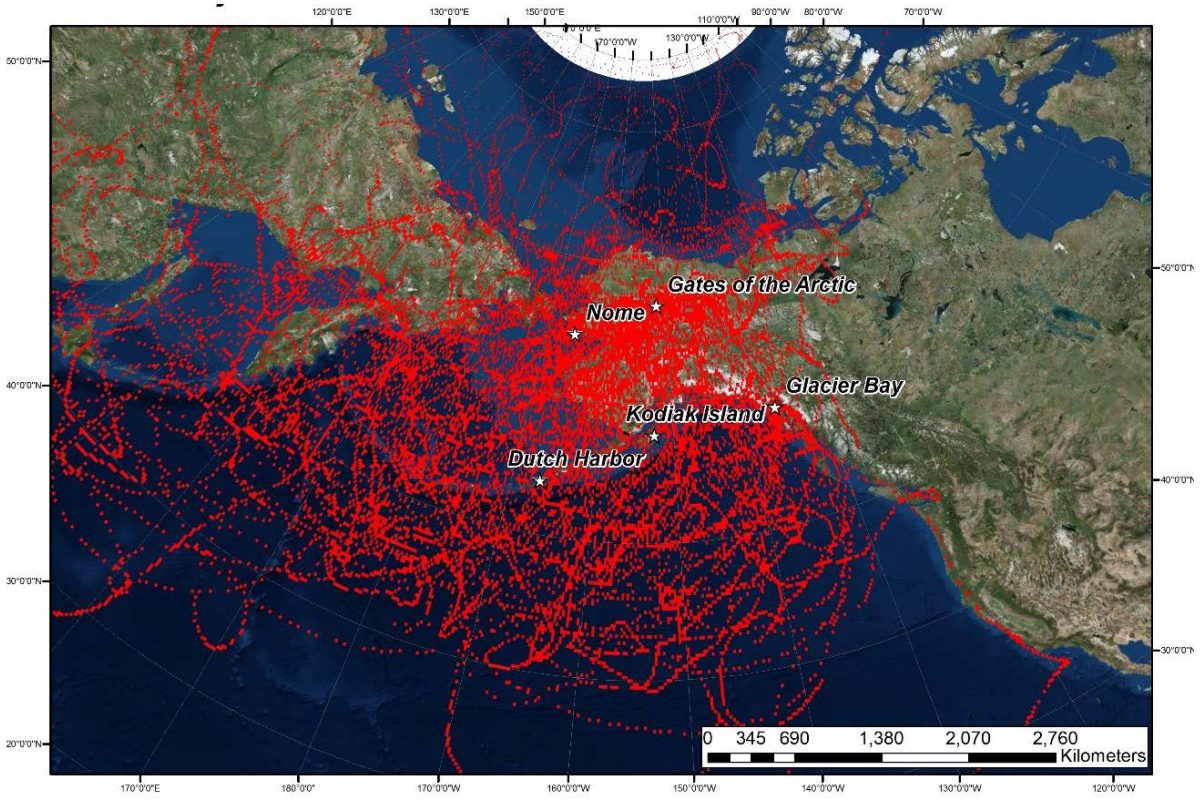
Gates of the Arctic
Nome
Glacier Bay
Kodiak Island
Dutch Harbor
0 345 690 1,380 2,070 2,760
Kilometers

b)

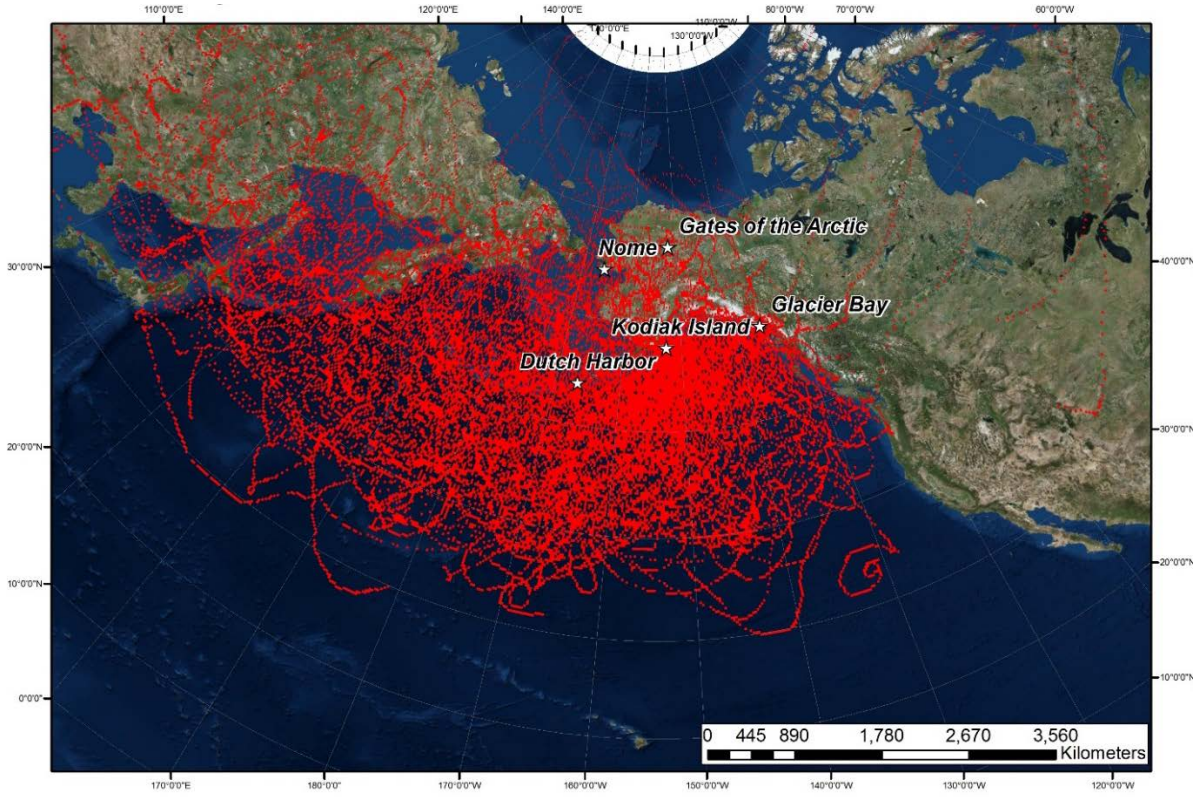

c)

Figure 19. Individual back trajectory traces showing all deposition events in 2014 for a) Nome, b) Gates of the Arctic, and c) Kodiak Island.

7.2. Normalized backtrajectory frequency maps for 2014

In order to visualize footprint areas for both precipitation and Hg deposition, we here show normalized backtrajectory frequency maps for all precipitation and deposition events for the entire year 2014. For Kodiak Island, trajectory frequency maps show almost identical patterns for precipitation and Hg deposition maps. Both show highest trajectory frequencies in the vicinity from the deposition station as well as to the south. This makes sense since each trajectory is passing through the grid cell prior to arriving at the deposition station, so the vicinity of the station always shows high contributions both for precipitation and Hg deposition. In addition, major source origins for both precipitation and Hg wet deposition stem mainly from the Gulf of Alaska, with additional contributions further south in the eastern Pacific Ocean, to about a distance of 2,500 km south of Kodiak Island. *For this station, we conclude that based on the similarity of the precipitation maps and the Hg deposition map, the origins of Hg deposition are very closely related to the origin of precipitation. In other words, for Kodiak Island, we cannot delineate zones of particularly enhanced Hg contributions that go beyond the contributions that are expected based on the origin of the precipitation.*

A similar pattern is observable for Gates of the Arctic, where we also find close agreement between the source origins of precipitation and Hg deposition. High contributions to annual Hg deposition and annual precipitation are observed again in the vicinity of the station as all trajectory pass through the grid cells adjacent to the station. In addition, major regions of storm activity that similarly contribute to Hg deposition are observed from the center of the Bering Sea as well as

from the Gulf of Alaska. There are only a few occasions where storms or deposition events can be tracked far into the western Pacific. *We conclude that at Gates of the Arctic, there are similar source regions for precipitation and Hg deposition, which both mainly originate in the Bering Sea and the Gulf of Alaska.*

A different pattern was evident for Nome. Here, the frequency distributions of trajectories differ between precipitation and Hg wet deposition. While precipitation origin again shows a high frequency in the vicinity of the station, they also show a relatively wide distribution across the Bering Sea, the central Pacific, and the western Pacific. For Hg, increased contributions relative to precipitation are clearly visible originating in the western Pacific, downwind of East Asia. *We conclude that for Nome, backtrajectory frequency maps for Hg deposition show increased relative contributions to Hg deposition loads from the western Pacific, contributions that go beyond what would merely be expected based on storm activities that originate in that respective area.*

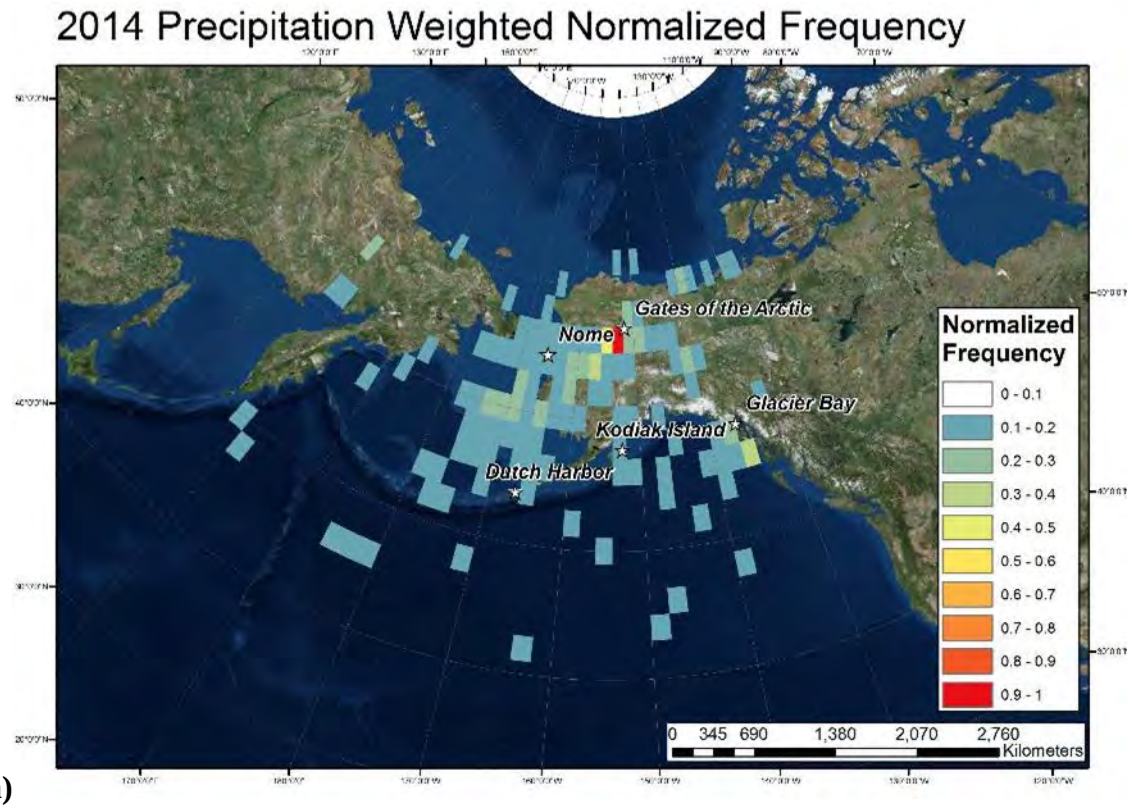

a)

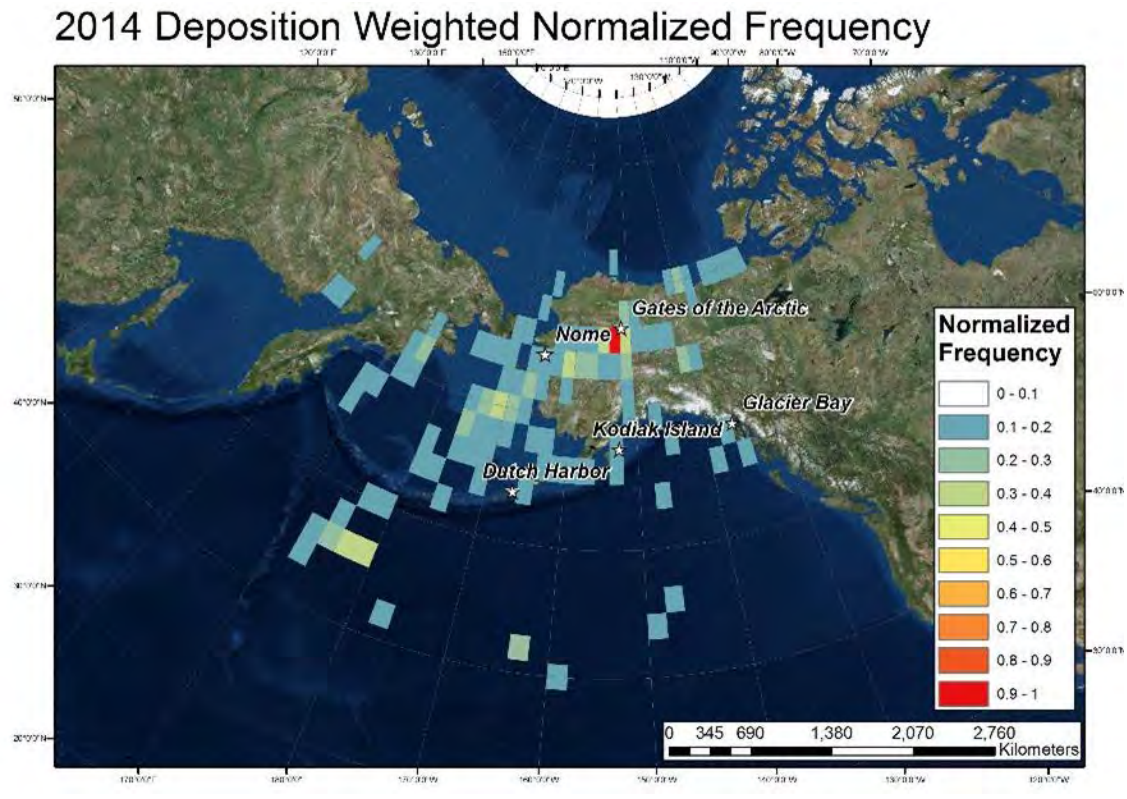

b)

Figure 20. Gates of the Arctic normalized-frequency maps weighted by a) precipitation and b) Hg deposition.

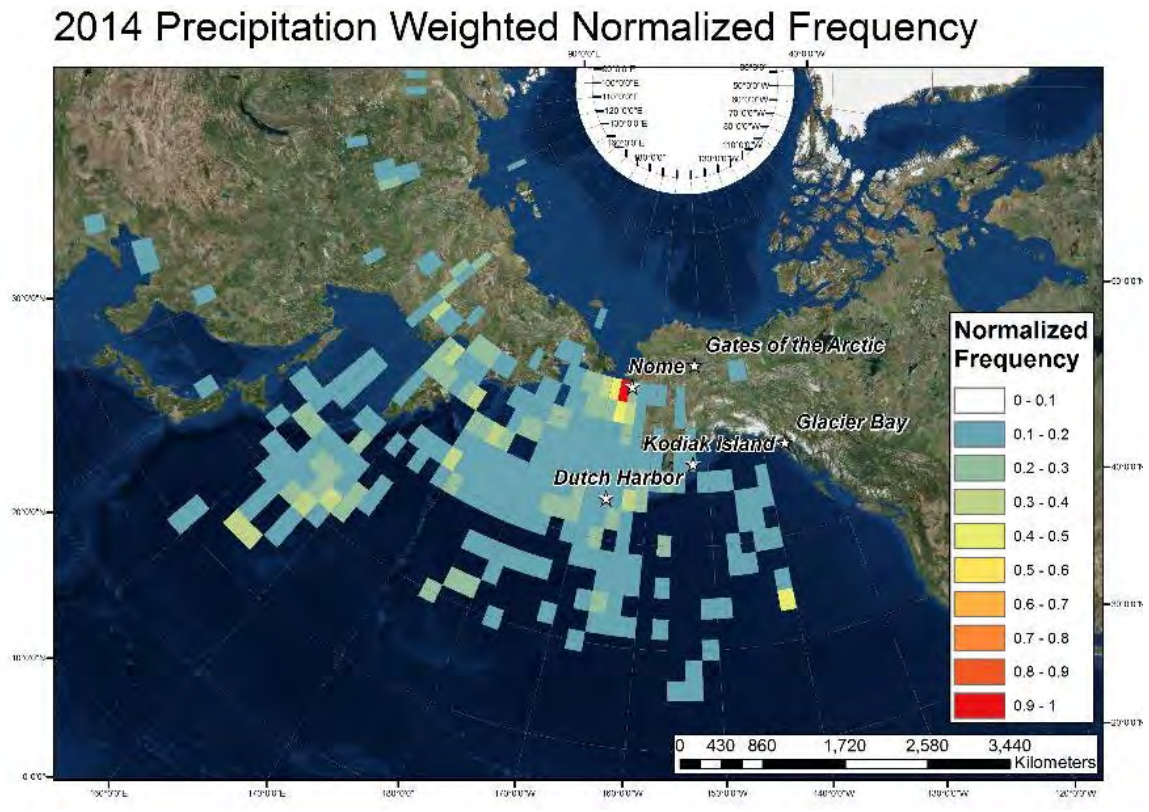

a)

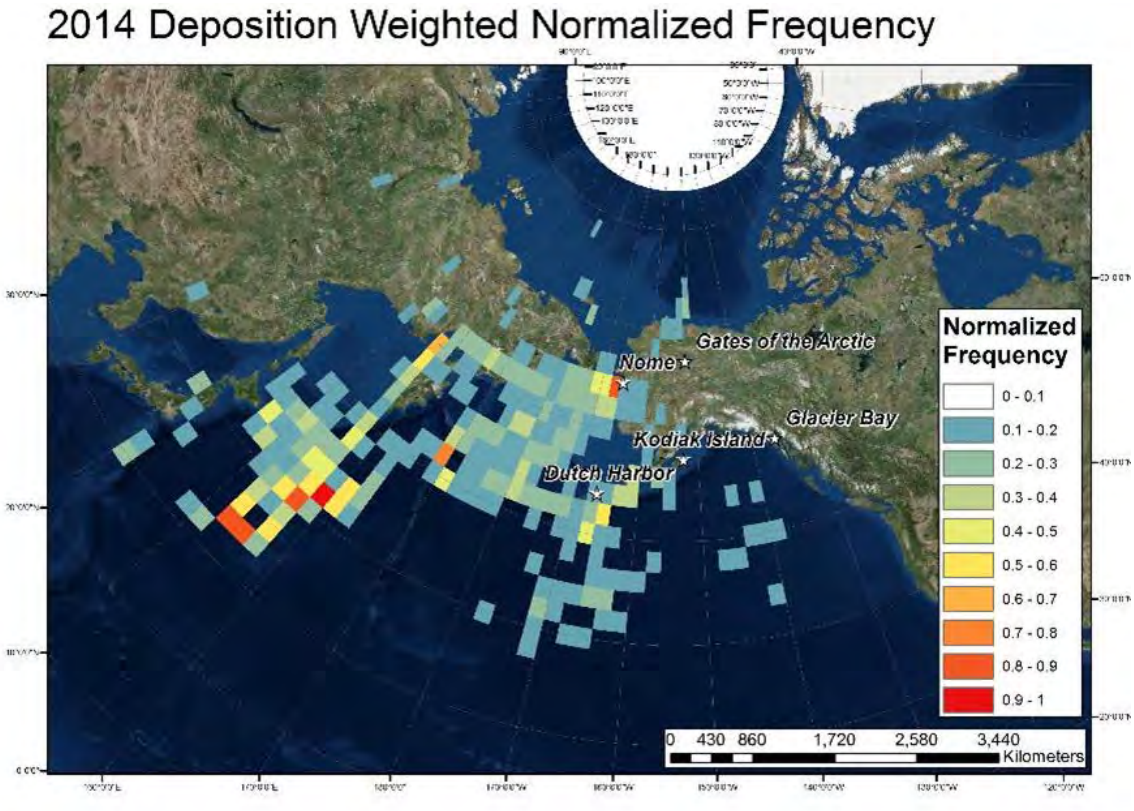

b)

Figure 21. Nome normalized-frequency maps weighted by a) precipitation and b) Hg deposition.

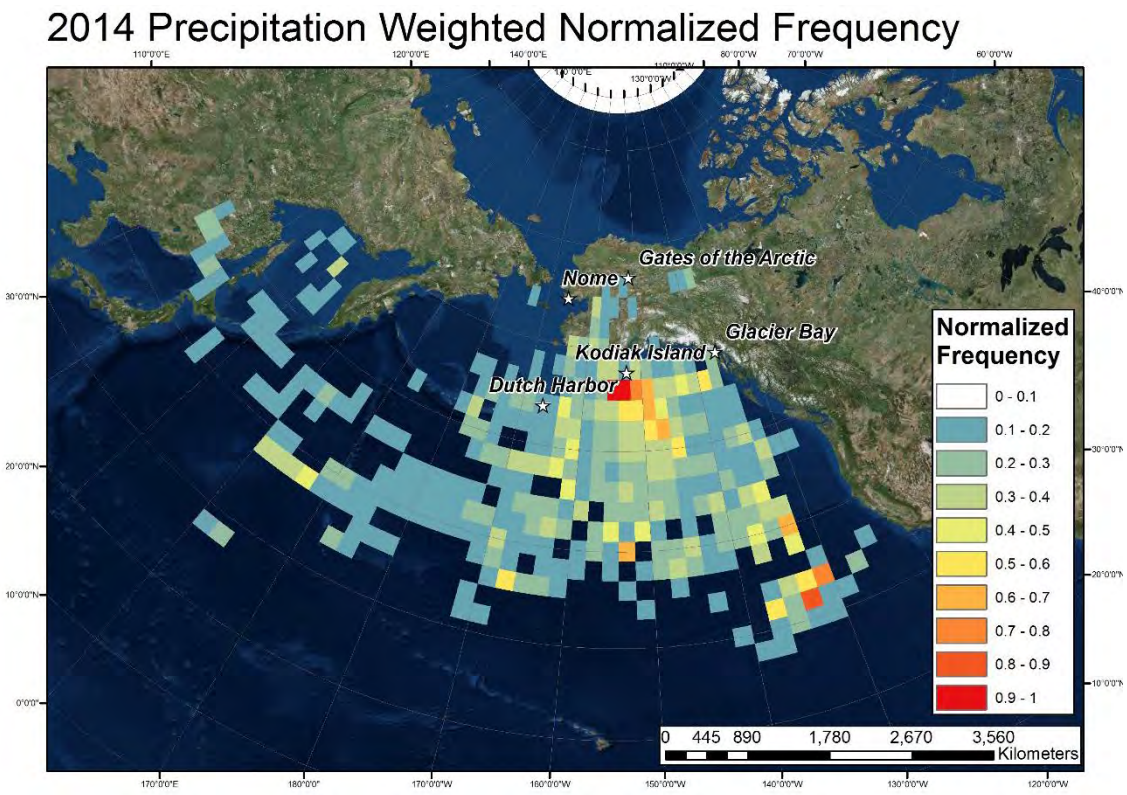

a)

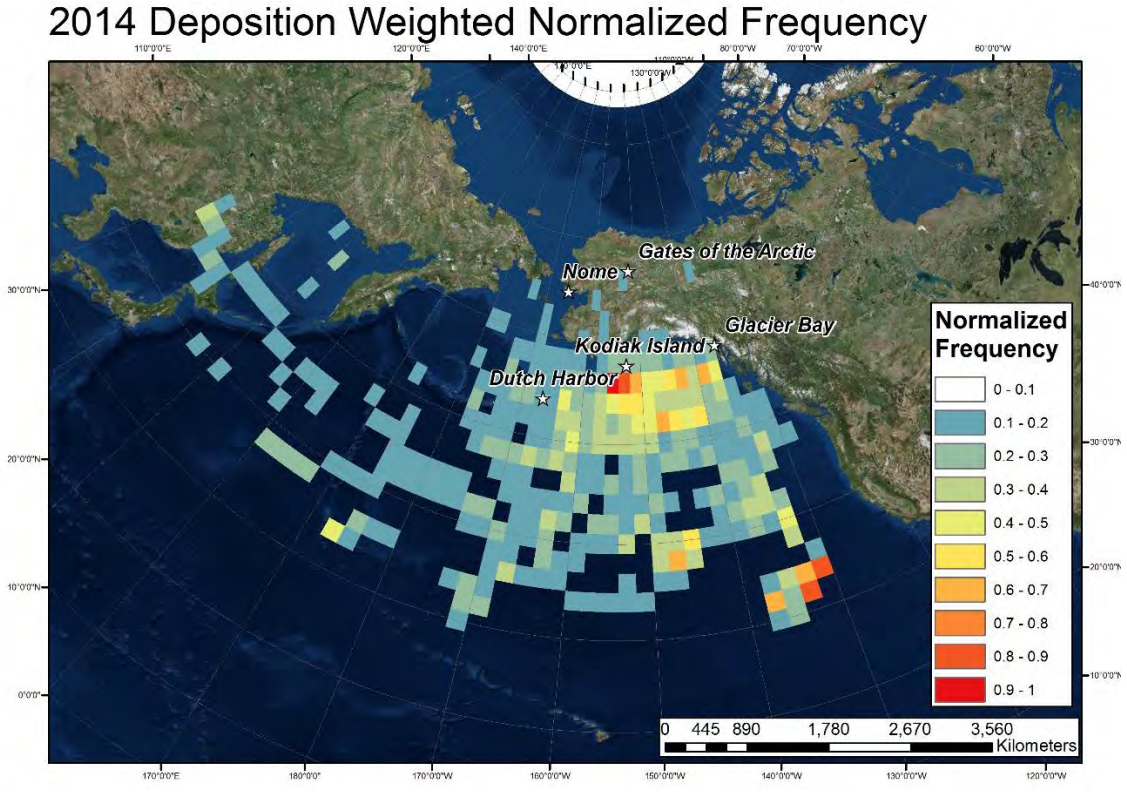

b)

Figure 22. Kodiak Island normalized-frequency maps weighted by a) precipitation and b) Hg deposition.

To visualize the enhanced contributions of the western Pacific region to Hg deposition loads at all sites, we calculated the ratio of relative frequencies for deposition to that of precipitation. A ratio of > 1 indicates relatively enhanced contributions to Hg deposition above the contributions expected based on precipitation only; ratios <1 shows lower contributions to Hg deposition compared to that expected based on precipitation. At all sites, there are a number of individual grid cells with very high or low ratios, but it is important to relate these with the importance of precipitation and deposition. For example, at Kodiak Islands, there seems to be a range of grid cells in the far north that show potentially enhanced contributions to Hg deposition, but these grid cells contribute very little to annual Hg deposition, so the high rations here are not important. However, there is a different case at Nome: here, a range of high ratios in the western Pacific is associated with an area that we described to have significant contributions to Hg deposition to that station. Many of the grid cells in the western Pacific Ocean show ratios of 1.5 to 3, which we interpret as contributions that are about three times the regular contributions expected based on the origin of precipitation only. *We conclude that at Nome, high backtrajectory frequencies originate from the western Pacific Ocean, and these high frequencies also show that this area contributes more to deposition than can be expected based on the origin of precipitation only. In all other areas, the origin of Hg wet deposition closely matches that of precipitation, suggesting no specific source of Hg deposition besides what can be expected based on the origins of storms.*

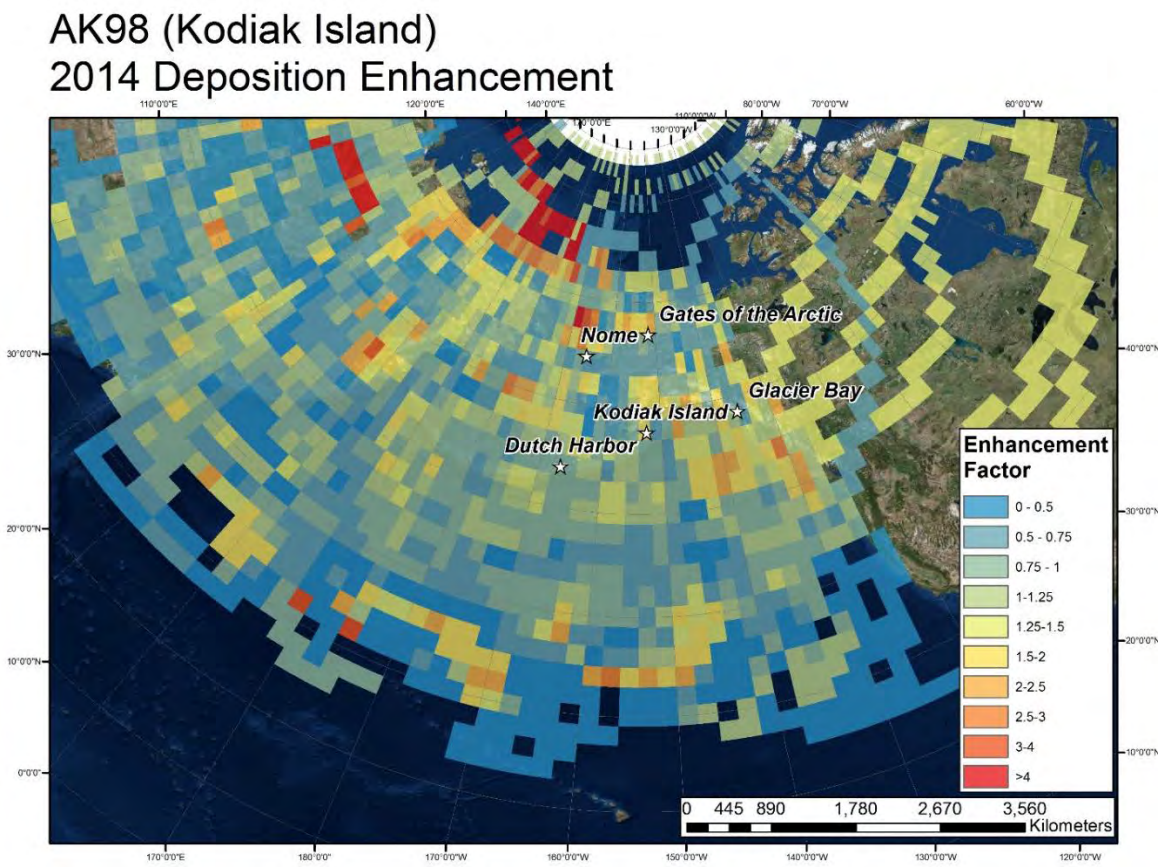

a)

b)

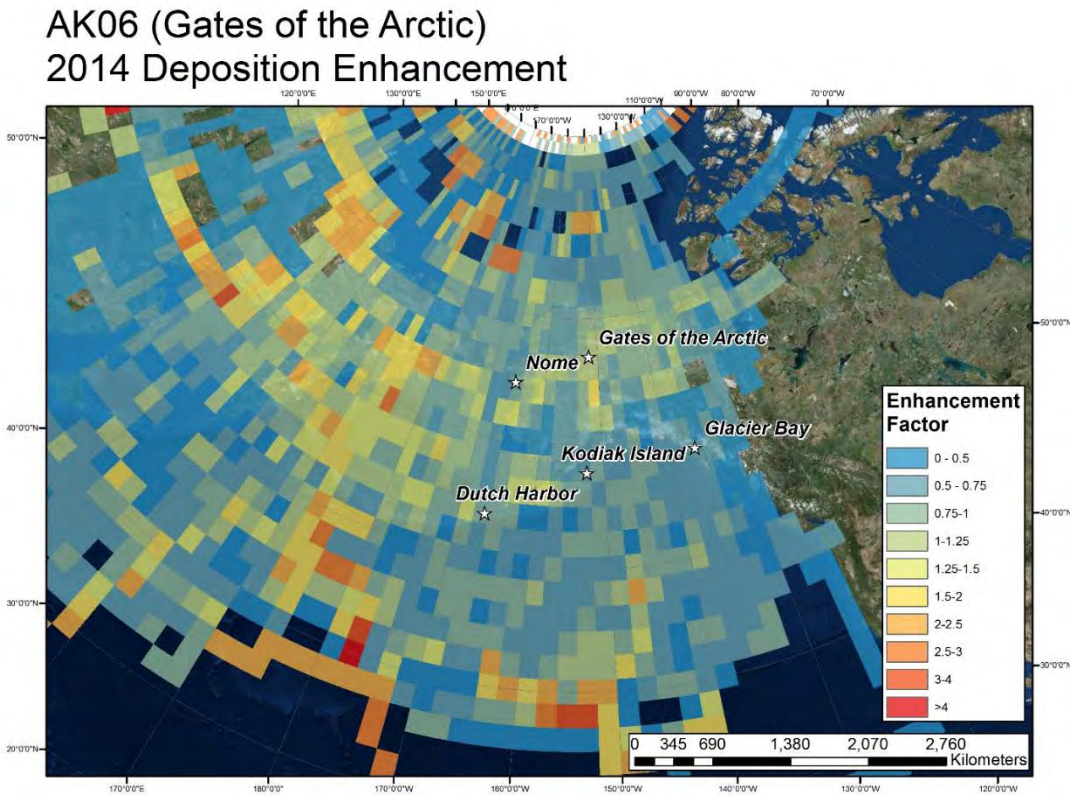

c)

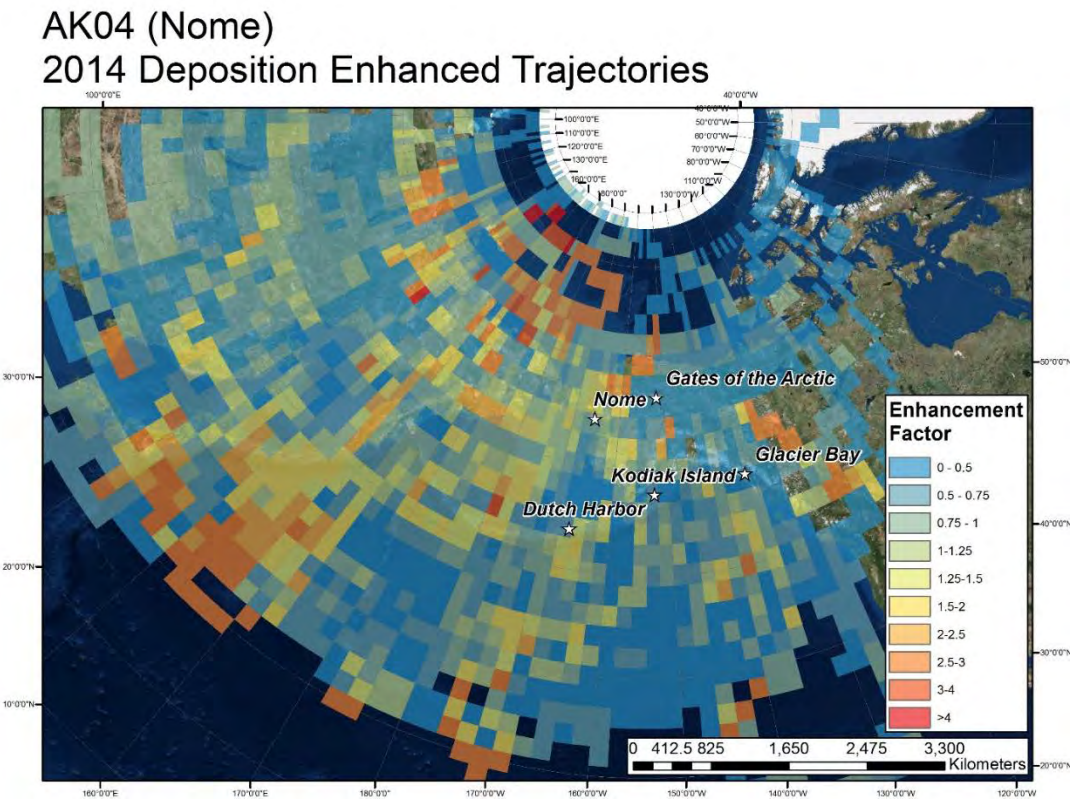

Figure 23. Deposition enhancement maps for a) Kodiak Island, b) Gates of the Arctic, and c) Nome.

8 How important is Hg wet deposition and are we measuring the right thing?

Terrestrial landscapes are the largest receptor areas of atmospheric Hg deposition due to their large surface area and as such upland runoff often contributes the main source of Hg to rivers and lakes (Lorey and Driscoll, 1999), a process particularly relevant in northern rivers lakes with large catchment areas (Meili, 1991). For the arctic ocean, modeling work by Fisher et al. (2012) suggested that riverine sources may be the dominant Hg source to the Arctic Ocean as well, in support of large Hg fluxes measured in riverine runoff to the Arctic Ocean (Leitch et al., 2007). Although subsequent work suggests that riverine fluxes may be lower than atmospheric deposition as an overall contributor to Arctic Hg input, riverine runoff still is an important source to ocean Hg loading (Amos et al., 2014; Dastoor and Durnford, 2014). For large ocean basins, direct atmospheric deposition clearly is important and likely the dominant source for Hg contributions, as discussed for the Arctic Ocean above. Therefore, characterizing deposition fluxes that stems from direct wet deposition is an important component to ocean Hg loading, in particular in areas of greater distance to coastal runoff areas.

For terrestrial ecosystems, however, recent work suggests that contributions of wet deposition to Hg loads may be much smaller than previously assumed and are small compared to other atmospheric sources. This line of evidence is based on different observations and findings, including: (i) measured deposition fluxes in (forested) terrestrial ecosystems; (ii) observed spatial patterns across landscape gradients; (iii) stable Hg isotope evidence; and (iv) modelling studies. In regards to (i), it has been known for a long time that in forested landscapes, the contributions of plant-derived deposition (such as litterfall and throughfall deposition) often dominate over direct wet deposition, for example with litterfall alone exceeding direct wet deposition by at least a factor of 2 (Bishop and Lee, 1997; Grigal et al., 2000; Iverfeldt, 1991; Lindberg, 1996; Munthe et al., 1995; Rea et al., 1996; St. Louis et al., 2001). Much of the plant-derived deposition is derived from atmospheric elemental Hg uptake, and some contributions may also derived from sorption of GOM (Demers et al., 2013; Ericksen et al., 2003; Jiskra et al., 2015b; Obrist, 2007; Zheng et al.). Several studies have indicated that these additional atmospheric deposition exceeding direct wet deposition in large parts drive spatial patterns of soil Hg distribution (Grigal, 2002; Grigal, 2003; Hararuk et al., 2013; Obrist et al., 2015). In a recent study using nearly 2000 sampling points across the western United States (Obrist et al., 2015), we found that soil Hg concentrations were significantly enhanced (by about a factor 2.5) in forested upland soils compared to shrublands and barren soils, and attributed this to an overwhelming effects plant productivity and vegetation-derived deposition for terrestrial Hg accumulation. These effects are confirmed by (iii) isotopic studies whereby several studies have shown that most Hg stored in litter and soils show a isotopic signature that is consistent with a dominant deposition of elemental Hg by plants (Demers et al., 2013; Enrico et al., 2016; Jiskra et al., 2015a). In soils, these studies also show that contributions Hg from precipitation and dry GOM deposition are consistently low, estimated at 16% in a Wisconsin the northeastern Wisconsin forest (Demers et al., 2013) and only 10% in an northern Sweden forest (Jiskra et al., 2015a). In the first larger-scale isotope study across 10 sites in the contiguous U.S. Zheng et al. (2016) estimate that atmospheric Hg^{II} (i.e., wet deposition and GOM deposition together) account on average for only 20±11% of total soil Hg. Finally, modeling studies (iv) also increasingly show the importance of dry deposition processes. The global-scale GEOS-Chem

model that has been used to assess deposition sources of Hg in Alaska in a previous report (Jaeglé, 2010) estimated that dry deposition of Hg^0 is responsible for 60% of total deposition to Alaska. They estimate wet deposition to Alaska of 7 Tg/yr, in comparison to a dry deposition of 18 Tg/yr. Dry deposition was predicted to be dominated by deposition of Hg^0, in comparison with only 3 Tg yr^{-1} for GOM and PHg deposition. Although the model predicts a higher wet deposition component (i.e., 28%) compared to most field studies (10-20%), the model is consistent that wet deposition is not a dominant deposition pathway.

Recent measurements based on 2 full years of measurements of all major Hg deposition fluxes at Toolik field station funded by the National Science Foundation Arctic Natural Science program ("Collaborative Research: Soil-Snow-Atmosphere Exchange of Mercury in the Interior Arctic Tundra Award Number 1304305; PI: D. Obrist, Co-PI: D. Helmig) support this notion for a high-latitude northern tundra site. Based on continuous micrometeorological measurements using a gradient-based tower system, we find that Hg deposition is strongly dominated by deposition of Hg^0, particularly enhanced by summertime plant uptake. The results are currently prepared for publication in peer-reviewed journals (Agnan et al., in preparation; Hedge et al., in preparation; Obrist et al., in preparation), and will be shared with the state of Alaska after publication.

All these studies show increasing evidence that terrestrial deposition is dominated by deposition of the elemental Hg^0, driven in large parts by plant uptake and subsequent transfer to soils by litterfall and plant senescence. The fact that wet deposition generally accounts for a minor component of terrestrial deposition, in the range of 10-20%, strongly suggests a need for re-assessment of monitoring strategies. In fact, the abundance of wet deposition stations, in comparison to much smaller networks of gaseous monitoring studies, does not seem as an appropriate focus in monitoring efforts. *We conclude that wet deposition is a minor contributor to deposition in most terrestrial ecosystems, and in order to capture the dominant deposition loads monitoring of dry Hg deposition, in particular of the gaseous elemental Hg^0, is needed.*

9 Concentrations of other trace elements at Dutch Harbor (AK00), Kodiak Island (AK98), and Nome (AK04)

9.1. Data coverage, data quality

We analyzed a corresponding data set on deposition of other trace elements at three of the five Hg deposition stations: Dutch Harbor, Kodiak Island, and Nome. Available analysis of other trace elements include the following 10 elements: arsenic (As), beryllium (Be, cadmium (Cd), chromium (Cr), copper (Cu), lead (Pb), nickel (Ni), Selenium (Se), and zinc (Zn). Seven of these trace elements are listed on EPA's list of hazardous air pollutants (EPA, 2016a), including As, Be, Cd, Cr, Pb, Ni, and Se.

In total, there were 132 observations of trace element deposition samples. Dutch Harbor has a total of 24 samples collected between 9/24/20113 through 4/28/2015; Nome has a total of 42 samples between 10/30/2013 and 4/28/2015, and Kodiak Island has a total of 65 samples between 9/17/2013 and 4/28/2015 (**Figure 24**). We assume that the different numbers and large gaps in data coverage are due to low sample volumes collected during deposition samples which often did not allow measurements of these trace metals.

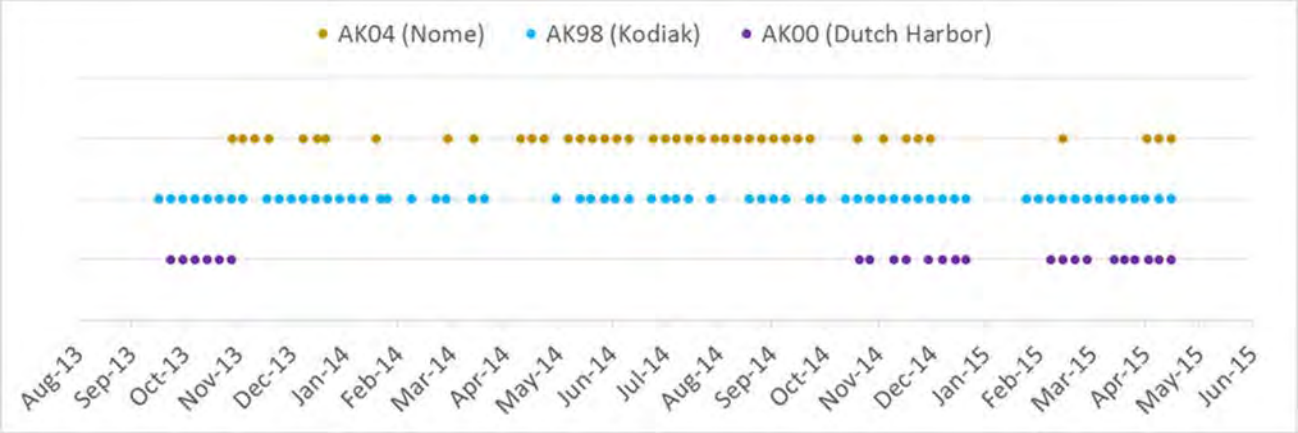

Figure 24. Time series of available trace metal measurements. Gaps in the record correspond to interruptions (>1 week) in sample collection.

A significant number of samples showed trace element concentrations below the detection limit of the analyses. These detection limits are reported as shown in **Table 15**, including the reported limit of detection. The percentage of samples below detection limits are as follows, starting with highest to lowest percentage: Cd: 80%, Be (56%), and Ni 44%, As (36%), and Cr (34%). All other elements have observations below reported detection limits less than 6%. Due to the large number of missing values for Cd and Be, we were not able to conduct a comprehensive analysis of these two trace elements: reasons for this is that any analysis would be highly biased by substitution. A second reason is that when using statistical tests and correlation matrices and PCAs to analyze associations among different trace elements, inclusion of these elements would result in a significant number of missing values.

Table 15. Summary of below detection limit values for each element.

n=131	n < MDL	% < MDL	MDL Mean	MDL Median	MDL Max
Arsenic	47	35.9%	0.02275	0.01	0.06
Beryllium	73	55.7%	0.004794	0.004	0.022
Cadmium	105	80.2%	0.009542	0.008	0.043
Chromium	45	34.4%	0.02389	0.02	0.11
Copper	1	0.8%	0.02389	0.02	0.11
Lead	7	5.3%	0.005954	0.005	0.027
Nickel	57	43.5%	0.04824	0.04	0.22
Selenium	31	23.7%	0.03847	0.02	0.1
Zinc	2	1.5%	0.1909	0.16	0.87
Mercury	0	0.0%	NA	NA	NA

9.2. Trace element summary statistics

For calculations of summary statistics, we performed both substitution of below detection limit (BDL) values with ½ of the detection limit as well as maximum likelihood estimation (MLE) techniques using the NADA package (Lee, 2013) in the statistical software program "R" (R-Core-

Team, 2014). MLE and non-parametric techniques are used to deal with non-detect values since replacement of data (e.g., using ½ detection limits) can be problematic (Helsel, 2012). MLE has been shown to produce unbiased estimates of mean, median, and standard deviation without substitution for minimally censored data sets with n >50 (Helsel, 2012). A lognormal distribution was assumed for MLE estimation.

Across all three stations and deposition samples, we found the following order of median concentrations (MLE-based) of trace elements: Zn (1.40 µg L^{-1}) > As (0.19 µg L^{-1}) > Cu (0.14 µg L^{-1}) > Se (0.06 µg L^{-1}) > Ni (0.04 µg L^{-1}) > Pb (0.04 µg L^{-1}) > Cr (0.02 µg L^{-1}) > Hg (0.002 µg L^{-1}). By far highest concentrations were observed for Zn, which exceeded all other concentrations by more than an order of magnitude. Similarly, by far lowest concentrations were observed for Hg, which was below concentrations of all other elements by at least one order of magnitude. Similar patterns of trace element concentrations, but higher in concentrations, have been observed in snow samples at lower latitudes: for example, in a study in Utah snowpack, Carling et al. (2012) observed highest bulk (unfiltered) concentrations of Ni, in the range of 3-4 µg L^{-1}, with concentrations that exceeded that of other trace metals several fold, and similarly, Hg concentrations were about one order of magnitude below concentrations of other trace elements. In the Everest region in the Himalayas, Lee et al. (2008) similarly observed higher concentrations of Zn (0.48 µg L^{-1}) as well, compared to many other trace elements (e.g., 0.11 for Cr, 0.08 for Pb and Ni, <0.01 for As). Concentrations in the latter study were in similar range as those observed in Alaska. In fresh snow in the French Alps, Veysseyre et al. (2001) observed concentrations of Zn up to 0.75 µg L^{-1}, again the highest compared to other trace metals (e.g., up to Cu: 0.2 µg L^{-1}) although Pb showed some high values in that study as well (max. of 1.76 µg L^{-1}).

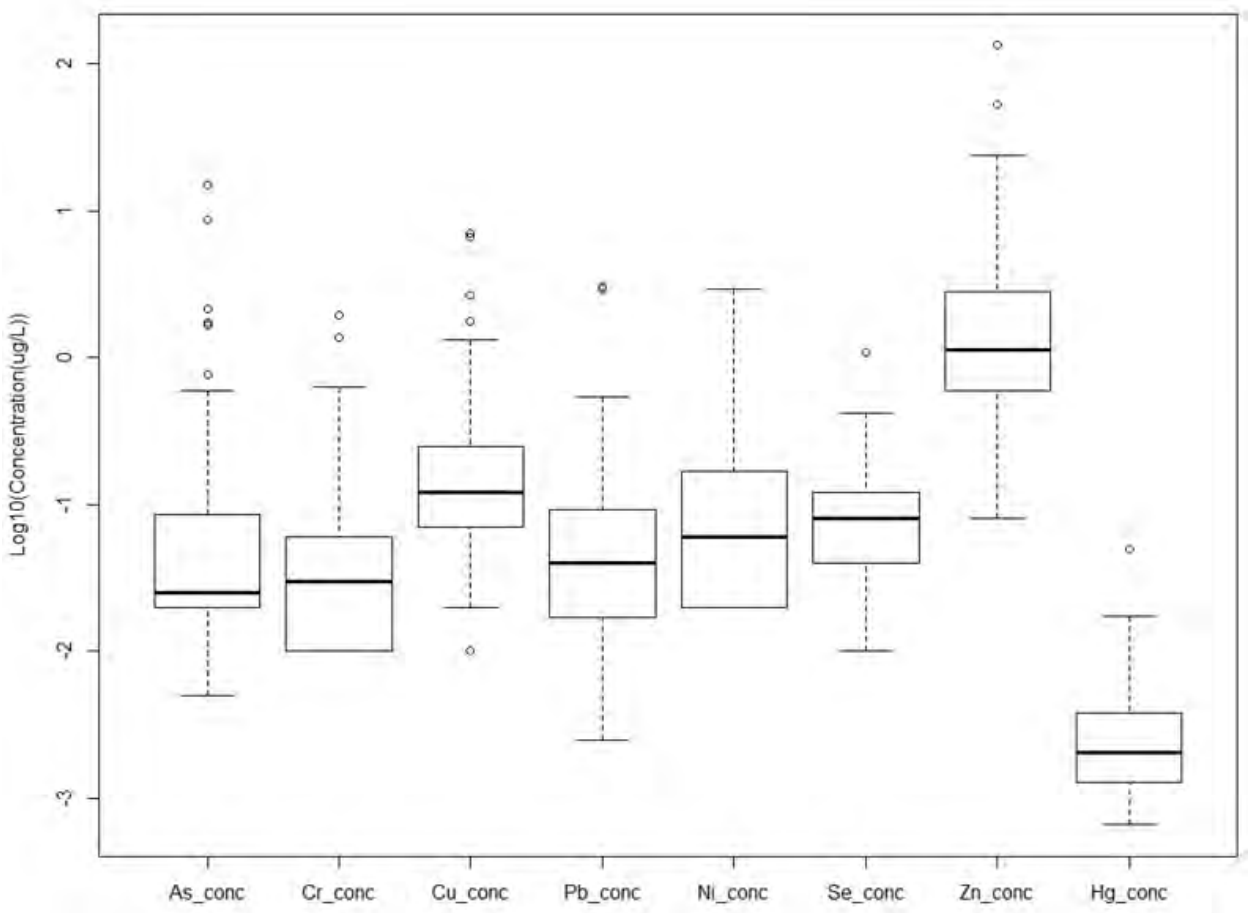

Figure 25. Summary boxplot of trace metal concentrations for all sites.

Table 16. Trace metal summary statistics for all sites using both ½ MDL replacement and Maximum Likelihood Estimation techniques.

½ MDL Substitution					
Concentration (ug L^{-1})	mean	std. deviation	median	min	max
Arsenic	0.29	1.51	0.02	0.00	14.90
Chromium	0.08	0.22	0.03	0.01	1.93
Copper	0.33	0.88	0.12	0.01	7.04
Lead	0.12	0.37	0.04	0.00	3.02
Nickel	0.17	0.37	0.06	0.02	2.90
Selenium	0.11	0.12	0.08	0.01	1.09
Zinc	3.86	12.72	1.13	0.08	133.00
Mercury	0.0038	0.0054	0.0021	0.0007	0.0493

Maximum Likelihood Summary Statistics				
n=131	n < MDL	median	mean	std. deviation
Arsenic	47	0.0216	0.1936	1.7240
Chromium	45	0.0222	0.0793	0.2719
Copper	1	0.1370	0.2525	0.3907
Lead	7	0.0389	0.1080	0.2799
Nickel	57	0.0360	0.2782	2.1331
Selenium	31	0.0635	0.1125	0.1646
Zinc	2	1.4033	2.9077	5.2769

An outlier analysis using the interquartile range (IQR) rule showed the following outlier concentrations (**Table 17**). There were only few points characterized as outliers, i.e., only 1 or 2 (for Se, Cr, Zn, Hg) to a maximum of 6 data points (for As). Similar to the analyses of Hg concentrations, outlier concentrations were observed mainly at very low precipitation amounts, suggesting a quality issue when low amount of wet deposition were collected. For example, the median precipitation of outliers (any of the elements) was 0.46 cm precipitation. In contrast, the median precipitation of all samples was 2.7 cm, or six time larger. Therefore, we find evidence that at low precipitation events, there are some quality issues with samples, likely due to high blanks that result in unusually high concentrations. For further analysis and statistics, we therefore chose to remove outlier concentrations as many statistical tests are sensitive to these.

Table 17. Outlier summary based on 1.5xIQR Rule and ½ substitution of BDL values.

Concentration (ug L^{-1})	Concentration	# of Outliers
Arsenic	0.60	6
Chromium	0.63	2
Copper	1.31	4
Lead	0.54	2
Nickel	2.90	0
Selenium	0.42	1
Zinc	24.00	2
Mercury	0.0174	2

*10 different samples contained outliers and were removed for Correlation, PCA, and Cluster Analyses

9.3. Differences in trace element concentrations between stations

We find statistically significant differences in deposition concentrations between the three measurement stations for all individual elements ($P<0.01$). One-way ANOVAs and Bonferroni post-hoc comparisons show the following statistical differences in concentrations between the stations.

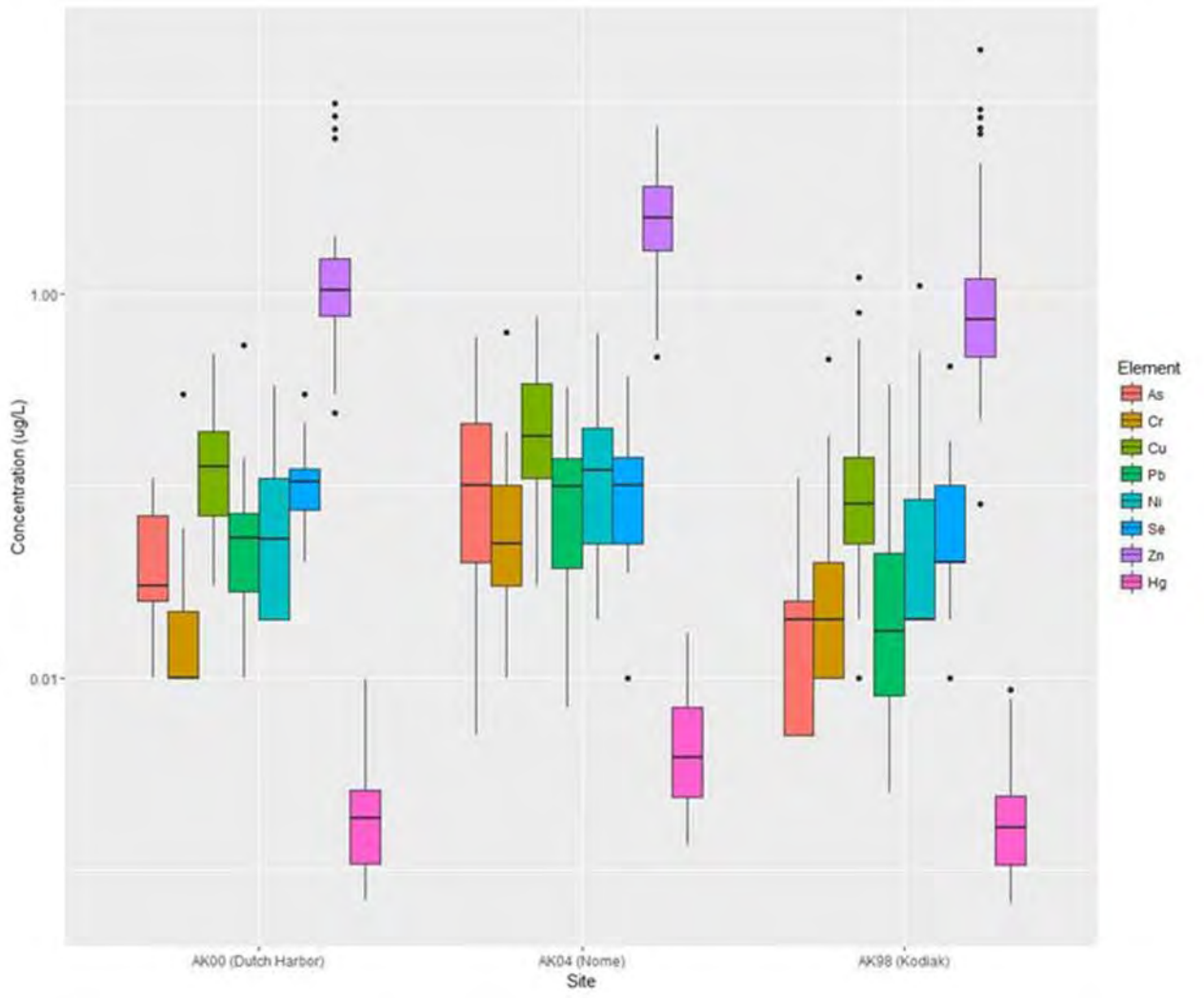

Figure 26. Boxplot of trace metal concentrations separated by site.

Table 18. ANOVA and post-hoc comparison results for each showing significant differences among sites for each individual element.

Log10(Element))~Site

Arsenic (ug L^{-1})	Df	SS	RSS	AIC	F-value	P-value
Site	2	14.794	32.302	-157.8	49.853	<0.001
Post-Hoc Comparisons						
Site	Diff	Lower	Upper	P-value		
Dutch Harbor-Nome	0.4259	0.1806	0.6711	<0.001		
Dutch Harbor-Kodiak	-0.3915	-0.6104	-0.1727	<0.001		
Nome-Kodiak	-0.8174	-1.0133	-0.6214	<0.001		
Chromium (ug L^{-1})	Df	SS	RSS	AIC	F-value	P-value
Site	2	4.2964	21.763	-205.58	14.512	<0.001
Post-Hoc Comparisons						
Site	Diff	Lower	Upper	P-value		
Dutch Harbor-Nome	0.4925	0.2475	0.7375	<0.001		
Dutch Harbor-Kodiak	0.1098	-0.1088	0.3284	0.4602		
Nome-Kodiak	-0.3827	-0.5784	-0.1870	<0.001		
Copper (ug L^{-1})	Df	SS	RSS	AIC	F-value	P-value
Site	2	2.355	17.43	-232.45	9.2173	<0.001
Post-Hoc Comparisons						
Site	Diff	Lower	Upper	P-value		
Dutch Harbor-Nome	0.2043	-0.0233	0.4319	0.0880		
Dutch Harbor-Kodiak	-0.1243	-0.3274	0.0787	0.3172		
Nome-Kodiak	-0.3287	-0.5105	-0.1469	<0.001		
Lead (ug L^{-1})	Df	SS	RSS	AIC	F-value	P-value
Site	2	7.6574	33.531	-153.28	17.461	<0.001
Post-Hoc Comparisons						
Site	Diff	Lower	Upper	P-value		
Dutch Harbor-Nome	0.1767	-0.1215	0.4748	0.3410		
Dutch Harbor-Kodiak	-0.3872	-0.6533	-0.1212	0.0022		
Nome-Kodiak	-0.5639	-0.8021	-0.3257	<0.001		
Nickel (ug L^{-1})	Df	SS	RSS	AIC	F-value	P-value
Site	2	3.5104	27.428	-177.59	8.6593	<0.001
Post-Hoc Comparisons						
Site	Diff	Lower	Upper	P-value		
Dutch Harbor-Nome	0.3148	0.0281	0.6015	0.0277		
Dutch Harbor-Kodiak	-0.0838	-0.3396	0.1720	0.7175		
Nome-Kodiak	-0.3986	-0.6276	-0.1695	<0.001		

Selenium (ug L^{-1})	Df	SS	RSS	AIC	F-value	P-value
Site	2	2.1295	14.899	-251.43	9.8387	<0.001
Post-Hoc Comparisons						
Site	Diff	Lower	Upper	P-value		
Dutch Harbor-Nome	-0.0071	-0.2166	0.2024	0.9964		
Dutch Harbor-Kodiak	-0.2698	-0.4568	-0.0829	0.0024		
Nome-Kodiak	-0.2627	-0.4301	-0.0954	<0.001		
Zinc (ug L^{-1})	Df	SS	RSS	AIC	F-value	P-value
Site	2	4.0216	23.808	-194.72	11.992	<0.001
Post-Hoc Comparisons						
Site	Diff	Lower	Upper	P-value		
Dutch Harbor-Nome	0.2835	0.0227	0.5442	0.0296		
Dutch Harbor-Kodiak	-0.1463	-0.3789	0.0864	0.2982		
Nome-Kodiak	-0.4298	-0.6381	-0.2215	<0.001		
Mercury (ug L^{-1})	Df	SS	RSS	AIC	F-value	P-value
Site	2	3.9168	14.434	-255.27	21.973	<0.001
Post-Hoc Comparisons						
Site	Diff	Lower	Upper	P-value		
Dutch Harbor-Nome	0.4041	0.2140	0.5942	<0.001		
Dutch Harbor-Kodiak	0.0001	-0.1695	0.1698	1.0000		
Nome-Kodiak	-0.4039	-0.5558	-0.2521	<0.001		

Concentrations between Nome (AK04) and Kodiak Island (AK98) were statistically significant different for all elements, with a common pattern that concentration at Kodiak Islands were always lower compared to those observed at the northernmost Nome station. In a similar way, element concentrations between Nome (AK04) and Dutch Harbor (AK00) were statistically different for most elements (for Cu at $P<0.1$), with the exception of the two elements Pb and Se. Similar to the above patterns, concentrations at the lower latitude station Dutch Harbor were consistently lower compared to concentrations at the far-northern Nome station. Further, some elements also showed differences between Kodiak and Dutch Harbor, although these differences were inconsistent.

Site differences for Hg showed strong statistically significant differences between the two northern stations Gates of the Arctic and Nome, compared to Kodiak Island and Glacier Bay further to the south. Therefore, the patterns we observed for mercury are quite consistent and also hold for all other trace elements, although for these we have fewer stations. As discussed in detail some of the differences for Hg were explained by different precipitation patterns among stations. Specifically, precipitation amounts at lower latitude stations are much higher compared to those observed at Nome (i.e., lower weekly precipitation, lower annual sums, lower individual storm sizes). We previously discussed that lower precipitation amounts lead to less wash-out effects explaining enhanced concentrations (section 4.4). To asses if different precipitation patterns are related to differences among stations for other trace elements as well, we calculate correlations of trace element concentrations in the section 10.5. *We conclude that similar to Hg, we observe consistently*

higher trace metal concentrations at the northern stations Nome compared to Kodiak Island further to the south, with concentrations at Dutch Harbor in-between.

9.4. Seasonal differences in trace element concentrations

There were differences in seasonal coverage of deposition samples; for example, fall had the best data coverage with 43 samples overall, followed by spring (33 data points) and winter (33 data points). The lowest data coverage was observed for summer with 21 samples. It is important to note that such different seasonal coverage could potentially induce a seasonal bias. Yet, we find that trace element concentrations were not statistically significantly different across seasons (data not shown).

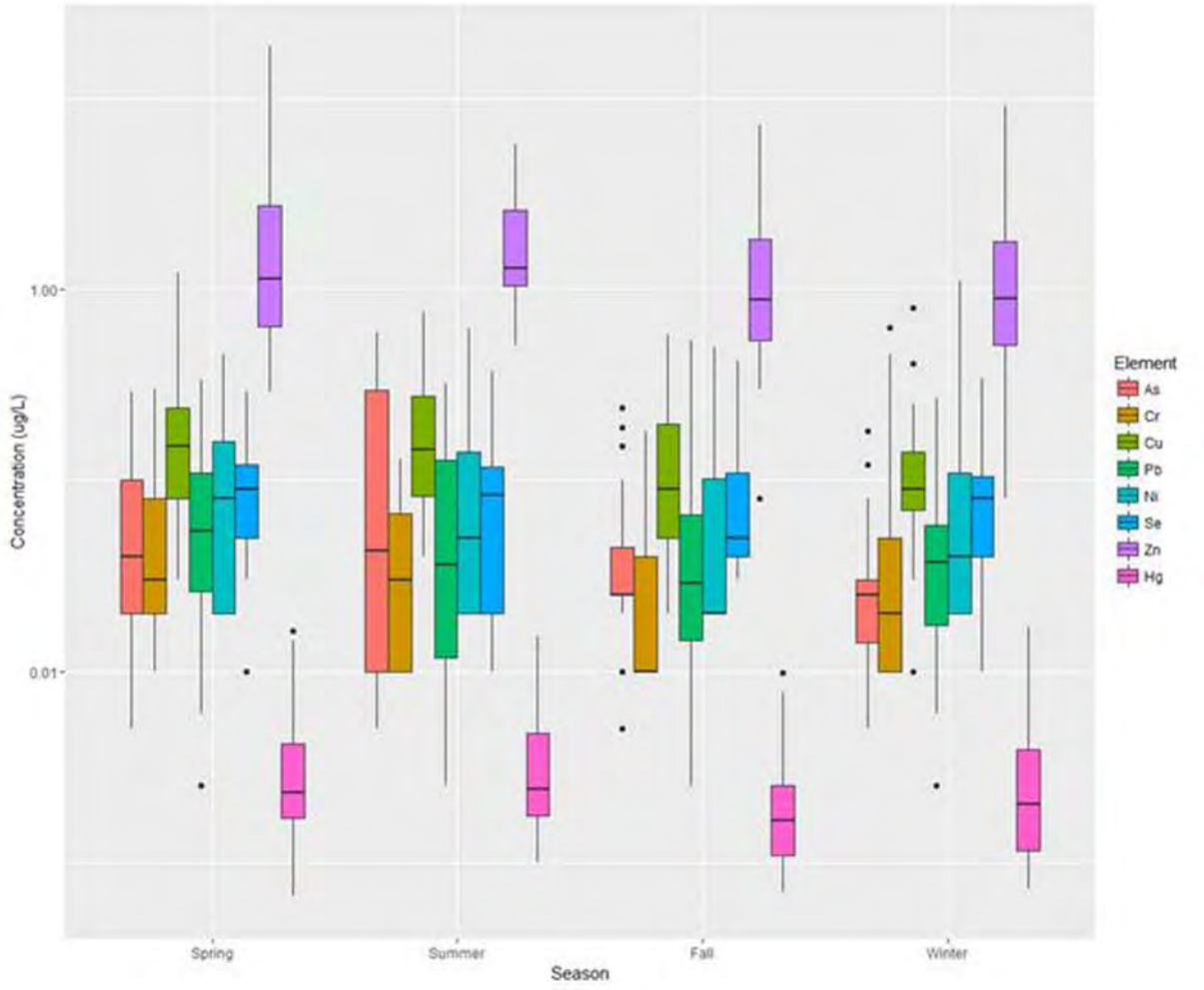

Figure 27. Boxplot of trace metal concentrations separated by season.

The lack of seasonal differences is in stark contrast to statistically significant seasonal differences observed for Hg (section 4.5). It is possible that a lack of seasonal differences, including for Hg in this smaller trace element dataset, is due to relative low sample numbers reducing our statistical power. However, even in this smaller dataset we observe a trend (yet not statistically significant) towards highest Hg concentrations in the summer, followed by spring, winter, and lowest in fall, similar to seasonal patterns described for Hg. Hence, the order of seasonal Hg concentrations of

this smaller dataset is fully consistent with seasonal patterns described for Hg in section 3.4. It is further noteworthy that for all other trace elements as well, we found similar seasonal (yet also not statistically significant) patterns with summer median concentrations consistently highest (with the exception of Ni where summer and spring concentrations were equal; see Figure 25). Further, springtime concentrations of other trace metals also were second highest. Finally, winter and fall concentrations were always lower compared to spring and summer, with some elements showing values less than half of the values observed in summer and spring (e.g., for As and Ni). *We conclude that even though we did not observe statistically significant seasonal differences for any of the trace elements, we find similar trends of highest summer concentrations of all trace elements in summer and spring and lower concentrations in fall and winter, but due to a lack of statistical difference, we did not explore seasonal patterns further.*

9.5. Concentration-precipitation relationships and washout effects

In section 4.4, we discussed that precipitation strongly affected Hg concentrations, which we attributed in large parts to a wash-out effect. We performed similar analyses of the relationships of Hg concentrations and precipitation, and statistically significant relationships between different elements and precipitation are shown in the correlation matrix shown below.

Kendall Tau correlation tests revealed significant negative correlations of elements to weekly precipitation amounts, indicative of wash-out effects. This effect was consistent for Hg in both the full Alaska MDN record and trace metal subset. It is very interesting that Hg shows the strongest correlation to precipitation of all elements, showing strongest P-value and Kendall Tau coefficients. A similarly strong P-value and Tau-value was only observed for Cr. Two further elements, Zn ($P = 0.05$) and Pb ($P = 0.08$) show negative correlations to precipitation as well, but these were only significant at the 10% level. Other elements did not show statistically significant correlations to precipitation (As, Ni, and Cu). Se was the only element showing a significant positive correlation, indicating a substantially different behavior of Se compared to all other elements.

The different behavior of these elements in regard to precipitation are somewhat puzzling. For example, sources for both Cr and Ni have been are considered both driven by crustal (i.e., dust) contributions, and we find that this is likely also the case for observed wet deposition in Alaska (see section on enrichment factors below). If this is the case, we would expect similar behavior of these two elements in regards to potential washout effects, but this is not the case. Therefore, the patterns of this analysis is somewhat inconclusive. Yet, there are two important points that merit further discussion: first, Hg, a trace element which is well known to have a variety of different forms in the atmosphere (particulate and gaseous forms in various oxidation states) is the element that shows the strongest washout effect compared to all other elements, many of which occur either uniquely in particulate-phases or have minor gas phases only (e.g., As). Therefore, the strong washout effect for Hg may be unique and is apparently not present in similar magnitudes in most other elements that are mainly dominated by particulate forms. It is possible that this difference indicates a significant contribution to Hg deposition through precipitation-scavenging of gaseous forms, in particulate GOM with its high solubility.

Second, the only other element with a significant gas phase, Se, is the only element that shows a positive concentration dependence to precipitation amounts. Se is quite different to most other trace elements reported here: Se has a number of natural and anthropogenic sources, but natural sources of Se are dominant on a global scale accounting for 50-65% of total emissions (Mosher et al., 1987). Especially in marine environments such as in the Pacific Ocean, it was found (Mosher et al., 1987) that Se is related to primary productivity due to volatile methylated emissions from the water, which dominate over the oceans as compared to transport from continental sources. In fact, marine biogenic Se is the dominant natural source accounting for 5000-8000 tons (Mosher et al., 1987). In addition, there are significant Se emissions from wetlands, although this source is much smaller (Vriens et al., 2014). It is well possible that the unique marine source of Se, maybe in conjunction with its unique gas phase or gas-to-particulate condensation, explains the different relationship of Se to precipitation compared to all other trace elements. *We conclude that wash-out effects are visible in some trace elements, with Hg showing the strongest dependence on precipitation and other elements such as Cr, Zn, and Pb also showing negative correlations of concentrations to precipitation amounts. Se, a unique trace element with a strong ocean degassing source, is the only element that shows a positive correlation of concentrations to precipitation.*

9.6. Correlation matrix among trace elements

In this section, we analyze relationships of wet deposition concentrations among different trace elements using Kendall's Tau correlation matrices. Non-parametric Kendall Tau testing was performed to account for the high number of BDL values and tied rankings. Overall, concentrations of elements are all significantly and positively correlated to each other, both when using P-values adjusted for multiple comparisons as well as when using unadjusted values (**Table 19**, **Figure 28**). Two exceptions are lack of correlations between Hg to Se and Hg to Pb. Yet, most of these correlations are very weak with low correlation coefficients. A detailed look, however, shows that some associations among elements are much stronger than others. Patterns of strong correlations suggests commonalities of element either respective to their sources or, alternatively, in respect to their environmental fate such as, for example, atmospheric scavenging processes.

Based on Kendall Tau's values we delineate two groups of elements that seem closely associated: the strongest Tau is between As and Pb, with a Tau-value of 0.62. This correlation is quite strong considering that the data is measured across three different stations, across different seasons, and across different years. The close association may support similar source origins for these two elements. Sources for both elements are considered mainly from anthropogenic sources: for As, major sources include coal combustion processes and metal smelters (Wai et al., 2016; Walsh et al., 1979), and similarly Pb sources include metal smelters, waste incinerators, utilities, and others (EPA, 2016b). In environmental matrices such as snow, ice, and even lichen, both As and Pb are often attributed to anthropogenic sources (Agnan et al., 2015b; Carling et al., 2012; Veysseyre et al., 2001). We therefore interpret the correlation between As and Pb to common sources. Interestingly, for As a recent modeling study has attributed 70% to 80% of total As deposition over the western part of North America and 39% of arctic region deposition to long-range transport of anthropogenic Asian emissions (Wai et al., 2016). In addition, Cu and

Se also show strong correlation with As. We already discussed that Se sources are distinctly different from those of As and Pb.

Another strong correlation is observed between Cr and Ni. Both of these elements are often associated with crustal sources; for example, they show small Enrichment Factors (see section below) in comparison to typical geogenic tracers such as Al, Fe, or Ti and as such have been attributed to be dominated by natural dust deposition (Agnan et al., 2015b; Carling et al., 2012; Veysseyre et al., 2001). No other elements show Tau-values of 0.5 with either Cr or Ni. We therefore suggest that the associations between Cr and Ni may be driven by a common crustal source of these elements, which is not mirrored in any of the other elements.

Table 19. Kendall Tau correlation matrix showing relationships between all elements.

Kendall's Tau	Arsenic	Chromium	Copper	Lead	Nickel	Selenium	Zinc	Mercury
Arsenic								
Chromium	0.31							
Copper	0.39	0.36						
Lead	0.62	0.29	0.47					
Nickel	0.33	0.56	0.41	0.33				
Selenium	0.46	0.27	0.41	0.49	0.36			
Zinc	0.36	0.32	0.5	0.41	0.42	0.29		
Mercury	0.18	0.28	0.21	0.17	0.26	0.07	0.24	
Prcp (mm)	-0.23	-0.29	-0.21	-0.09	-0.26	-0.02	-0.28	-0.25

P-values	Arsenic	Chromium	Copper	Lead	Nickel	Selenium	Zinc	Mercury	Prcp
Arsenic		0.010	<0.001	<0.001	0.010	<0.001	<0.001	0.240	0.080
Chromium	<0.001		<0.001	0.020	<0.001	0.030	0.010	0.030	0.020
Copper	<0.001	<0.001		<0.001	<0.001	<0.001	<0.001	0.140	0.140
Lead	<0.001	<0.001	<0.001		<0.001	<0.001	<0.001	0.270	0.970
Nickel	<0.001	<0.001	<0.001	<0.001		<0.001	<0.001	0.050	0.050
Selenium	<0.001	<0.001	<0.001	<0.001	<0.001		0.020	0.970	0.970
Zinc	0.000	<0.001	<0.001	<0.001	<0.001	<0.001		0.070	0.030
Mercury	0.050	<0.001	0.020	0.070	<0.001	0.480	0.010		0.060
Prcp (mm)	0.010	<0.001	0.020	0.320	<0.001	0.790	<0.001	0.010	

*Lower-left not adjusted for multiple tests
**Upper-right adjusted for multiple tests.

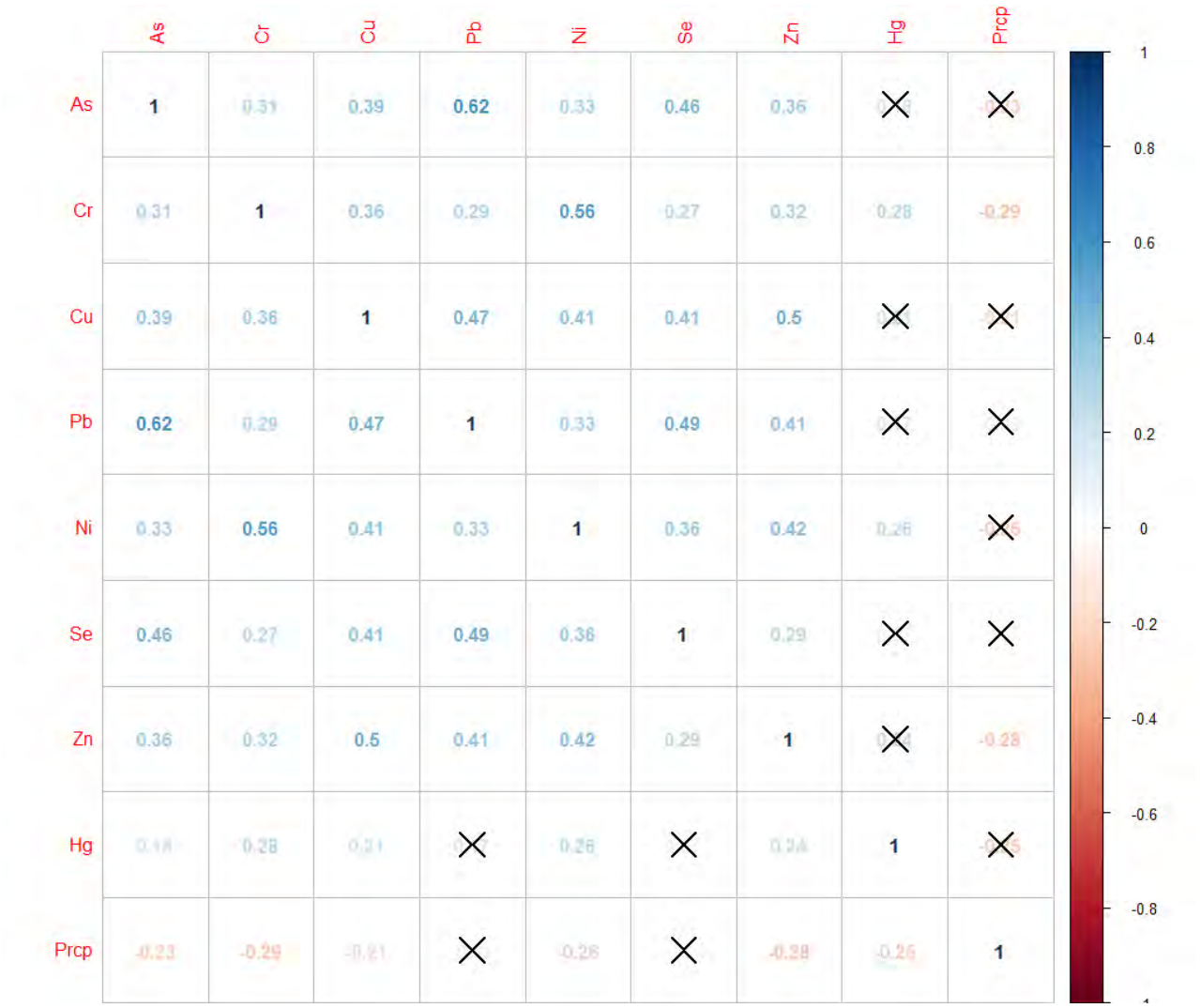

Figure 28. Kendall Tau correlation matrix summary figure. X's signify non-significant results. Lower-left significance testing is not adjusted for running multiple tests. Upper-right significance testing is adjusted for running multiple tests (Holm-Bonferroni).

9.7. Principal component analyses of the full trace element concentration dataset

In this section, we use Principal Component Analysis (PCAs) to further explore commonalities of elements, both using the entire dataset across the three stations as well as for individual stations. According to Reimann et al., (2008), large geochemical dataset can use PCA to graphically inspect the data and reduce data into few components that explain as much variability of the complete data set as possible.

The first PCA using all data from all three station shows four principal components with eigenvalues above 1, whereby the most important two components are graphically shown in **Figure 29**. The first principal components has an eigenvalue of 2.4 and explains 30% of the overall variance of the data set. Principal component two has an eigenvalue of 1.5 explaining 19% of the data variance; finally, a third component has an eigenvalue of 1.4 and explains 14% of the variance. The graphical representation show a separation of several elements along the first component

(representing the x-axis for both panels), most pronounced by Ni and Cr on one side of the axis and Pb and As that are on the opposite side of the first component. Along this separation, we find weaker associations of Hg along with Ni and Cr, and on the opposite side of Se with Pb and As. The first component of this PCA therefore is very consistent with the correlation matrix shown in **Figure 29**, showing the relatively strong association of Ni and Cr on the one hand and As and Pb on the other hand. We interpret this analysis the same way as above: Ni and Cr may be associated due to their common source profile, possibly driven by crustal, natural sources. Interestingly, Hg is slightly located along that component as well, yet the factor loading for Hg is very weak (also note the weak correlation coefficient in the correlation matrix above). Therefore, we would not suggest that Hg is primarily drive by similar natural sources as Ni and Cr. On the opposite loading of this first principal component we find Pb and As; again, this association, as well as their different loading on the first component, would be consistent with a different source origin. As discussed above, we suggest that As and Pb are primarily driven by anthropogenic, industrial emissions sources such as smelters and combustion processes, and that these may at least in part be derived from long-range transport from Asia.

It is possible, however, that factor loading are also related to site effects, since we did not find fully consistent patterns of elements across different sites. To repeat, we observed that (i) all elements were statistically higher in concentrations at Nome compared to Kodiak Island; (ii) all elements except Pb and Se were statistically higher at Nome compared to Dutch Harbor; but (iii) only As, Pb, and Se were statistically higher at Dutch Harbor compared to Kodiak Island. It is therefore possible that factor 1 may reflect a somewhat different behavior of As, Pb, and Se compared to most other elements (or particularly Ni and Cr). To test to what degree component 1 is related to such site differences, we used the graphical representation of biplots, which allows to visualize scores and directions of principal component analysis simultaneously, including separation of scores and loadings by major groups to determine grouping of variables and driving processes. In the biplot below, we visualize principal components 1 (x-axis) and 2 (y-axis), and group the scores and loading by sites represented by different colors. The graph indicates that among principal component 1, we observe very little separation of the two locations Kodiak Island (AK98) and Dutch Harbor (AK00), with the third locations Nome (AK04) located in-between. Therefore, we don't consider that site differences are responsible for the different component loadings.

In support of this, we find that the same first component separating Cr and Ni from As and Pb is consistent across all sites individually. In all site-specific PCAs, principal component 1 always shows eigenvalues above 2 and explains between 25 and 33% of the variability in each respective datasets. A consistent pattern at all three sites is the strong loading of Ni and Cr on one side of the first component and the opposite loading of As and Pb. Therefore, the patterns observed in the PCA 1 in **Figure 29** is evident at each station individually, in support of different source origins that consistently affect all stations. In contrast to the consistent patterns for Ni and Cr and As and Pb, none of the other elements are consistently associated across the three individual sites. Hg, Cu, Se, and Zn show highly different loadings and locations. *We conclude that across all sites, we find two distinct profiles with Cr and Ni versus As and Pb, which we attribute to possibly different source origins, with Ni and Cr possibly driven by crustal (e.g., dust sources) and As and Pb determined by anthropogenic inputs possibly enhanced by long-range transport from Asia.*

Mercury nor any of the other trace elements is not consistently associate with either of the four other elements suggesting more diffuse and possibly different source origins.

Table 20. Rank-based principal component analysis summary show % variance explained by each factor for PCA containing all sites and each site separately.

% Variance Explained			
	Component 1	Component 2	Component 3
All Sites	54.55	14.29	8.99
AK00 (Dutch Harbor)	45.85	15.00	12.47
AK04 (Nome)	59.44	12.67	10.90
AK98 (Kodiak)	39.93	19.52	13.01

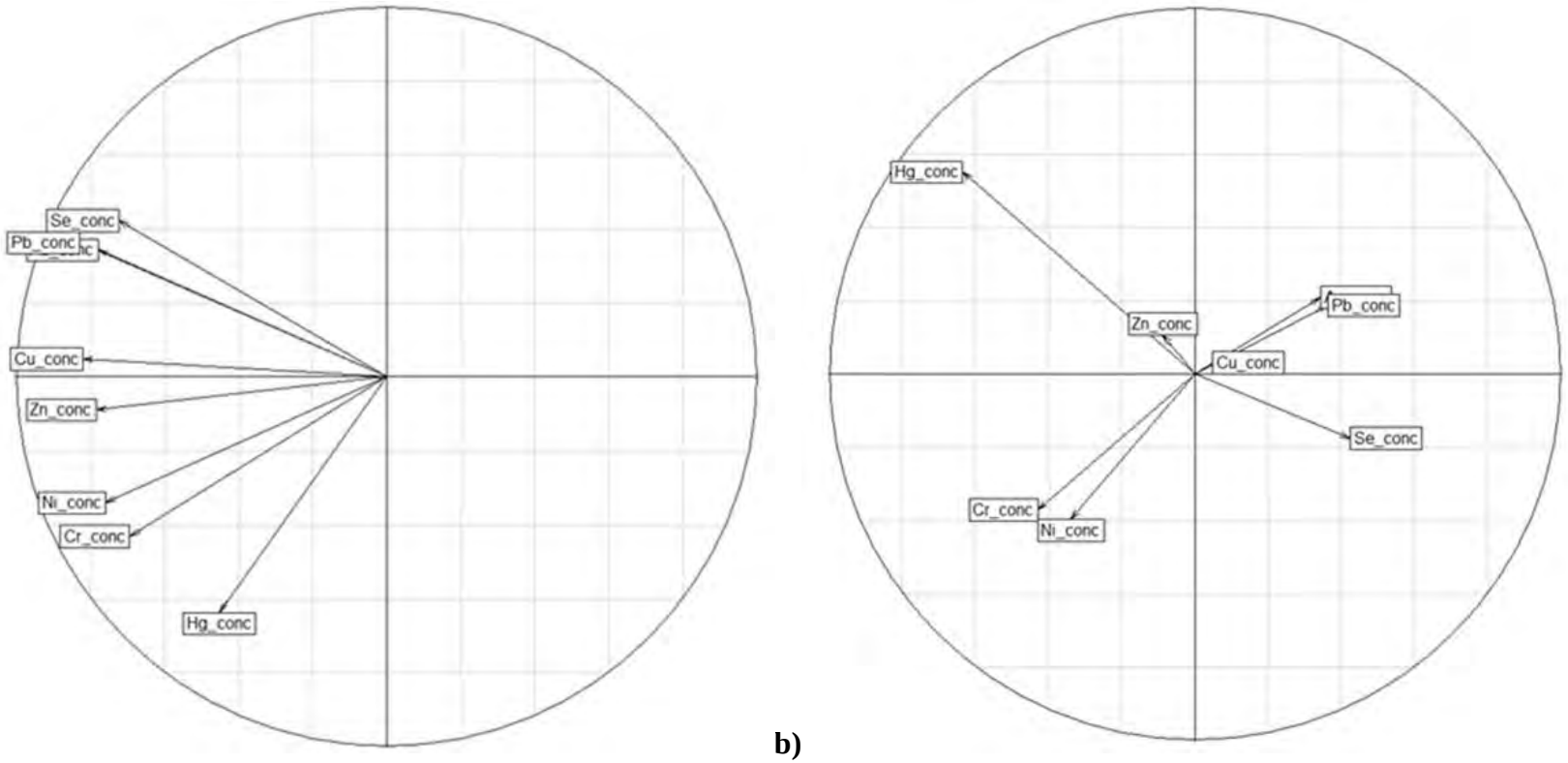

a) **b)**

Figure 29. Trace metal rank-based principal component analysis bipolots for all sites: a) component 1 versus component 2 b) component 2 versus component 3.

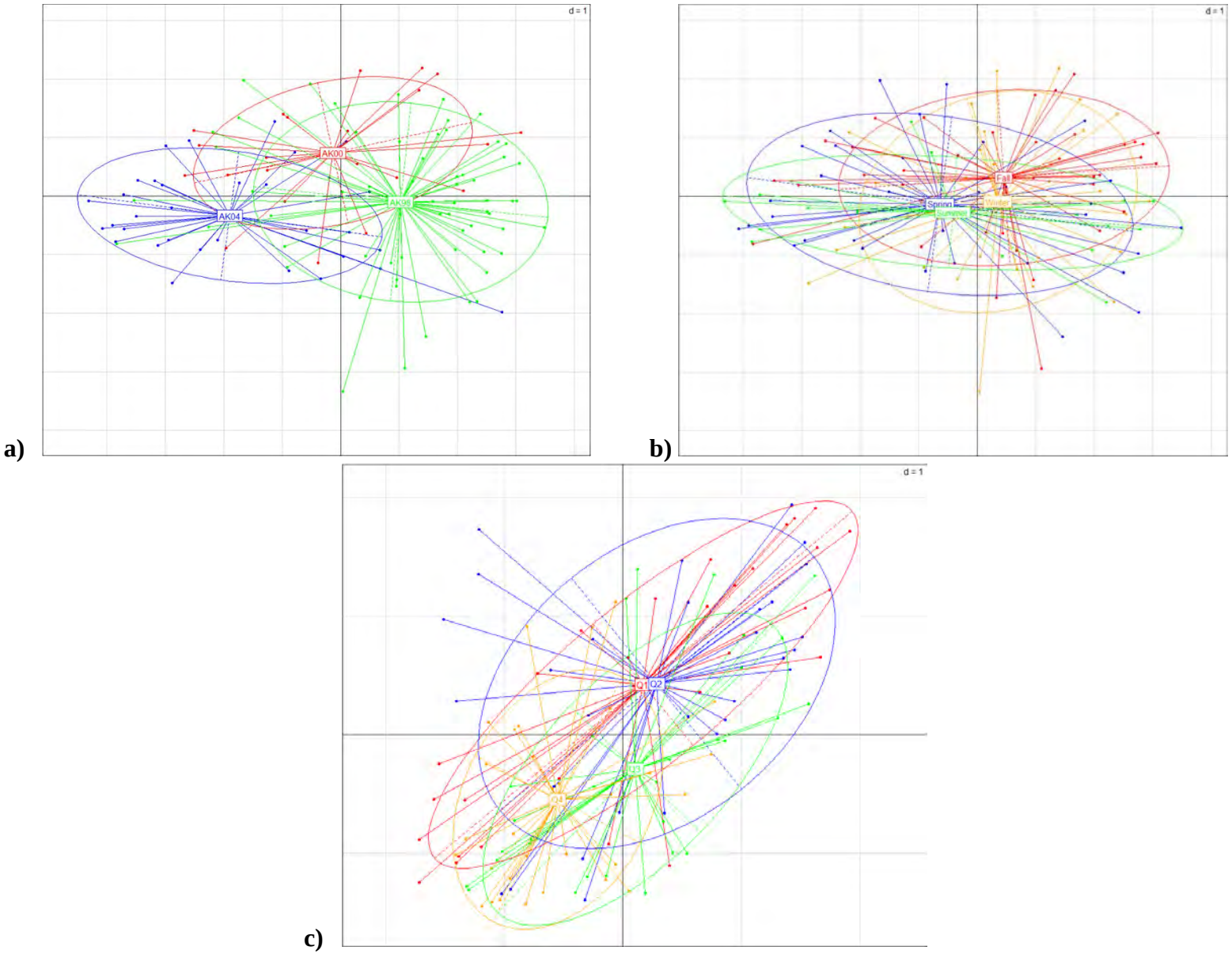

Figure 30. PCA biplots of component 1 versus component 2 grouped by a) site, b) season, and c) precipitation quantile.

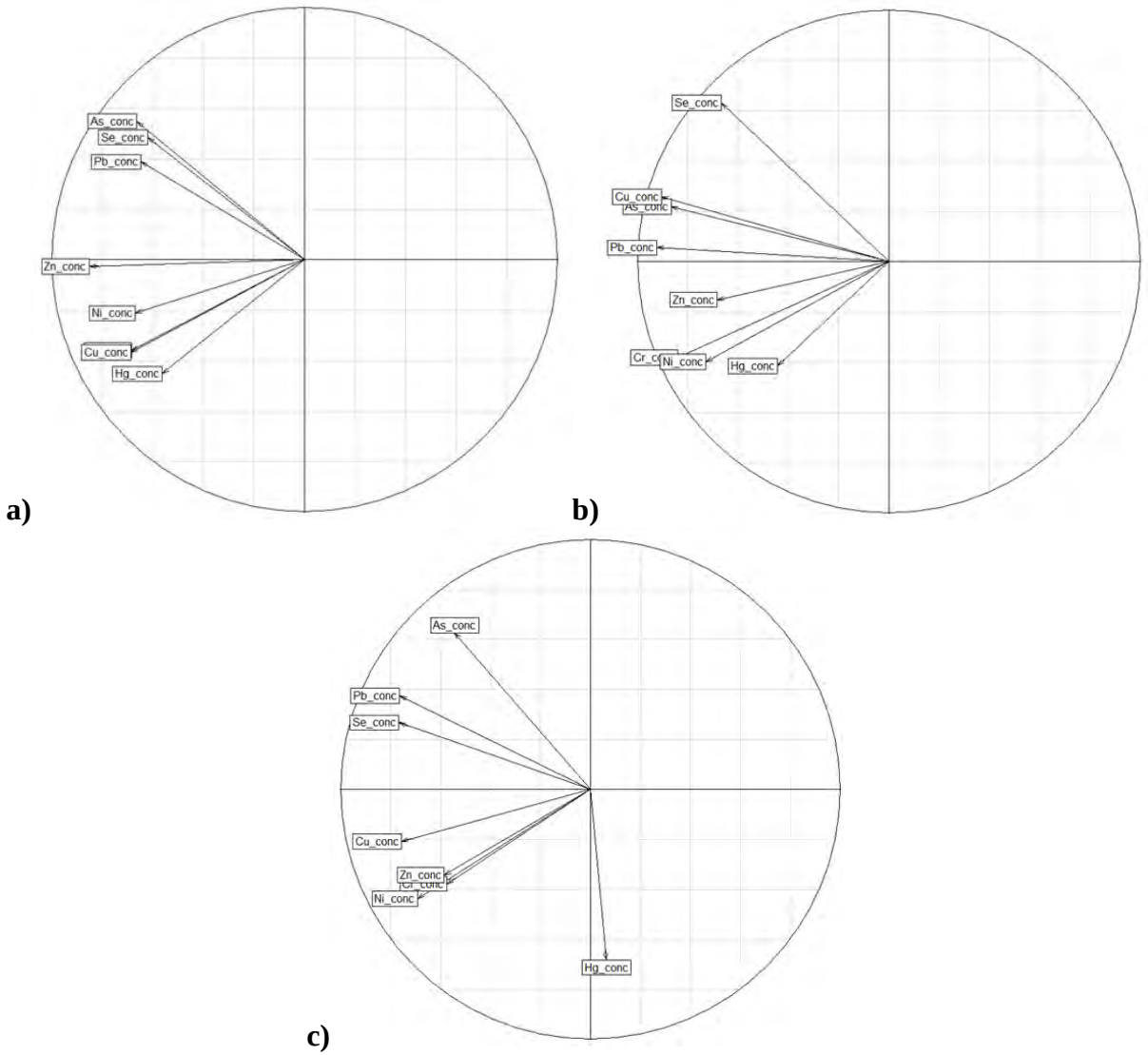

Figure 31. Trace metal PCA biplots showing component 1 versus component 2 for a) Dutch Harbor, b) Nome, and c) Kodiak Island.

9.8. Enrichment factors of trace elements to assess geogenic (dust) and other sources including anthropogenic contributions

A supporting analysis of the notion of natural dust origins versus anthropogenic sources can be derived from calculations of enrichment factors. The method of upper continental crustal enrichment factors, (EF_{ucc}), calculates ratios of elements of interest to a conservative crustal element such as Al. Al is a good tracer for crustal and rock elements, and as such can indicate crustal contributions such as from dust. Using normalized ratios of other elements to that of upper continental crust (Wedepohl, 1995), the method calculates enrichments of elements above what is expected from purely natural sources. Enrichment factors are calculated following equation 3 (e.g., Carling et al., 2012):

Equation 3:
$$EF_{ucc} = \frac{{}^{[X]_s}/_{[Al]_s}}{{}^{[X]_{ucc}}/_{[Al]_{ucc}}}$$

Unfortunately, the dataset on wet deposition we have available does not have data for Al nor other commonly used conservative geogenic tracers such as Ti or Fe. In order to still perform calculations of enrichment factors, we decided to use Cr and Ni instead as two possible reference elements. Both these elements often show low enrichment factors compared to Al, indicating similar crustal sources as observed for Al, (Agnan et al., 2015b; Carling et al., 2012; Veysseyre et al., 2001). Uncertainties in the methodology includes that local or regional soil elemental composition can be different from used reference crustal composition.

Calculated EF_{ucc} are shown in **Figure 32** for all data from all three stations. EF_{ucc} between 0.1 to 10 are often indicated that dominant sources are from soils, dust, or rocks; high EF_{ucc} values are indicative of other natural or anthropogenic sources, whereby ratios between 10 to 500 are moderately enriched and values above 500 are strongly enriched and indicative of anthropogenic contributions (Carling et al., 2012; Lee et al., 2008). Based on this, we would classify Cr, Pb, and Ni with median values below 10 primarily deriving from crustal contributions. The only element we would clearly characterize as strongly enriched compared to crustal composition is Se with a median EF_{ucc} of 1054. Moderately enriched EF_{ucc} factor are observed for Cu, As, Zn, and Hg, with EF_{ucc} values between 11 to 57. **Figure 32** shows that the range and order of EF_{ucc} is very consistent among the three stations, always showing a separation of element with distinctly different EF_{ucc} values: low values for Cr, Pb, and Ni, median ranges for Cu, As, Zn, and Hg, and the highest value for Se.

This analysis suggests that the clustering of the elements Cr and Ni in the PCA analysis above is in fact likely to be driven by their common crustal origin. The results are in partial support of the notion that opposite loading on the first principal component for Se and As could in part be driven by other sources (natural [e.g., for Se] or anthropogenic [e.g., for As]) sources. Yet, the analysis would not be in support of the PCA results that Pb also is driven by other sources than crustal contributions as low EF_{ucc} for Pb suggests primarily crustal sources similar to Cr and Ni. *We conclude that enrichment factors for Cr and Ni are showing low enrichment factors in support of predominantly crustal sources, while high enrichment factors for Pb and Se suggest additional*

anthropogenic and natural sources. For most other elements enrichment factors are in-between not indicating clear crustal or anthropogenic sources.

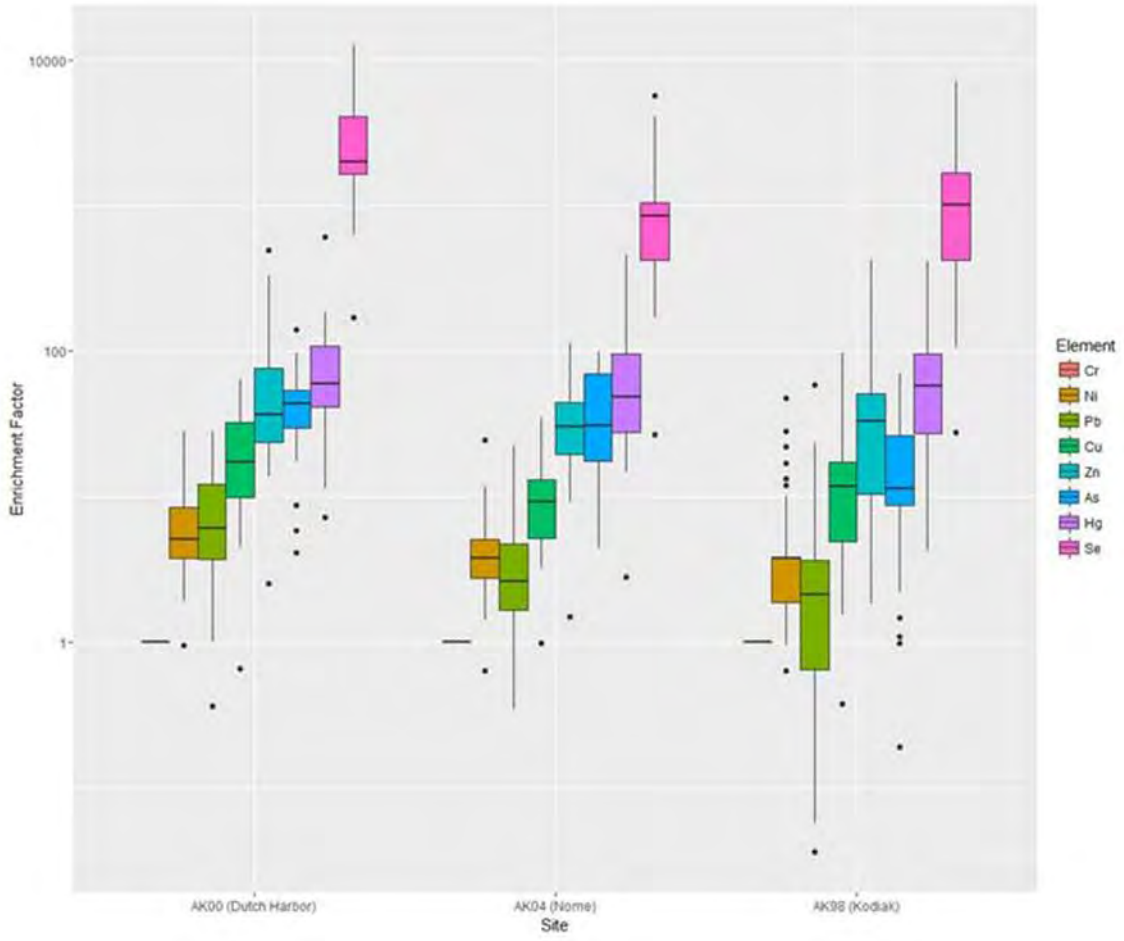

Figure 32. Summary boxplot of enrichment factors separated by site. Enrichment factors are calculated using Chromium as the conservative tracer.

9.9. Annual deposition sums of trace elements in Alaska

Here, we estimate annual deposition loads for all trace elements. We follow similar protocols that we use in section 5 for calculation of Hg deposition; annual deposition is based on precipitation-weighed concentrations for each station, multiplied by annual deposition. We use the MDN provided annual precipitation for 2014 for all stations and calculate precipitation-weighed concentrations based on NADP protocols.

However, due to the much lower number of samples, it needs to be emphasized that these annual deposition loads are not fulfilling the data coverage normally needed to fulfill quality measured given for example by MDN. For example, these deposition loads are only based on 24 observations of concentration measurements at Dutch Harbor, 22 observations at Nome, and 64 observations at Kodiak Island, and therefore would not fulfill the ≥75% concentration coverage required by the MDN. The lower temporal coverage also can bias numbers seasonally (e.g., the majority of the

Dutch observations occur during winter between Oct-April, while observations at Kodiak Island are more evenly distributed throughout the year.

Table 21. Annual deposition estimates for each trace metal. Precipitation-weighted mean concentrations were calculated separately for each site using all available data and combined with average annual precipitation from NADP MDN annual precipitation totals.

	Dutch Harbor (AK00)	Nome (AK04)	Kodiak (AK98)
Precipitation (mm)	1657.4	380.0	2249.4
PWM (ug L^{-1})			
Arsenic	0.0373	0.1514	0.0172
Chromium	0.0209	0.0964	0.0292
Copper	0.1436	0.2351	0.1090
Lead	0.0748	0.0968	0.0346
Nickel	0.0757	0.1207	0.0575
Selenium	0.1011	0.1154	0.0630
Zinc	1.4429	2.3080	1.0600
Mercury	0.0016	0.0055	0.0029
Deposition (μg m^{-2})			
Arsenic	61.77	57.53	38.70
Chromium	34.56	36.64	65.66
Copper	237.96	89.34	245.18
Lead	123.99	36.79	77.76
Nickel	125.54	45.86	129.25
Selenium	167.50	43.84	141.63
Zinc	2391.47	876.97	2384.35
Mercury	2.65	2.08	6.43

Still, calculated deposition loads show patterns that are mostly consistent with observations of Hg deposition described before. In general, the two more lower latitude stations Dutch Harbor and Kodiak Island receive the highest deposition loads, in agreement with higher precipitation loads, although the order between Kodiak and Dutch Harbor is not consistent: Kodiak Island, the station with the highest precipitation in 2014, receives highest deposition of Cr, Cu, Ni, and Hg, while Dutch Harbor receives highest deposition loads of As, Pb, Se, and Zn. The lowest trace element deposition are generally observed for Nome analogue to its low precipitation, although an exception to this is As that shows higher deposition compared to Kodiak and almost similarly high loads as Dutch Harbor. We previously determined that Nome is influenced by Asian long-range transport for Hg deposition (section 7.2.), and it is possible that the relatively high As deposition observed at Nome may be further evidence of Asian influence given that models predict high proportions of As depositions in the western U.S. and the arctic due to Asian outflow (Wai et al., 2016). It is possible that the relatively higher deposition of As, Pb, and Zn at Dutch Harbor may

be related to such long-range transport effects, and that the high Se deposition at that station may be related to its proximity to ocean evasion sources (Mosher et al., 1987). Yet, without further detailed analysis, and given the sparse data coverage of deposition records for these stations that complicate estimation of annual deposition loads, these conclusions need further confirmation. *We conclude the order of annual deposition of other trace metals can deviate from that of Hg which was very closely linked to precipitation patterns. Relatively high deposition of As at Nome relatively higher levels at Dutch Harbor of As, Pb, and Zn may be related to Asian sources, and higher deposition of Se at Dutch Harbor may be related to its proximity to Ocean evasion sources. However, given the sparse data record available to calculate annual deposition loads, this needs further confirmation.*

9.10. Summary backtrajectory frequencies for trace metal deposition for all three stations for 2014

We performed similar backtrajectory analysis for select elements for the year 2014 as we performed for Hg in section 7.2. The frequency maps for all measured deposition events for 2014 are given in the figures below. Please note that due to fewer data points, we decided to combine the trajectory analysis for all three stations.

The trajectory analyses are in support of the patterns described above. For Cr and Ni, for example, we notice a diffuse source patterns that is widely distributed over the Pacific Ocean, the Gulf of Alaska, and Bering Sea, without any clear source zones that are particularly highlighted from specific areas. However, for these elements, we also did not observed specific continental origins of deposition loads as might be expected if =dust contributions were a major source. Arsenic is an example of an element that shows contributions from the western Pacific Ocean, which would be in support of above hypothesized and referenced long-range transport sources and contribution from east Asian emissions, and to a lower degree some influence is also observable for lead as well, although not nearly as strong. Finally, for Se, we did not observe a particularly different source origin compared to most other trace elements, in spite of its potentially ocean-driven, natural sources; yet, all major contributions occur from ocean areas for Se. *We conclude that backtrajectory frequency analyses are in support of an influence of Asian long-range transport contributions for As and Pb, similar to what we previously observed for Hg deposition for the station Nome, and that all other trace elements seem to have diffuse source origins that are mainly located over the upwind ocean areas.*

Chromium-weighted Frequency Map

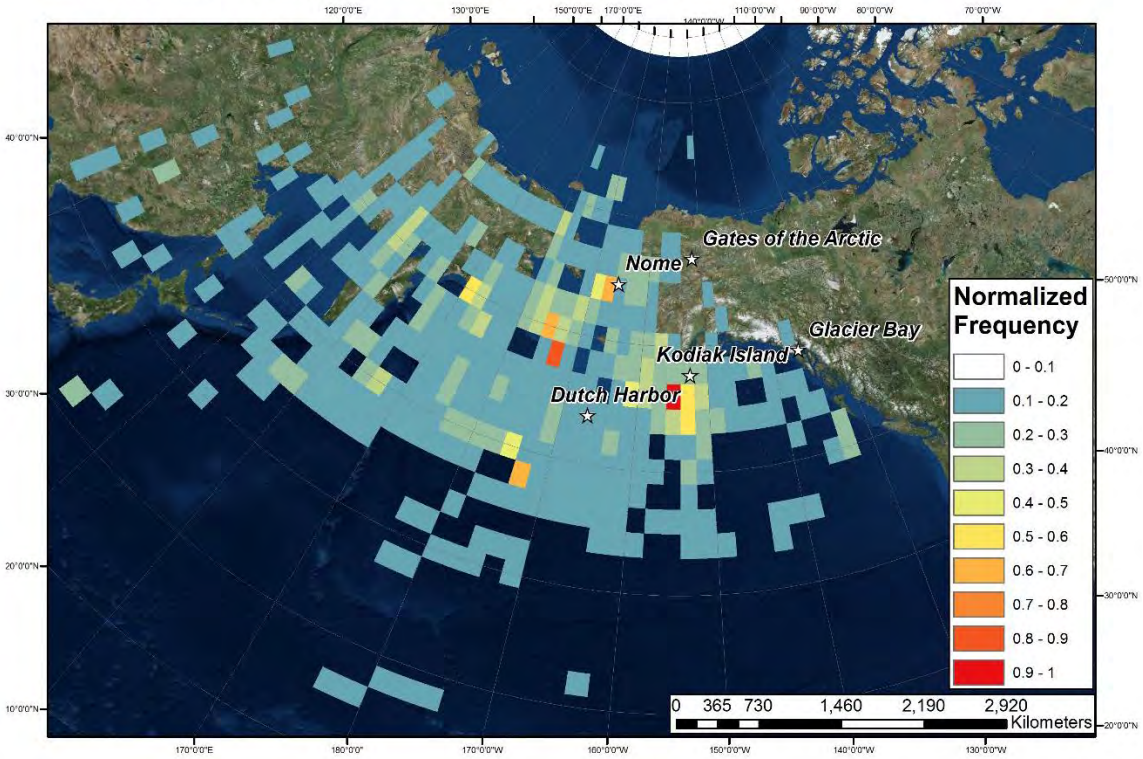

a)

Nickel-weighted Frequency Map

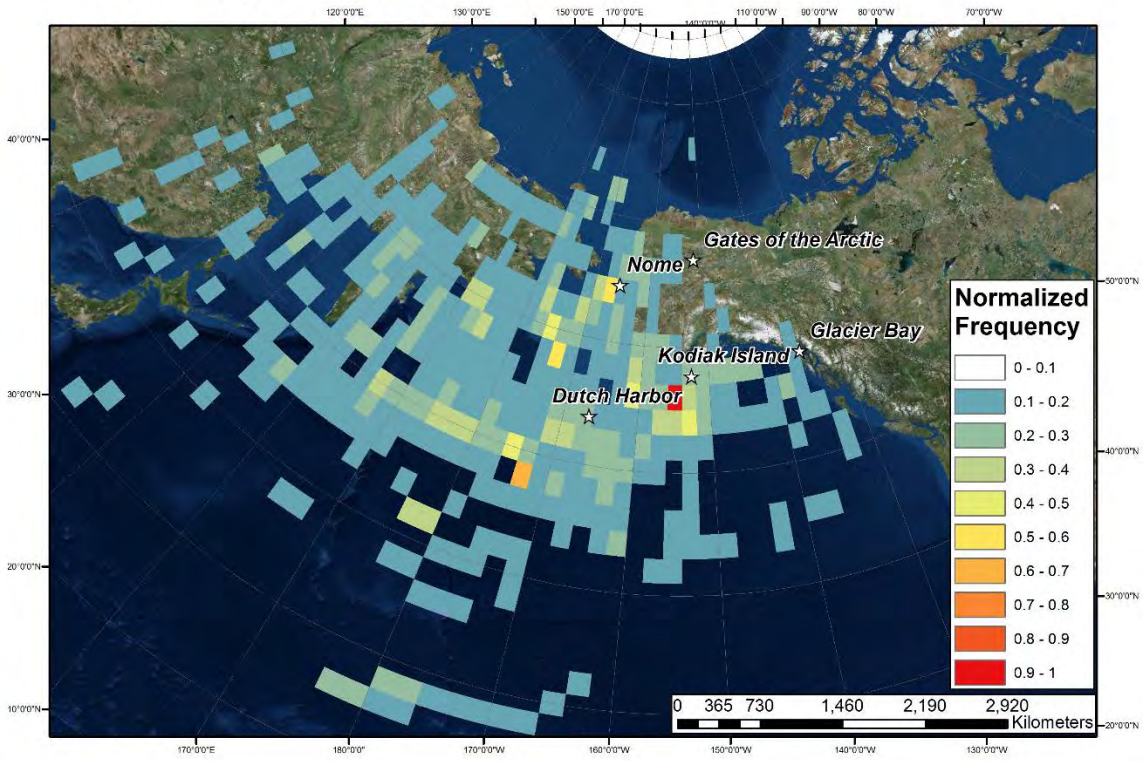

b)

Lead-weighted Frequency Map

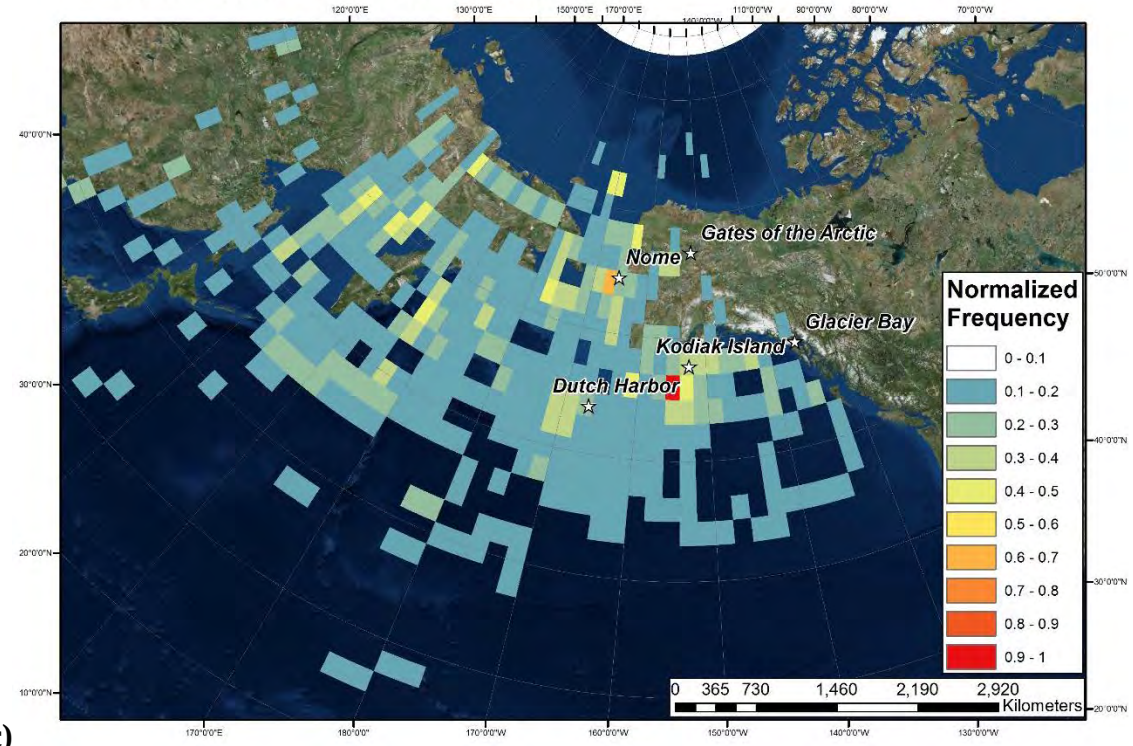

c)

Arsenic-weighted Frequency Map

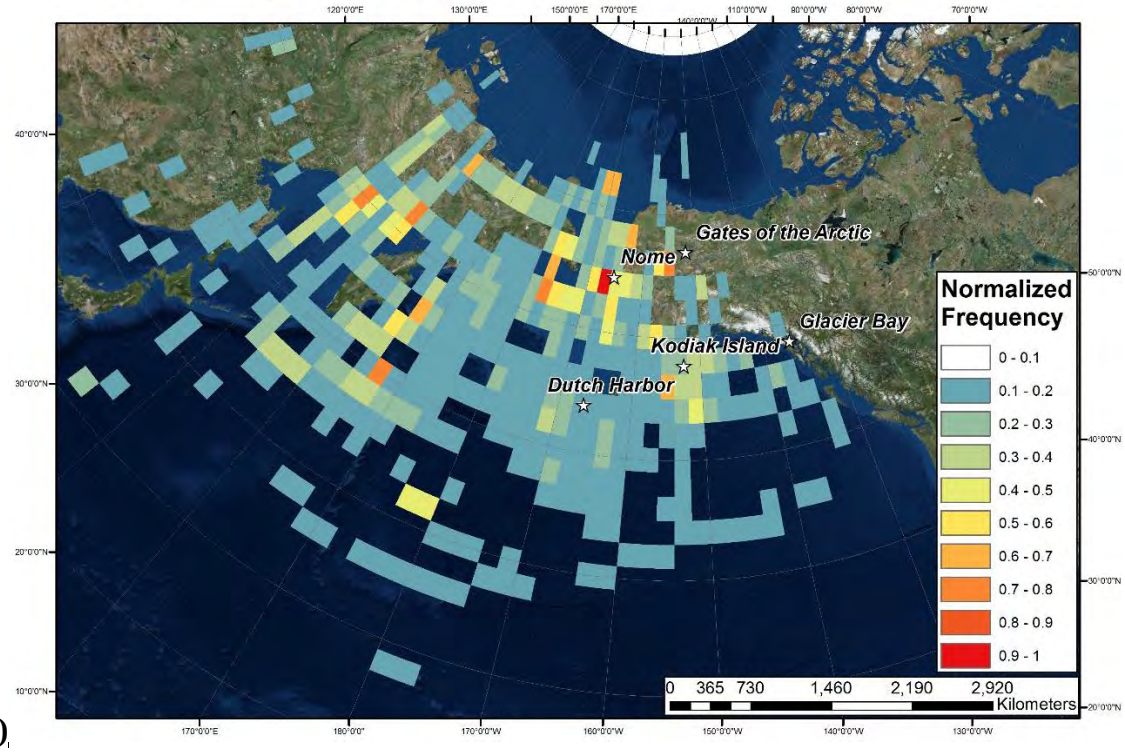

d)

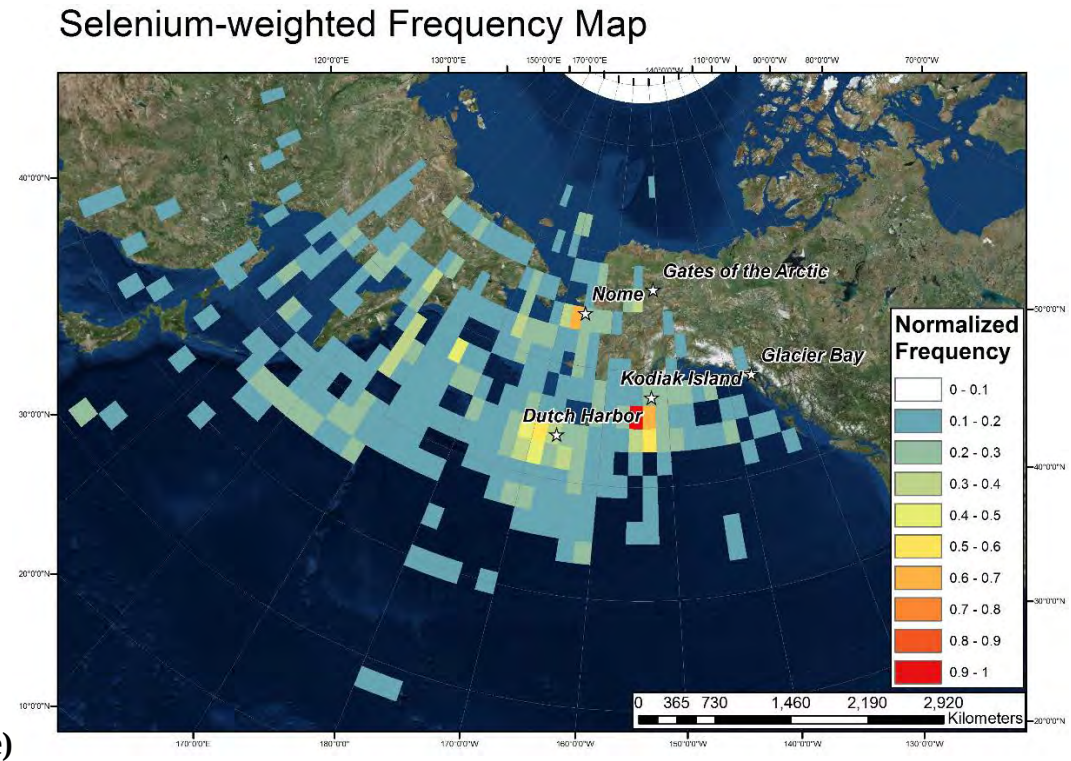

e)

Figure 33. Backtrajectory frequency maps weighted by a) Cr, b) Ni, c) Pb, d) As, and e) Se for all trace metal deposition data at AK04 (Nome), AK00 (Dutch Harbor), and AK98 (Kodiak Island).

10 Recommendations

For continued monitoring work of atmospheric deposition in Alaska, we have the following key recommendations based on our analyses of observed patterns:

(1) Given the strong gradients in Hg wet deposition between coastal and inland, more northern sites strongly following precipitation patterns, we recommend continued wet deposition monitoring to include a station with high precipitation regime and a site with low precipitation conditions. Give a relatively narrow range of Hg concentrations, however, the number of stations could probably be reduced to one station representing each precipitation regime. In our view, it would be best to continue monitoring wet Hg deposition at the two deposition stations with the longest deposition record, each one located in a high and an a low precipitation area, in order to build upon an existing multiyear record: Kodiak Island and Gates of the Arctic. This strategy would allow to analyze inter-annual variability in Hg wet deposition as well as analyze temporal trends.

(2) Given low wet deposition amounts of Hg across most of Alaska that are below the deposition loads of most other areas in the U.S., we recommend to focus deposition monitoring on dry deposition processes. The focus should be on assessing the dry deposition of the gaseous elemental mercury (Hg^0) which has been shown to dominate deposition loads in most terrestrial ecosystems, including in northern Alaska (see section 8). The methodologies for accurate dry deposition monitoring are complex and

challenging, with the methods that allow direct quantification of whole ecosystem Hg^0 fluxes generally limited to micrometeorological techniques (Bash and Miller, 2008; Fritsche et al., 2008a; Fritsche et al., 2008b; Marsik et al., 2005; Olofsson et al., 2005; Pierce et al., 2014; Zhang et al., 2009). Alternatively, litterfall measurements have been proposed as a proxy for atmospheric dry deposition, and have been implemented by NADP in a litterfall deposition network (Risch et al., 2012; Zhang et al., 2012a; Zhang et al., 2012b), although this has not been implemented in non-forest ecosystem yet. It needs to be pointed out that litterfall deposition, however, is not equal to net deposition of elemental Hg^0 as it includes both oxidized Hg^{II} and Hg^0 dry deposition and does not account for re-volatilization losses of Hg^0 after deposition.

(3) Hg^{II} dry deposition can be an important component of arctic Hg dynamics particularly during MDE in the polar spring along the coasts, as for example shown in Alaska by studies from Barrow (Brooks et al., 2006; Douglas et al., 2005; Lindberg et al., 2001a; Lindberg et al., 2002; Moore et al., 2014). Yet, there is evidence that the effects of MDE are limited spatially to the proximity of high-northern coastal regions (Douglas and Sturm, 2004), and that significant re-emissions of deposited Hg^{II} may limit the impacts of MDE (Douglas et al., 2012). Although wet deposition concentrations did not indicate high atmospheric Hg^{II} levels, impacts of MDEs in the high arctic and a possible presence of Hg^{II} along coastal locations should be not be disregarded.

(4) Quantification of wet Hg deposition is not sufficient to account for Hg loading to freshwater ecosystems, coastal ecosystems, and oceans. The sources for these systems are often dominated by runoff processes from upland terrestrial areas and wetland dynamics (Amos et al., 2014; Dastoor and Durnford, 2014; Fisher et al., 2012; Leitch et al., 2007; Lorey and Driscoll, 1999; Meili, 1991), and these inputs need to be accounted for to understand aquatic Hg loads.

(5) To determine source-receptor relationships, multi-tracer approaches present a good opportunity to better quantify different sources. Yet, for a better assessment of different sources, we suggest to develop a comprehensive monitoring strategy that involves additional tracers. Depending on the specific interests and goals, such tracers should include geogenic/dust tracers such as Al, Fe, or Ti; major cations and anions (such as Na, Mg, Cl) to identify marine sources; and gas traces such as CO, CO_2, NO_x, O_3, SO_4 (e.g., for combustion sources) or 222Rn (e.g., as boundary layer signature).

(6) The inclusion of multiple elements allows to analyze commonalities of elements in deposition and thereby help to identify possibly common sources. Yet, the approach is limited as results can be inconclusive and patterns can also be independent of sources, e.g., driven by similar environmental fate processes. The State of Alaska should develop a list of the most critical trace elements that are of interest and based on this develop specific monitoring approaches which may go beyond monitoring in wet deposition samples.

11 References

Ackerman JT, Eagles-Smith CA, Herzog MP, Hartman CA, Peterson SH, Evers DC, et al. Avian mercury exposure and toxicological risk across western North America: a synthesis. Science of the Total Environment 2016.

Agnan Y, Jiskra M, Colegrove D, Douglas T, Helmig D, Sonke JE, et al. The dynamics of mercury in tundra snow pack: deposition, seasonal loads, gaseous exchange, and inputs during snowmelt, in preparation.

Agnan Y, LeDantec T, Moore C, Edwards G, Obrist D. New constraints on terrestrial surface-atmosphere fluxes of gaseous elemental mercury using a global database. Environmental Science & Technology 2015a; 19: 507-524.

Agnan Y, Obrist D, Moore C. A comprehensive database of global soil-snow-atmosphere flux studies of mercury. American Geophysical Union Fall Meeting, San Francisco, 2014.

Agnan Y, Sejalon-Delmas N, Claustres A, Probst A. Investigation of spatial and temporal metal atmospheric deposition in France through lichen and moss bioaccumulation over one century. Science of the Total Environment 2015b; 529: 285-296.

AMAP. AMAP Assessment 2002: Heavy Metals in the Arctic. Arctic Monitoring and Assessment Programme (AMAP), Oslo, Norway, 2005, pp. xvi + 265 pp.

AMAP. Arctic Pollution 2009. Arctic Monitoring and Assessment Programme. Arctic Monitoring and Assessment Programme (AMAP), Oslo, Norway, 2009a, pp. 83.

AMAP. Assessment 2009: Human Health in the Arctic. Arctic Monitoring and Assessment Programme, Oslo, Norway, 2009b.

AMAP. Arctic Pollution 2011. Arctic Monitoring and Assessment Programme (AMAP), Oslo, Norway, 2011, pp. 38.

Amirbahman A, Ruck PL, Fernandez IJ, Haines TA, Kahl JA. The Effect of Fire on Mercury Cycling in the Soils of Forested Watersheds: Acadia National Park, Maine, U.S.A. Water, Air, & Soil Pollution 2004a; 152: 315-331.

Amirbahman A, Ruck PL, Fernandez IJ, Haines TA, Kahl JS. The effect of fire on mercury cycling in the soils of forested watersheds: Acadia National Park, Maine, USA. Water Air and Soil Pollution 2004b; 152: 313-331.

Amos HM, Jacob DJ, Kocman D, Horowitz HM, Zhang YX, Dutkiewicz S, et al. Global Biogeochemical Implications of Mercury Discharges from Rivers and Sediment Burial. Environmental Science & Technology 2014; 48: 9514-9522.

Andreae MO, Berresheim H, Andreae TW, Kritz MA, Bates TS, Merrill JT. Vertical-Distribution of Dimethylsulfide, Sulfur-Dioxide, Aerosol Ions, and Radon over the Northeast Pacific-Ocean. Journal of Atmospheric Chemistry 1988; 6: 149-173.

Ariya PA, Dastoor AP, Amyot M, Schroeder WH, Barrie L, Anlauf K, et al. The Arctic: a sink for mercury. Tellus Series B-Chemical and Physical Meteorology 2004; 56: 397-403.

Baeyens W, Leermakers M, Papina T, Saprykin A, Brion N, Noyen J, et al. Bioconcentration and biomagnification of mercury and methylmercury in North Sea and Scheldt estuary fish. Archives of Environmental Contamination and Toxicology 2003; 45: 498-508.

Bash JO, Miller DR. A relaxed eddy accumulation system for measuring surface fluxes of total gaseous mercury. Journal of Atmospheric and Oceanic Technology 2008; 25: 244-257.

Bergan T, Rodhe H. Oxidation of elemental mercury in the atmosphere; Constraints imposed by global scale modelling. Journal of Atmospheric Chemistry 2001; 40: 191-212.

Bishop K, Lee Y. Catchments as a source of mercury/methylmercury in boreal surface waters. Metal Ions in Biological Systems 1997; 34: 113-130.

Biswas A, Blum JD, Keeler GJ. Mercury storage in surface soils in a central Washington forest and estimated release during the 2001 Rex Creek Fire. Science of the Total Environment 2008; 404: 129-138.

Bjerregaard P, Hansen JC. Organochlorines and heavy metals in pregnant women from the Disko Bay area in Greenland. Science of the Total Environment 2000; 245: 195-202.
Bocharova N, Treu G, Czirják GÁ, Krone O, Stefanski V, Wibbelt G, et al. Correlates between Feeding Ecology and Mercury Levels in Historical and Modern Arctic Foxes (<italic>Vulpes lagopus</italic>). PLoS ONE 2013; 8: e60879.
Boutron CF, Vandal GM, Fitzgerald WF, Ferrari CP. A forty year record of Mercury in central Greenland snow. Geophys. Res. Lett. 1998; 25: 3315-3318.
Braune BM, Gaston AJ, Gilchrist HG, Mallory ML, Provencher JF. A geographical comparison of mercury in seabirds in the eastern Canadian Arctic. Environment International 2014; 66: 92-96.
Brooks S, Arimoto R, Lindberg S, Southworth G. Antarctic polar plateau snow surface conversion of deposited oxidized mercury to gaseous elemental mercury with fractional long-term burial. Atmospheric Environment 2008; 42: 2877-2884.
Brooks S, Saiz-Lopez A, Skov H, Lindberg S, Plane J, Goodsite M. The mass balance of mercury in the springtime arctic environment. GEOPHYSICAL RESEARCH LETTERS 2006; 33: L13812.
Brunke EG, Labuschagne C, Slemr F. Gaseous mercury emissions from a fire in the Cape Peninsula, South Africa, during January 2000. Geophysical Research Letters 2001; 28: 1483-1486.
Carling GT, Fernandez DP, Johnson WP. Dust-mediated loading of trace and major elements to Wasatch Mountain snowpack. Science of the Total Environment 2012; 432: 65-77.
Castello L, Zhulidov AV, Gurtovaya TY, Robarts RD, Holmes RM, Zhulidov DA, et al. Low and Declining Mercury in Arctic Russian Rivers. Environmental Science & Technology 2014; 48: 747-752.
Corbitt ES, Jacob DJ, Holmes CD, Streets DG, Sunderland EM. Global Source-Receptor Relationships for Mercury Deposition Under Present-Day and 2050 Emissions Scenarios. Environmental Science & Technology 2011; 45: 10477-10484.
Dastoor AP, Durnford DA. Arctic Ocean: Is It a Sink or a Source of Atmospheric Mercury? Environmental Science & Technology 2014; 48: 1707-1717.
Demers JD, Blum JD, Zak DR. Mercury isotopes in a forested ecosystem: Implications for air-surface exchange dynamics and the global mercury cycle. Global Biogeochemical Cycles 2013; 27: 222-238.
Dietz R, Outridge PM, Hobson KA. Anthropogenic contributions to mercury levels in present-day Arctic animals-A review. Science of the Total Environment 2009; 407: 6120-6131.
Dommergue A, Sprovieri F, Pirrone N, Ebinghaus R, Brooks S, Courteaud J, et al. Overview of mercury measurements in the Antarctic troposphere. Atmos. Chem. Phys. 2010; 10: 3309-3319.
Douglas TA, Loseto LL, Macdonald RW, Outridge P, Dommergue A, Poulain A, et al. The fate of mercury in Arctic terrestrial and aquatic ecosystems, a review. Environmental Chemistry 2012; 9: 321-355.
Douglas TA, Sturm M. Arctic haze, mercury and the chemical composition of snow across northwestern Alaska. Atmospheric Environment 2004; 38: 805-820.
Douglas TA, Sturm M, Simpson WR, Brooks S, Lindberg SE, Perovich DK. Elevated mercury measured in snow and frost flowers near Arctic sea ice leads. Geophysical Research Letters 2005; 32.
Dray S, Dufour AB. The ade4 package: implementing the duality diagram for ecologist. Journal of Statistical Software 2007; 22: 1-20.
Durnford D, Dastoor A, Figueras-Nieto D, Ryjkov A. Long range transport of mercury to the Arctic and across Canada. Atmospheric Chemistry and Physics 2010; 10: 6063-6086.
Eagles-Smith CA, Ackerman JT, Willacker JJ, Tate MT, Lutz MA, Fleck JA, et al. Spatial and temporal patterns of mercury concentrations in freshwater fish across the western United States and Canada. . Science of the Total Environment 2016.
Engle MA, Tate MT, Krabbenhoft DP, Kolker A, Olson ML, Edgerton ES, et al. Characterization and cycling of atmospheric mercury along the central US Gulf Coast. Applied Geochemistry 2008; 23: 419-437.
Enrico M, Roux GL, Marusczak N, Heimbürger L-E, Claustres A, Fu X, et al. Atmospheric Mercury Transfer to Peat Bogs Dominated by Gaseous Elemental Mercury Dry Deposition. Environmental Science and Technology 2016; 50: 2405-2412.

EPA. U.S. Environmental Protection Agency: Initial List of Hazardous Air Pollutants with Modifications, 2016a.
EPA US. U.S. EPA Toxics Release Inventory 2014. 2016, 2014.
EPA US. U.S. Environmental Protection Agency: Lead (Pb) air pollution. 2016b.
Ericksen JA, Gustin MS, Schorran DE, Johnson DW, Lindberg S, Coleman JS. Accumulation of atmospheric mercury in forest foliage. Atmospheric Environment 2003; 37: 1613-1622.
Evans MS, Lockhart WL, Doetzel L, Low G, Muir D, Kidd K, et al. Elevated mercury concentrations in fish in lakes in the Mackenzie River Basin: The role of physical, chemical, and biological factors. Science of the Total Environment 2005; 351: 479-500.
Faïn X, Ferrari CP, Dommergue A, Albet MR, Battle M, Severinghaus J, et al. Polar firn air reveals large-scale impact of anthropogenic mercury emissions during the 1970s. Proceedings of the National Academy of Sciences of the United States of America 2009a; 106: 16114-16119.
Faïn X, Obrist D, Hallar AG, McCubbin I, Rahn T. High levels of reactive gaseous mercury observed at a high elevation research laboratory in the Rockies Mountains. Atmos. Chem. Phys. 2009b; 9: 8049-8060.
Faïn X, Obrist D, Pierce A, Barth C, Gustin MS, Boyle DP. Whole-watershed mercury balance at Sagehen Creek, Sierra Nevada, CA. Geochimica et Cosmochimica Acta 2011; 75: 2379-2392.
Ferrara R, Maserti B, Petrosino A, Bargagli. Mercury levels in rain and air and the subsequent washout mechanism in a central Italian region. Atmospheric Environment 1986; 20: 125-128.
Ferrara R, Mazzolai B, Lanzillotta E, Nucaro E, Pirrone N. Volcanoes as emission sources of atmospheric mercury in the Mediterranean basin. The Science of The Total Environment 2000; 259: 115-121.
Fisher JA, Jacob DJ, Soerensen AL, Amos HM, Steffen A, Sunderland EM. Riverine source of Arctic Ocean mercury inferred from atmospheric observations. Nature Geoscience 2012; 5: 499-504.
Fitzgerald WF, Engstrom DR, Lamborg CH, Tseng CM, Balcom PH, Hammerschmidt CR. Modern and historic atmospheric mercury fluxes in northern Alaska: Global sources and Arctic depletion. Environmental Science & Technology 2005; 39: 557-568.
Friedli H, Radke L, Lu J. Mercury in smoke from biomass fires. Geophysical Research Letters 2001; 28: 3223-3226.
Friedli H, Radke L, Prescott R, Li P, Woo J, Carmichael G. Mercury in the atmosphere around Japan, Korea, and China as observed during the 2001 ACE-Asia field campaign: Measurements, distributions, sources, and implications. Journal of Geophysical Research-Atmospheres 2004a; 109: -.
Friedli HR, Radke LF, Prescott R, Li P, Woo JH, Carmichael GR. Mercury in the atmosphere around Japan, Korea, and China as observed during the 2001 ACE-Asia field campaign: Measurements, distributions, sources, and implications. Journal of Geophysical Research-Atmospheres 2004b; 109.
Fritsche J, Obrist D, Zeeman MJ, Conen F, Eugster W, Alewell C. Elemental mercury fluxes over a sub-alpine grassland determined with two micrometeorological methods. Atmospheric Environment 2008a; 42: 2922-2933.
Fritsche J, Wohlfahrt G, Ammann C, Zeeman M, Hammerle A, Obrist D, et al. Summertime elemental mercury exchange of temperate grasslands on an ecosystem-scale. Atmospheric Chemistry and Physics 2008b; 8: 7709-7722.
Gallant AL, Binnian EF, Omernik JM, Shasby MB. Level III Ecorgeions of Alaska 1995 - reproduced 2010. 2016, 1995.
GDAL. GDAL - Geospatial Data Abstraction Library: Version 2.1.1, Open Source Geospatial Foundation, 2016.
Glass GE, Sorensen JA. Six-year trend (1990-1995) of wet mercury deposition in the Upper Midwest, USA. Environmental Science and Technology 1999; 33: 3303-3312.
Google Earth Engine Team. Google Earth Engine: A planetary-scale geospatial analysis platform, 2015.
Grigal D, Kolka R, Fleck J, Nater E. Mercury budget of an upland-peatland watershed. Biogeochemistry 2000; 50: 95-109.

Grigal DF. Inputs and outputs of mercury from terrestrial watersheds: a review. Environmental Review 2002; 10: 1-39.
Grigal DF. Mercury sequestration in forests and peatlands: A review. Journal of Environmental Quality 2003; 32: 393-405.
Gustin MS, Lindberg SE, Weisberg PJ. An update on the natural sources and sinks of atmospheric mercury. Applied Geochemistry 2008; 23: 482-493.
Hararuk O, Obrist D, Luo Y. Modeling the sensitivity of soil mercury storage to climate-induced changes in soil carbon pools. Biogeosciences 2013; 10: 2393–2407.
Hare AA, Stern GA, Kuzyk ZZA, Macdonald RW, Johannessen SC, Wang F. Natural and Anthropogenic Mercury Distribution in Marine Sediments from Hudson Bay, Canada. Environmental Science & Technology 2010; 44: 5805-5811.
Hedge C, Obrist D, Kretzschmar R, Wiederhold I, Biester H, Chow J, et al. Soil and plant mercury concentrations and pools in the Arctic tundra of northern Alaska. International Conference on Mercury as a Global Pollutant, Jeju, South Korea, 2015.
Hedge C, Obrist D, Kretzschmar R, Wiederhold I, Biester H, Chow J, et al. Soil and plant mercury concentrations and pools in the Arctic tundra of northern Alaska, in preparation.
Helsel D. Statistics for Censored Environmental Data Using Mintab and R: Wiley Publishing, 2012.
Hermanson MH. Anthropogenic mercury deposition to arctic lake sediments. Water Air and Soil Pollution 1998; 101: 309-321.
Husar RB, Tratt DM, Schichtel BA, Falke SR, Li F, Jaffe D, et al. Asian dust events of April 1998. Journal of Geophysical Research-Atmospheres 2001; 106: 18317-18330.
Iverfeldt Å. Mercury in forest canopy throughfall water and its relation to atmospheric deposition. Water, Air, and Soil Pollution 1991; 56: 553-564.
Jaeglé L. Atmospheric long-range transport and deposition of mercury to Alaska. Department of Atmospheric Sciences, University of Washington, Seattle, A report to the Alaska Department of Environmental Conservation, 2010.
Jaffe D, Anderson T, Covert D, Kotchenruther R, Trost B, Danielson J, et al. Transport of Asian air pollution to North America. GEOPHYSICAL RESEARCH LETTERS 1999; 26: 711-714.
Jaffe D, McKendry I, Anderson T, Price H. Six 'new' episodes of trans-Pacific transport of air pollutants. ATMOSPHERIC ENVIRONMENT 2003a; 37: 391-404.
Jaffe D, Prestbo E, Swartzendruber P, Weiss-Penzias P, Kato S, Takami A, et al. Export of atmospheric mercury from Asia. Atmospheric Environment 2005; 39: 3029-3038.
Jaffe D, Price H, Parrish D, Goldstein A, Harris J. Increasing background ozone during spring on the west coast of North America. GEOPHYSICAL RESEARCH LETTERS 2003b; 30: -.
Jaffe D, Snow J, Cooper O. The 2001 Asian Dust Events: Transport and Impact on Surface Aerosol Concentrations in the U.S. Eos 2003c; 84: 501-516.
Jiskra M, Wiederhold JG, Skyllberg U, Kronberg R-M, Hajdas I, Kretzschmar R. Mercury Deposition and Re-emission Pathways in Boreal Forest Soils Investigated with Hg Isotope Signatures. Environmental Science and Technology 2015a.
Jiskra M, Wiederhold JG, Skyllberg U, Kronberg RM, Hajdas I, Kretzschmar R. Mercury deposition and re-emission pathways in boreal forest soils investigated with Hg isotope signatures. Environmental Science & Technology 2015b; 49: 7188-7196.
Karagas MR, Choi AL, Oken E, Horvat M, Schoeny R, Kamai E, et al. Evidence on the Human Health Effects of Low-Level Methylmercury Exposure. Environmental Health Perspectives 2012; 120: 799-806.
Kelly EN, Schindler DW, St Louis VL, Donald DB, Vlaclicka KE. Forest fire increases mercury accumulation by fishes via food web restructuring and increased mercury inputs. Proceedings of the National Academy of Sciences of the United States of America 2006; 103: 19380-19385.
Laird BD, Goncharov AB, Egeland GM, Chan HM. Dietary Advice on Inuit Traditional Food Use Needs to Balance Benefits and Risks of Mercury, Selenium, and n3 Fatty Acids. Journal of Nutrition 2013; 143: 923-930.

Lamborg CH, Fitzgerald WF, Vandal GM, Rolfhus KR. Atmospheric mercury in Northern Wisconsin : sources and species. Water Air and Soil Pollution 1995; 80: 189-198.
Landis MS, Vette AF, Keeler GJ. Atmospheric Mercury in the Lake Michigan Basin: Influence of the Chicago/Gary Urban Area. Environmental Science & Technology 2002; 36: 4508-4517.
Laurier FJG, Mason RP, Whalin L, Kato S. Reactive gaseous mercury formation in the North Pacific Ocean's marine boundary layer: A potential role of halogen chemistry. Journal of Geophysical Research-Atmospheres 2003; 108: 12.
Lawson NM, Mason RP. Accumulation of mercury in estuarine food chains. Biogeochemistry 1998; 40: 235-247.
Lee K, Hur SD, Hou S, Hong S, Qin X, Ren J, et al. Atmospheric pollution for trace elements in the remote high-altitude atmosphere in central Asia as recorded in snow from Mt. Qomolangma (Everest) of the Himalayas. Science of the Total Environment 2008; 404: 171-181.
Lee L. NADA: Nondetects And Data Analysis for environmental data. R package version 1.5-6. 2015, 2013.
Leitch DR, Carrie J, Lean D, Macdonald RW, Stern GA, Wang FY. The delivery of mercury to the Beaufort Sea of the Arctic Ocean by the Mackenzie River. Science of the Total Environment 2007; 373: 178-195.
Lindberg S, Brooks S, Lin C, Scott K, Meyers T, Chambers L, et al. Formation of Reactive Gaseous Mercury in the Arctic: Evidence of Oxidation of Hg◦ to Gas-Phase Hg-II Compounds After Arctic Sunrise. Water, Air, and Soil Pollution 2001a; Focus 1: 295-302.
Lindberg SE. Forest and the global biogeochemical cycle of mercury: The importance of understanding air/vegetation exchange processes. In: Aeyens W., Ebinghaus R., And Vasiliev O. (eds) Global and Regional Mercury Cycles: Sources, Fluxes and Mass Balances. NATOASI Series. Vol 21. Kluwer Academic Publishe3rs, Dordreacht 1996: 359-380.
Lindberg SE, Brooks S, Lin C-J, Scott K, Meyers T, Chambers L, et al. Formation of Reactive Gaseous Mercury in the Arctic: Evidence of Oxidation of Hg° to Gas-Phase Hg-II Compounds after Arctic Sunrise. Water Air and Soil Pollution 2001b; 1: 295-302.
Lindberg SE, Brooks S, Lin C-J, Scott KJ, Landis MS, Stevens RK, et al. Dynamic Oxidation of Gaseous Mercury in the Arctic Troposphere at Polar Sunrise. Environmental Science and Technology 2002; 36: 1245-256.
Lorey P, Driscoll CT. Historical trends of mercury deposition in Adirondack lakes. Environmental Science & Technology 1999; 33: 718-722.
Loseto LL, Stern GA, Ferguson SH. Size and biomagnification: How habitat selection explains beluga mercury levels. Environmental Science & Technology 2008; 42: 3982-3988.
Lu JY, Schroeder WH, Barrie LA, Steffen A, Welch HE, Martin K, et al. Magnification of atmospheric mercury deposition to polar regions in springtime: the link to tropospheric ozone depletion chemistry. Geophysical Research Letters 2001; 28: 3219-3222.
Lyman SN, Gustin MS. Speciation of atmospheric mercury at two sites in northern Nevada, USA. Atmospheric Environment 2008; 42: 927-939.
Macdonald RW, Bewers JM. Contaminants in the arctic marine environment: Priorities for protection. Ices Journal of Marine Science 1996; 53: 537-563.
Mann JL, Long SE, Shuman CA, Kelly WR. Determination of mercury content in a shallow firn core from Greenland by isotope dilution inductively coupled plasma mass spectrometry. Water Air and Soil Pollution 2005; 163: 19-32.
Marsik F, Keeler G, Lindberg S, Zhang H. Air-surface exchange of gaseous mercury over a mixed sawgrass-cattail stand within the Florida Everglades. Environmental Science & Technology 2005; 39: 4739-4746.
Mason RP, Fitzgerald WF, Morel FMM. The biogeochemical cycling of elemental mercury - anthropogenic influences. Geochimica Et Cosmochimica Acta 1994; 58: 3191-3198.
Mason RP, Lawson NM, Sheu GR. Annual and seasonal trends in mercury deposition in Maryland. Atmospheric Environment 2000; 34: 1691-1701.

Mason RP, Lawson NM, Sullivan KA. The concentration, speciation and sources of mercury in Chesapeake Bay precipitation. Atmospheric Environment 1997; 31: 3541-3550.
Mather TA, Pyle DM. Volcanic emissions of mercury to the atmosphere: global and regional inventories. Comment. Science of the Total Environment 2004; 327: 323-329.
Meili M. The coupling of mercury and organic matter in the biogeochemical cycle - towards a mechanistic model for the boreal forest zone. Water Air and Soil Pollution 1991; 56: 333-347.
Mitchell CPJ, Kolka RK, Fraver S. Singular and Combined Effects of Blowdown, Salvage Logging, and Wildfire on Forest Floor and Soil Mercury Pools. Environmental Science & Technology 2012; 46: 7963-7970.
Moore CW, Obrist D, Steffen A, Staebler RM, Douglas TA, Richter A, et al. Convective forcing of mercury and ozone in the Arctic boundary layer induced by leads in sea ice. Nature 2014; 506: 81-84.
Mosher BW, Duce RA, Prospero JM, Savoie DL. Atmospheric Selenium - Geographical-Distribution and Ocean to Atmosphere Flux in the Pacific. Journal of Geophysical Research-Atmospheres 1987; 92: 13277-13287.
Muir DCG, Wang X, Yang F, Nguyen N, Jackson TA, Evans MS, et al. Spatial Trends and Historical Deposition of Mercury in Eastern and Northern Canada Inferred from Lake Sediment Cores. Environmental Science & Technology 2009; 43: 4802-4809.
Munthe J, Hultberg H, Iverfeldt A. Mechanisms of Deposition of Methylmercury and Mercury to Coniferous Forests. Water Air and Soil Pollution 1995; 80: 363-371.
Murphy D, Cziczo D, Froyd K, Hudson P, Matthew B, Middlebrook A, et al. Single-particle mass spectrometry of tropospheric aerosol particles. JOURNAL OF GEOPHYSICAL RESEARCH-ATMOSPHERES 2006; 111.
NADP. National Atmospheric Deposition Program (NADP): about the NADP concentration and deposition maps, 2016.
NPS US. WACAP - Western Airborne Contaminants Assessment Project. A window into the contaminant situation at 20 national parks from the Arctic to the Mexican border, 2008.
Nriagu J, Becker C. Volcanic emissions of mercury to the atmosphere: global and regional inventories. Science of the Total Environment 2003; 304: 3-12.
Obrist D. Atmospheric mercury pollution due to losses of terrestrial carbon pools? Biogeochemistry 2007; 85: 119-123, doi 10.1007/s10533-007-9108-0.
Obrist D, Agnan Y, Helmig D, Moore C, Jiskra M, Hueber J, et al. A global mercury sink for atmospheric mercury observed in the arctic tundra. in preparation.
Obrist D, Hallar AG, McCubbin I, Stephens BB, Rahn T. Atmospheric mercury concentrations at Storm Peak Laboratory in the Rocky Mountains: Evidence for long-range transport from Asia, boundary layer contributions, and plant mercury uptake. Atmospheric Environment 2008a; 42: 7579-7589.
Obrist D, Moosmueller H, Schuermann R, Chen LWA, Kreidenweis SM. Particulate-phase and gaseous elemental mercury emissions during biomass combustion: Controlling factors and correlation with particulate matter emissions. Environmental Science & Technology 2008b; 42: 721-727.
Obrist D, Pearson C, Webster J, Kane T, Che-Jen L, Aiken G, et al. Terrestrial mercury in the western United States: Spatial distribution defined by land coer and plant productivity. Science of the Total Environment 2015; http://dx.doi.org/10.1016/j.scitotenv.2015.11.104.
Obrist D, Tas E, Mordechai P, Matveev V, Faïn X, Asaf D, et al. Bromine-induced oxidation of mercury in the temperate atmosphere. Nature Geoscience 2010: in press.
Olofsson M, Sommar J, Ljungstrom E, Andersson M, Wangberg I. Application of relaxed eddy accumulation technique to quantify Hg-0 fluxes over modified soil surfaces. WATER AIR AND SOIL POLLUTION 2005; 167: 331-352.
Outridge PM, Macdonald RW, Wang F, Stern GA, Dastoor AP. A mass balance inventory of mercury in the Arctic Ocean. Environmental Chemistry 2008; 5: 89-111.
Parrish DD, Hahn CJ, Williams EJ, Norton RB, Fehsenfeld FC, Singh HB, et al. Indications of Photochemical Histories of Pacific Air Masses from Measurements of Atmospheric Trace Species at Point Arena, California. Journal of Geophysical Research-Atmospheres 1992; 97: 15883-15901.

Pierce AM, Moore CW, Wohlfahrt G, Hörtnagel L, Kljun N, Obrist D. Eddy covariance flux measurements of gaseous elemental mercury using cavity ring-down spectroscopy. Environmental Science & Technology 2014; 49.
Poissant L, Pilote M. Mercury concentrations in single event precipitation in southern Quebec. The Science of The Total Environment 1998; 213: 65-72.
Porvari P, Verta M, Munthe J, Haapanen M. Forestry practices increase mercury and methyl mercury output from boreal forest catchments. Environmental Science & Technology 2003; 37: 2389-2393.
Price H, Jaffe D, Cooper O, Doskey P. Photochemistry, ozone production, and dilution during long-range transport episodes from Eurasia to the northwest United States. JOURNAL OF GEOPHYSICAL RESEARCH-ATMOSPHERES 2004; 109: -.
Pyle DM, Mather TA. The importance of volcanic emissions for the global atmospheric mercury cycle. Atmospheric Environment 2003; 37: 5115-5124.
PythonSoftwareFoundation. Python Language Reference, version 2.7.
R-Core-Team. R: a language and environment for statistical computing. R Foundation for Statistical Computing, Vienna, Austria, 2014.
Rasmussen R, Baker B, Kochendorfer J, Meyers T, Landolt S, Fischer AP, et al. HOW WELL ARE WE MEASURING SNOW? The NOAA/FAA/NCAR Winter Precipitation Test Bed. Bulletin of the American Meteorological Society 2012; 93: 811-829.
Rea A, Keeler G, Scherbatskoy T. The deposition of mercury in throughfall and litterfall in the lake champlain watershed: A short-term study. Atmopsheric Environment 1996; 30: 3257-3263.
Revelle W. psych: Procedures for Personality and Psychological Research, Northwestern University, Evanston, Illinois, USA 2014.
Risch MR, DeWild JF, Krabbenhoft DP, Kolka RK, Zhang LM. Litterfall mercury dry deposition in the eastern USA. Environmental Pollution 2012; 161: 284-290.
Saha S, et al. NCEP Climate Forecast System Version 2 (CFSv2) 6-hourly Products. Research Data Archive at the National Center for Atmospheric Research, Computational and Information Systems Laboratory, 2011.
Sanei H, Outridge PM, Goodarzi F, Wang F, Armstrong D, Warren K. Wet deposition mercury fluxes in the Canadian sub-Arctic and southern Alberta, measured using an automated precipitation collector adapted to cold regions. Atmospheric Environment 2010; 44: 1672-1681.
Savina M, Schäppi B, Molnar P, Burlando P, Sevruk B. Comparison of a tipping-bucket and electronic weighing precipitation gage for snowfall. Atmospheric Research 2012; 103: 45-51.
Schroeder WH, Anlauf KG, Barrie LA, Lu JY, Steffen A, Schneeberger DR, et al. Arctic springtime depletion of mercury. Nature 1998; 394: 331-332.
Schroeder WH, Munthe J. Atmospheric mercury - An overview. Atmospheric Environment 1998; 32: 809-822.
Schuster PF, Krabbenhoft DP, DeWild JF, Sabin TG. A paleoenvironmental record of atmospheric mercury deposition in a permafrost core EOS Transaction, AGU, Fall Meeting suppl. Abstract B13C-0452, San Franc, 2008.
Schuster PF, Krabbenhoft DP, Naftz DL, Cecil LD, Olson ML, Dewild JF, et al. Atmospheric Mercury Deposition during the Last 270 Years: A Glacial Ice Core Record of Natural and Anthropogenic Sources. Environmental Science & Technology 2002; 36: 2303-2310.
Schuster PF, Striegl RG, Aiken GR, Krabbenhoft DP, Dewild JF, Butler K, et al. Mercury Export from the Yukon River Basin and Potential Response to a Changing Climate. Environmental Science & Technology 2011; 45: 9262-9267.
Seigneur C, Vijayaraghavan K, Lohman K, Karamchandani P, Scott C. Global source attribution for mercury deposition in the United States. Environmental Science & Technology 2004; 38: 555-569.
Selin NE, Jacob DJ. Seasonal and spatial patterns of mercury wet deposition in the United States: Constraints on the contribution from North American anthropogenic sources. Atmospheric Environment 2008; 42: 5193-5204.

Selin NE, Jacob DJ, Park RJ, Yantosca RM, Strode S, Jaegle L, et al. Chemical cycling and deposition of atmospheric mercury: Global constraints from observations. Journal of Geophysical Research-Atmospheres 2007; 112.
Semkin RG, Mierle G, Neureuther RJ. Hydrochemistry and mercury cycling in a High Arctic watershed. Science of the Total Environment 2005; 342: 199-221.
Sheu GR, Lin NH, Wang JL, Lee CT, Yang CFO, Wang SH. Temporal distribution and potential sources of atmospheric mercury measured at a high-elevation background station in Taiwan. Atmospheric Environment 2010; 44: 2393-2400.
Shotyk W, Goodsite ME, Roos-Barraclough F, Frei R, Heinemeier J, Asmund G, et al. Anthropogenic contributions to atmospheric Hg, Pb and As accumulation recorded by peat cores from southern Greenland and Denmark dated using the 14C "bomb pulse curve". Geochimica Et Cosmochimica Acta 2003; 67: 3991-4011.
Sigler J, Lee X, Munger W. Emission and long-range transport of gaseous mercury from a large-scale Canadian boreal forest fire. Environmental Science & Technology 2003; 37: 4343-4347.
Sigler JM, Mao H, Talbot R. Gaseous elemental and reactive mercury in Southern New Hampshire. Atmospheric Chemistry and Physics 2009; 9: 1929-1942.
Skov H, Christensen J, Goodsite M, Heidam NZ, Jensen B, Wahlin P, et al. Fate of elemental mercury in the Arctic during atmospheric mercury depletion episodes and the load of atmospheric mercury to the Arctic. Environmental Science and Technology 2004; 38: 2373-2382.
Slemr F, Schuster G, Seiler W. Distribution, speciation, and budget of atmospheric mercury. Journal of Atmospheric Chemistry 1985; 3: 407-434.
Sprovieri F, Pirrone N, Garfield K, Sommar J. Mercury speciation in the marine boundary layer along a 6000 km cruise path around the Mediterranean Sea Atmospheric Environment Part a-General Topics 2003.
St. Louis V, Rudd J, Kelly C, Hall B, Rolfhus K, Scott K, et al. Importance of the forest canopy to fluxes of methyl mercury and total mercury to boreal ecosystems. Environmental Science & Technology 2001; 35: 3089-3098.
Steffen A, Douglas T, Amyot M, Ariya P, Aspmo K, Berg T, et al. A synthesis of atmospheric mercury depletion event chemistry in the atmosphere and snow. Atmospheric Chemistry and Physics 2008; 8: 1445-1482.
Stow J, Krümmel E, Leech T, Donaldson S. What is the Impact of Mercury Contamination on Human Health in the Arctic? AMAP Assessment 2011: Mercury in the Arctic. Arctic Monitoring and Assessment Programme, Oslo, 2011, pp. pp. 159-170.
Streets DG, Devane MK, Lu Z, Bond TC, Sunderland EM, Jacob DJ. All-Time Releases of Mercury to the Atmosphere from Human Activities. Environmental Science & Technology 2011a; 45: 10485-10491.
Streets DG, Devane MK, Lu ZF, Bond TC, Sunderland EM, Jacob DJ. All-Time Releases of Mercury to the Atmosphere from Human Activities. Environmental Science & Technology 2011b; 45: 10485-10491.
Strode SA, Jaegle L, Jaffe DA, Swartzendruber PC, Selin NE, Holmes C, et al. Trans-Pacific transport of mercury. Journal of Geophysical Research-Atmospheres 2008; 113: 12 pp.
Swartzendruber PC, Jaffe DA, Prestbo EM, Weiss-Penzias P, Selin NE, Park R, et al. Observations of reactive gaseous mercury in the free troposphere at the Mount Bachelor Observatory. Journal of Geophysical Research-Atmospheres 2006; 111.
Tan SW, Meiller JC, Mahaffey KR. The endocrine effects of mercury in humans and wildlife. Critical Reviews in Toxicology 2009; 39: 228-269.
Taylor DA. Mercury - Forest fire fallout. Environmental Health Perspectives 2007; 115: A21-A21.
Turetsky M, Harden J, Friedli H, Flannigan M, Payne N, Crock J, et al. Wildfires threaten mercury stocks in northern soils. Geophysical Research Letters 2006a; 33: 6 pp.
Turetsky MR, Harden JW, Friedli HR, Flannigan M, Payne N, Crock J, et al. Wildfires threaten mercury stocks in northern soils. Geophys. Res. Lett. 2006b; 33: 6 pp.

Van Dam B, Helmig D, Burkhart JF, Obrist D, Oltmans SJ. Springtime boundary layer O3 and GEM depletion at Toolik Lake, Alaska. Journal of Geophysical Research: Atmospheres 2013; 118: 3382-3391.

Van Oostdam J, Gilman A, Dewailly E, Usher P, Wheatley B, Kuhnlein H, et al. Human health implications of environmental contaminants in Arctic Canada: a review. Science of the Total Environment 1999; 230: 1-82.

Veysseyre A, Moutard K, Ferrari C, Van de Velde K, Barbante C, Cozzi G, et al. Heavy metals in fresh snow collected at different altitudes in the Chamonix and Maurienne valleys, French Alps: initial results. Atmospheric Environment 2001; 35: 415-425.

Vriens B, Lenz M, Charlet L, Berg M, Winkel LHE. Natural wetland emissions of methylated trace elements. Nature Communications 2014; 5.

Wai KM, Wu SL, Li XL, Jaffe DA, Perry KD. Global Atmospheric Transport and Source-Receptor Relationships for Arsenic. Environmental Science & Technology 2016; 50: 3714-3720.

Walker JB, Houseman J, Seddon L, McMullen E, Tofflemire K, Mills C, et al. Maternal and umbilical cord blood levels of mercury, lead, cadmium, and essential trace elements in Arctic Canada. Environmental Research 2006; 100: 295-318.

Walsh PR, Duce RA, Fasching JL. Considerations of the Enrichment, Sources, and Flux of Arsenic in the Troposphere. Journal of Geophysical Research-Oceans and Atmospheres 1979; 84: 1719-1726.

Watras CJ, Bloom NS. Mercury and Methylmercury in Individual Zooplankton - Implications for Bioaccumulation. Limnology and Oceanography 1992; 37: 1313-1318.

Webster JP, Kane TJ, Obrist D, Ryan JN, Aiken GR. Estimating mercury emissions resutlign from wildfires in forests of the Western United States. Science of the Total Environment 2016.

Wedepohl KH. The Composition of the Continental-Crust. Geochimica Et Cosmochimica Acta 1995; 59: 1217-1232.

Weiss-Penzias P, Jaffe D, Swartzendruber P, Dennison J, Chand D, Hafner W, et al. Observations of Asian air pollution in the free troposphere at Mount Bachelor Observatory during the spring of 2004. Journal of Geosphysical Research-Atmospheres 2006; 111: -.

Weiss-Penzias P, Jaffe D, Swartzendruber P, Hafner W, Chand D, Prestbo E. Quantifying Asian and biomass burning sources of mercury using the Hg/CO ratio in pollution plumes observed at the Mount Bachelor Observatory. Atmospheric Environment 2007; 41: 4366-4379.

Wickham H. ggplot2: elegant graphic for data analysis. New York, USA: Springer Verlag, 2009.

Wiedinmyer C, Friedli H. Mercury emission estimates from fires: an initial inventory for the United States. Environmental Science & Technology 2007.

Wiedinmyer C, Quayle B, Geron C, Belote A, McKenzie D, Zhang X, et al. Estimating emissions from fires in North America for air quality modeling. Atmospheric Environment 2006; 40: 3419-3432.

Wilson S, Munthe J, Sundseth K, Kindbom K, Maxson P, Pacyna J, et al. Updating historical global inventories of anthropogenic mercury emissions to air. AMAP Technical Report 3, Oslo, 2010, pp. 1-12.

Yang D, Kane DL, Hinzman LD, Goodison BE, Metcalfe JR, Louie PYT, et al. An evaluation of the Wyoming Gauge System for snowfall measurement. Water Resources Research 2000; 36: 2665-2677.

Zhang L, Blanchard P, Gay DA, Prestbo EM, Risch MR, Johnson D, et al. Estimation of speciated and total mercury dry deposition at monitoring locations in eastern and central North America. Atmospheric Chemistry and Physics 2012a; 12: 4327-4340.

Zhang L, Blanchard P, Johnson D, Dastoor A, Ryzhkov A, Lin CJ, et al. Assessment of modeled mercury dry deposition over the Great Lakes region. Environmental Pollution 2012b; 161: 272-283.

Zhang LM, Wright LP, Blanchard P. A review of current knowledge concerning dry deposition of atmospheric mercury. Atmospheric Environment 2009; 43: 5853-5864.

Zheng W, Obrist D, Weis D, Bergquist B. Mercury isotope compositions across North American forests. Global Biogeochemical Cycles; in review.

Zheng W, Obrist D, Weis D, Bergquist BA. Mercury isotope compositions across North American forests. Global Biogeochemical Cycles 2016; in press.